MODIFICATION OF POLYMERIC MATERIALS BY ENERGETIC PROTONS

BY

SHYAMA PRASANNA TRIPATHY

THESIS SUBMITTED

IN FULFILMENT OF THE DEGREE OF

DOCTOR OF PHILOSOPHY IN PHYSICS

OF

NORTH-EASTERN HILL UNIVERSITY
SHILLONG - 793022
INDIA

Thesis

Dedicated to my

PARENTS

NORTH-EASTERN HILL UNIVERSITY
SHILLONG
November 2000

CERTIFICATE

I, Shyama Prasanna Tripathy, hereby, declare that the subject matter of this thesis entitled "Modification of Polymeric Materials by Energetic Protons" is the record of work done by me, that the contents of this thesis did not form basis of the award of any previous degree to me or to the best of my knowledge to anybody else, and that the thesis has not been submitted by me for any research degree in any other University/ Institute.

This is being submitted to the North-Eastern Hill University for the degree of Doctor of Philosophy in Physics.

Shyama Prasanna Tripathy.

Shyama Prasanna Tripathy
(Candidate)

Head
Department of Physics
North-Eastern Hill University

Dr. D. T. Khathing
(Supervisor)

Dr. K. K. Dwivedi
(Joint Supervisor)

Acknowledgements

Man is perfect by his own standards. Quest for excellence is a divinely bestowed attribute that triggers his adventurism. But it is the teachers who diagnosis the potency, provides impetus, sets a goal and unsets activities that help manifest the best in his student. I deem to avail this rare opportunity for expressing my humblest gratitude to my reverend teachers Dr. K. K. Dwivedi, Vice Chancellor, Arunachal University and Dr. D. T. Khathing, Head, Regional Sophisticated Instrumentation Centre, NEHU for their incessant supervision, inspiration, dynamic and invaluable guidance and above all personal care & concern throughout the entire period of my work with them. They have been more than providential in my pursuit.

Dr. D. Fink, HMI, Berlin whose keen interest in my work and his valuable advice have gone a long way in adding a touch of refinement is specially due for a very special & deep sense of gratitude. A note of appreciation is due to Dr. R. Brandt, Phillipines University, for his affectionate encouragement during his visit to India in 1998.

I take this opportunity to thank all the referees of my published manuscripts for their useful suggestions. I wish to express my wholehearted appreciation to all the eminent scientists and resource persons for their constructive criticisms during my presentations in the national and international conferences. I bow in reverence to all those luminaries who have already illuminated the hitherto impassable tracks of research & have provided opportunity of reference for my adventurism.

I am thankful to the scientific staff of Hahn Meitner Institute, Berlin and Nuclear Science Centre, New Delhi for providing proton and heavy ion irradiation facility. I express my gratefulness to Prof. Ajay Gupta, Director, Inter University Consortium, Indore for allowing me to carry out X-ray diffraction studies and Atomic Force Microscopy. I am equally thankful to the director of Institute of Physics, Bhubaneswar for permitting me to utilise the library facilities. I express my reverence to all the teachers from Physics and

Chemistry department as well as the scientific staff of Regional Sophisticated Instrumentation Centre, N.E.H.U., for their encouragement and also for giving me an easy assess to utilise all the available facilities. My heartfelt gratitude is due to my seniors Dr. S. Ghosh, Dr. D. Sinha, Dr. A. Kulshreshtha and Mr. S. C. Katiyar for their proficient help. I wish to express my wholehearted appreciation to my close friends J. Shukla (B.A.R.C.) & S. Swain (University of Hawaii) for their constant encouragement and support. I am thankful to all my seniors and friends in the Department of Chemistry and Physics for their co-operation and friendliness. I acknowledge my sincere thanks to all my well-wishers, who have been encouraging me to reach the acme of success and feel my success as theirs. I express my deep sense of gratitude to Dr. (Mrs.) R. Dwivedi and Mrs. N. Khathing for their love, affection and blessings.

I acknowledge the financial grant in the form of Junior Research Fellowship by N. S. C. -U. G. C. and in the form of Senior Research Fellowship by Council of Scientific and Industrial Research, New Delhi.

I acknowledge a very special thanks to my colleague Rosaline (Rosy) for her unfailing support, enlightening discussions and constructive suggestions that remarkably helped me in improving the quality of this work.

To sum up with it is the perennial fountain of love & blessings of Baba & Bou & their ideals of pursuit of excellence that has emboldened me in my endeavour to translate their dreams to reality, Bhaina & Bhauja who always encouraged me to take up new challenges, my sisters and brother-in-laws who have all in their infinite different ways instilled confidence in me. Had it not for them, I would not have been, where I assert myself.

I could make all my acknowledgements only because of All Mighty who abides with me throughout my life.

04.11.2000
Shillong

Shyama Prasanna Tripathy

CONTENTS

LIST OF TABLES

TABLE NO.	CONTENTS	PAGE NO.

TABLE NO.	CONTENTS	PAGE NO.

TABLE NO.	CONTENTS	PAGE NO.

LIST OF FIGURES

FIGURE NO.	CONTENTS	PAGE NO.

FIGURE NO.	CONTENTS	PAGE NO.

FIGURE NO.	CONTENTS	PAGE NO.

FIGURE NO.	CONTENTS	PAGE NO.
4.8.7.	SEM photographs of fission fragment tracks in PADC samples of stack S5 i) Pristine PADC (blank region) etched for 120 minutes, ii) Proton irradiated region etched for 120 minutes, iii) (Proton + C_{60}) region etched for 120 minutes.	134
4.8.8.	Etching time versus ^{28}Si track diameters for PADC samples of S6 stack adjacent to gold foil and that of S7 stack adjacent to aluminium foil, along with the pristine.	135
4.8.9.	Etching time versus ^{28}Si track lengths for PADC samples of S6 stack adjacent to gold foil and that of S7 stack adjacent to aluminium foil, along with the pristine.	136
4.8.10.	Photomicrographs of etched ^{28}Si tracks in i) Proton irradiated PADC of stack S6 adjacent to gold foil, ii) Proton irradiated PADC of stack S7 adjacent to aluminium foil, iii) Pristine PADC.	139


CHAPTER 1

CHAPTER 1

INTRODUCTION

1.1. IMPORTANCE OF RADIATION IN THE FIELD OF MATERIAL SCIENCE

Many fields - such as microelectronics and mechanics, biology and medicine, surface and membrane technology, magneto-optics and low temperature physics - require a high degree of geometric control on a microscopic scale. Ion irradiation offers a possibility to modify the properties of the materials in a controlled way on microscopic scale. Ionising radiations have a definite range of penetration, a high local confinement of deposited energy and can be generated conveniently in great quantity. The created damage zones can be stored indefinitely in many insulators and can be used to initiate a phase transformation process that modifies the material along the latent track. One ion suffices to induce - physically and chemically - a submicroscopic change in the target material and thereby can render it susceptible to the development process [1].

A lot of work in this field of ion beam treatment has been carried out to investigate the interaction of charged particles with matter. The

application of ion beams nowadays range from the use of low energy ions in the field of surface technology to the application of relativistic heavy ions in radiation therapy.

1.2. POLYMERS

Polymer is a generic name given to a vast number of materials of high molecular weight. Depending on their origin they can be grouped as natural and synthetic polymers. Owing to the presence of carbon in their backbone structure they can be classified as organic and inorganic polymers. They can be divided into thermoplastic and thermosetting polymers due to their response to application of heat. According to its ultimate form and use, a polymer can be classified as plastic, elastomer, fibre or liquid resin [2].

While the chemical structure of a macromolecule depends on the chemical nature of the monomeric units, the geometrical structure depends on the spatial arrangement of the monomeric units with respect to each other. Polymers exist only as solid or liquid but never as gas as they decompose before reaching their boiling point [3]. Because of their low cost, easy processibility, low weight, high corrosion resistance, high electric resistance, durability, etc., polymers are fast replacing metals and alloys in many applications and are

extensively used nowadays in the field of industries, science and technologies, particularly in space and nuclear technology.

The application of ionising radiations to polymeric materials has grown due to the fact that the physical and chemical properties of the polymers can be modified by suitable and controlled irradiation. Interest also evolved in the peculiar nature of the ion-polymer interactions. This field of polymer modification and characterisation by ion beam treatment has become a very challenging field owing to the vast technological implications.

1.3 EFFECTS OF ION IRRADIATION ON POLYMERS

The irradiation of energetic ions affects the physico-chemical properties of the polymeric materials. The primary phenomena associated with the interaction of radiation with the polymers are chain scission, chain aggregation, molecular emission and formation of double bonds [4]. Various gaseous molecular species are released during irradiation. The most prominent emission is of Hydrogen, followed by less abundant heavier molecular species which are scission products from the pendant side groups and chain-end segments.

Cross-linking occurs when two free dangling ions or radical pairs on neighbouring chains unite. Double and triple bonds are formed

when two neighbouring radicals in the same chain unite. Cross-linking enhances the modulus and hardness of the polymer. In partially crystalline polymers, it imparts a non-melting behaviour and above the crystalline melting point the cross-linked polymer exhibits rubber elasticity.

Radiation degradation is a random chain-scission process, which reduces the molecular weight of the polymer, thus, plasticising the material. All these effects depend on the composition, density, molecular weight of the polymer, temperature and time of irradiation, mass, energy, charge and fluence of the ion beam.

The energy deposition by the traversing ions triggers a wide range of complicated processes and may cause permanent changes in the spatially limited regions known as latent tracks [5]. The track of a highly ionising particle in a polymer consists of a core in which intensive destruction occurs and a halo where the cross-linking of macromolecules predominate. The process of creation of cross-linked region around the track core can be described by the following scheme [6]:

i) Generation of a number of hydrogen atoms and ions in the core.

ii) Their diffusion to the surrounding space and interaction with macromolecules initiating the formation of interior radicals.

iii) Recombination of radicals.

The ultimate changes in the polymer depend on the competition between the processes as well as the effects of delta electrons.

Chemical etching is the technique for amplification of these latent tracks. This technique is based on preferential attack of the chemical solution to the region along the particle trajectory [7]. The sensitivity of polymeric track detectors is known to be affected by various factors such as purity of the monomer, the molecular structure of the polymers, polymerisation conditions, environmental conditions during irradiations and etching.

Ion irradiation leads to modification in most of the polymeric properties like optical, thermal, mechanical and electrical properties.

- The solubility and molecular weight distribution are also affected by ion bombardment [8].
- Ion irradiation at high fluence leads to carbonisation of the polymer and the properties of the modified polymer resembles those of amorphous carbon [9,10].
- Optical properties of ion beam irradiated polymers have been characterised [11] and modification induced in the optical properties of the polymer due to energy deposition by the impinging ion beam have been reported [12,13].

- The effect of irradiation on the chemical structure of the polymer resulting in modification in the electrical properties of polystyrene, polyimide, polystersulphane have been studied [14]. Doping effects introduced by ion irradiation lead to modification in electrical conductivity of the polymers [15].
- Ion irradiation on ferroelectric polymer leads to a phase transition [16].
- The hardness, surface smoothness and wear resistance of the polymers can be improved by multiple ion beam treatment [17].
- Ion bombardment leads to a change in the refractive index of the polymer due to formation of a relatively high concentration of unsaturated bonds all along the irradiated polymer layer [18,19].
- A decrease in melting point and enthalpy of polymers has been observed by ion irradiation [20].
- Track registration properties such as the etch-rates, detection efficiency, sensitivity of the detectors, etc. can be highly influenced by ion irradiation [21-23].

1.4. IMPACT OF PROTON IRRADIATION ON POLYMERS

Three important phenomena that come into picture due to passage of a charged heavy particle through matter are:

(i) At sufficiently high velocities, the ion is stripped of all of its electrons and the energy loss is essentially through electronic excitation and ionisation of the stopping material.

(ii) At velocities comparable to the velocities of its K-shell electrons, the heavy ion starts to pick up electrons from the stopping material. The mechanism of energy loss is still essentially all electronic.

(iii) At velocities comparable to those of the valence electrons of the stopping material, the mechanism of energy loss becomes one of elastic collisions between the heavy ion and the atoms of the stopping material.

Proton is a kind of light ion and the stopping power in solids is small so that the probability of causing observable defect is small [24]. Literature survey indicates that a lot of work is going on to induce modification in polymeric materials using proton beam irradiation.

♦ Durrani et al. [25] gave massive doses (~10^{16} cm^{-2}) of 3 MeV protons to glass detectors both before and after their exposure to ^{252}Cf fission fragments and Fe ions. In both the cases, and particularly for the post-proton irradiations (Exposure to ^{252}Cf fission fragments and Fe

ions followed by proton irradiation), a significant diminution of the etched track diameters for heavily charged particles was observed. The reduction in diameters was accompanied by a fall in registration efficiency of the heavy particles.

- For proton irradiated CR-39, the sensitivity increases with increase in proton energy, reaching a maximum at about 0.5 to 0.8 MeV and then decreases with further increase in proton energy. This finding enhances the applicability of CR-39 in neutron dosimetry [26].
- The chemical registration of 1 to 2 MeV protons in CN-85 detectors were studied and it has been found that CN-85 has very high response to low energy protons. At each energy, there was a linearity between the track diameter and etching time and the slope of the line decreased with increase in particle energy. The registration efficiency for proton decreased with increase in their energy [27].
- For Polyallyldiglycol carbonate irradiated to 200 keV proton beam the refractive index was found to be an increasing function of the dose [19].
- A number of attempts have been made to improve the detection efficiency of CR-39 for protons. A co-polymer labeled USF-3 was developed by adding a small amount of anti-oxidant to CR-39, which

could record tracks of protons up to the energy of 16 MeV [28]. Another co-polymer of CR-39 with 3wt% of NIPAAM (N-isopropylacrylamide) showed a still higher sensitivity by recording normally incident protons up to 20 MeV energy [29]. Again another co-polymer CR-39/NIPAAM/Naugard445, composed in weight ratio of 99/1/0.01 is found to be highly sensitive to low LET (linear energy transfer) particles in the region below 10keV/μm of LET_{200eV} and able to record normally incident particles of LET_{200eV} down to ~1.5 keV/μm, recording protons up to energy 27 MeV [30].

- The thermal annealing of proton tracks of 4 to 6 MeV at temperatures ranging from 150 to 240°C in CR-39 polymeric detectors have been studied and the activation energy for the annealing process was found to be 0.2 ± 0.02 eV. This work is of considerable importance in neutron dosimetry [31].

1.5. THE PRESENT WORK

In this work, an attempt to characterise the effects of proton irradiation on the physico-chemical properties of some polymeric materials using various experimental techniques has been made. It is hoped that the findings in this work would be of important relevance to material science and applications of polymers.

Dose dependent modifications in optical, structural, topographical and thermal properties of eight different polymers by four different doses of 62 MeV proton irradiation has been quantified by various characterisation techniques. The work is further extended to the study of extra surface damage due to the deposition of additional amounts of energy by fullerene destruction in one of these polymers. Also, the effect of proton irradiation through thin metal foils has been studied in one of the polymers. In this dissertation an account of the work has been presented in the subsequent chapters as follows:

CHAPTER 2 gives a detailed account of structures, properties and utilities of all the eight polymers used (Makrofol-N, Triafol-TN, Polyethylene terephthalate, Triafol-BN, Polypropylene, Polyimide, Polytetrafluoro ethylene and Polyallyldiglycol carbonate). A brief description of the work already done on these polymers has also been reported. A detailed description of the different characterisation techniques, the principles and conditions of operations and the various parameters that can be studied through these techniques are also given.

CHAPTER 3 describes the irradiation parameters and conditions for ion (proton and ^{28}Si) irradiation. A detail information

about the doses used is also given. The experimental set up and conditions of the different characterisation techniques used in the present work to analyse the irradiated polymers are also discussed.

In **CHAPTER 4**, the results obtained from different technical studies showing the dose dependent modifications induced in the polymers by proton irradiation has been discussed in terms of **track registration property, activation energy for etching, optical band-gap, infra-red absorbance, surface roughness, thermal decomposition behaviour, melting, crystallisation** and **free radical formation.**

The effect of proton irradiation on fullerene, its destruction and the effect of the huge amount of energy released during the destruction process on the track registration property of the polymer Polyallyldiglycol carbonate (PADC) has been described. The effect of proton irradiation through some metal targets on the modification of track registration property has also been discussed.

CHAPTER 5 describes the important conclusions derived from the present investigation and the future perspectives. The proton-induced modifications as well as the utility of the modified polymers have been discussed in detail. A brief account is also given on the further investigations in this field and extension of the present work.

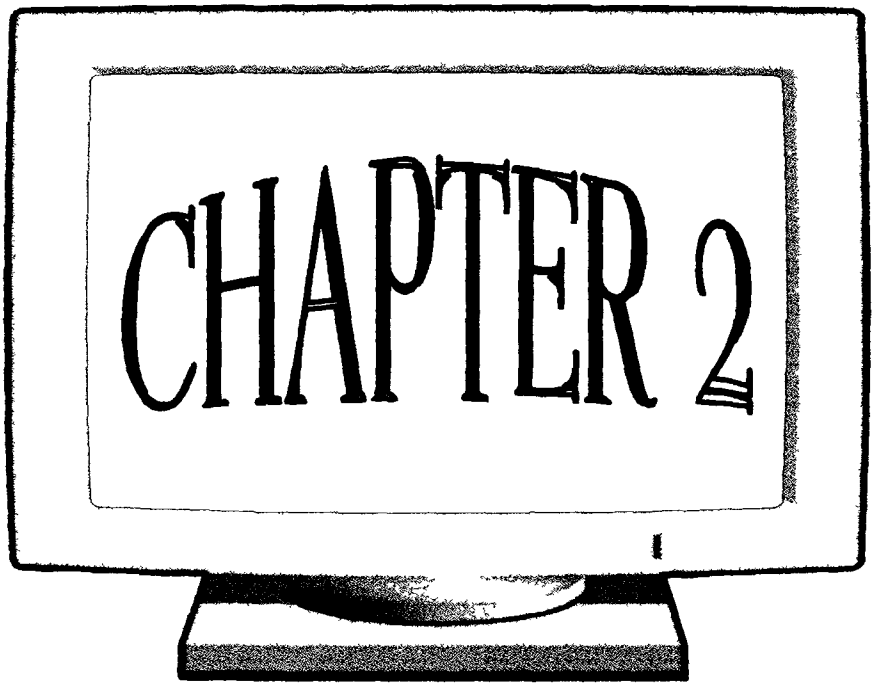
CHAPTER 2

CHAPTER 2

POLYMER SPECIFICATIONS & THEIR CHARACTERISATION TECHNIQUES

This chapter comprises of two sections. In the first section, the structures and utilities of the polymers used in the present work have been described briefly. In the second section, the theoretical concepts of the experimental techniques used to characterise the irradiated polymers are described.

2.1. POLYMER SPECIFICATIONS

In the present investigation eight different polymeric materials were used viz. **Makrofol-N, PADC (Homalite), Triafol-TN, Triafol-BN, Polypropylene, Polytetrafluoro ethylene, Polyethylene terephthalate and Polyimide**. Table 2.1 gives a brief description about the properties of the polymers used. The structure and utilities of the polymers are given below.

2.1.1. MAKROFOL-N (MFN)

The structure of Makrofol-N is given below.

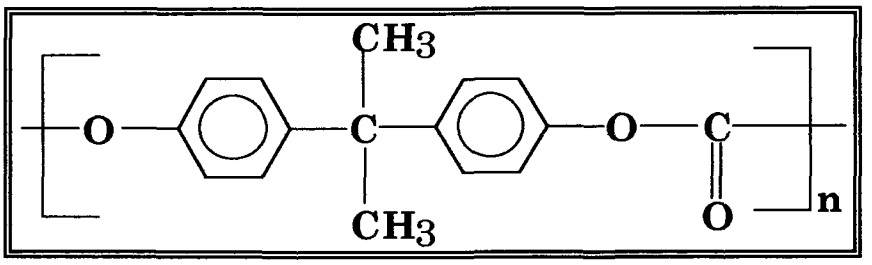

These are the polyesters of phenols and carbonic acid, produced by Bayer AG, FRG. Its chemical name is Bis-phenol-A-polycarbonate, commonly known as Lexan. The polymer is transparent and has high compact strength. It is resistant to water and many organic compounds. Thermal stability of Makrofol-N is more due to the presence of aromatic groups in the backbone and melts at around 265°C. It is used in manufacturing micro-filters, safety goggles, safety shields, telephone parts, machinery housings, bullet proof materials, etc. In polycarbonates (Makrofol-KG) irradiated by 125 MeV xenon ions, the etching rate of the ion tracks was found to decrease in the presence of atomic hydrogen [32]. Edmonds and Durrani [33] noticed the disappearance of ESR signals above 200-250°C in gamma irradiated polycarbonate (Lexan). The structural changes produced in polycarbonate (Lexan) track detectors were found to be a function of irradiated gamma dose [34].

2.1.2. TRIAFOL-TN (TTN)

Triafol-TN is a cellulose ester known as cellulose triacetate. First, Cellulose acetate of varying degree of substitution is prepared by treating it with acetic acid, acetic anhydride and a mineral acid catalyst. Mild hydrolysis of the product gives completely acetylated cellulose i.e. cellulose triacetate. Its structure is given below.

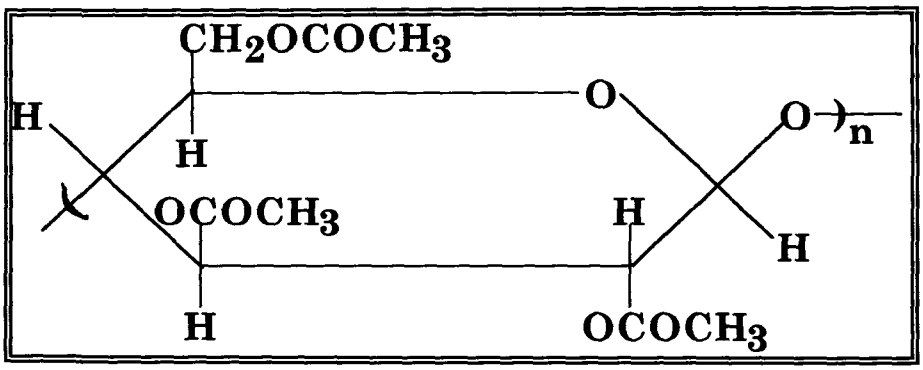

It is a transparent and soft thermoplastic polymer. It is used in manufacturing fibres, non-flammable safety cinematographic films, moulded articles, etc. Sinha et al. have found that gamma irradiation up to 10^5Gy on TTN produces no change in the properties of TTN, but at 10^6Gy the thermal stability decreased, the etch rate increased and TTN became brittle and turned to powder form [35]. UV radiation on TTN leads to formation of conjugated double bonds which in turn gives rise to electron excitation levels in the visible spectral range and produce discolouration and reduction in light transmission [36].

2.1.3. POLYETHYLENE TEREPHTHALATE (PET)

PET is one of the most popular and commercially available polymers marketed under the trade name of Terylene or Terene. The structure of PET is given below.

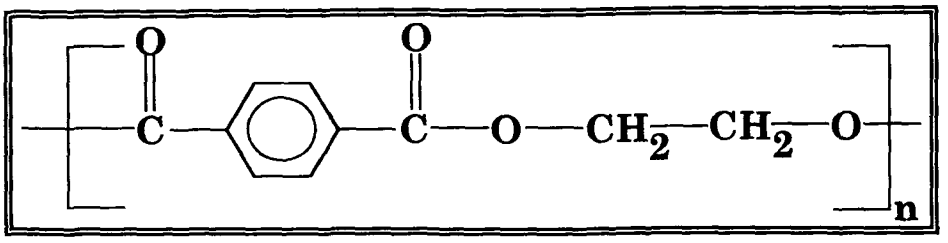

This polyester has a high melting point (≈265°C) due to presence of the aromatic ring in the polymeric structure. It is resistant to heat and moisture. It is virtually unattacked by many chemicals. It has a very good mechanical strength up to 175°C. It is soft, transparent and a thermoplastic polymer. It is used in garment manufacture, magnetic recording tapes, aluminised sheets, etc. In addition to chain scissioning, cross-linking, molecular emission and formation of double bonds which occurs by low LET radiations in PET, formation of an alkyne group is an additional effect in PET by swift heavy ions [37]. Heavy ion irradiation in keV - MeV range on PET results in hydrogen loss and decrease of optical band-gap. Heavy ion irradiation on PET leads to the production of hydroxyterephthalates and dihydroxyterephthalates in the polymer backbone as radiolysis

products and molecular orientation in the ion tracks [38]. Heavy ion irradiation leads to main chain scission in the aliphatic part of the main chain rather than destruction of benzene ring and thus leading to amorphisation of the polymer [39].

2.1.4. TRIAFOL-BN (TBN)

The structure is the same as Triafol-TN with 26%-29% acetyl and 17%-48% butyl groups. It is an important cellulose plastic known as cellulose acetate-butyrate. It is prepared by the esterification of cellulose with the mixture of acetic anhydride and butyric anhydride. It is a hard thermoplastic polymer having high impact strength, good dimensional stability and excellent compatibility with plasticisers. It has a much lower moisture absorption capacity as compared to Triafol-TN. It finds its applications in automobile components, safety goggles, etc. Sinha et al. have found that gamma irradiation up to a dose of 10^5 Gy on TBN produces no change in the polymer properties, but at 10^6 Gy TBN becomes brittle, the colour of the polymer fades due to destruction of purple dye, the thermal stability decreases and the etch-rate increases [35].

2.1.5. POLYPROPYLENE (PP)

PP is the lightest known industrial polymer. It exists in three forms: isotactic, syndiotactic or atactic. The isotactic polymer is highly crystalline and melts at 208°C. The polymer molecules are essentially linear and have configurations of 3_1 helical structure. Its structure is given below.

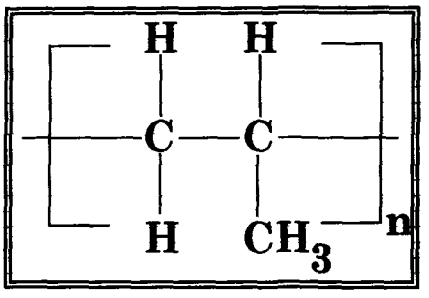

It is a transparent, soft and thermoplastic polymer. Being highly crystalline, it exhibits high stiffness, hardness and tensile strength. It has a very high strength-to-weight ratio. It is insoluble at room temperature in many of the known solvents, but can be dissolved in aromatic and chlorinated hydrocarbons above its melting temperature. It is resistant to many chemicals such as acids, alkalis and oils. It has excellent mechanical and dielectric properties. It is used in refrigerators, radios, televisions, package films, pipes, storage tanks, seat covers, monofilaments, ropes, sterilised moulded articles, etc. In PP irradiated by ^{235}U, a weaker influence is observed of the irradiation temperature on the track etch-rate of PP with high content of

antioxidant in the polymer [40]. In PP irradiated by 125 MeV xenon ions, a fading of ion tracks in the presence of atomic hydrogen was observed [41].

2.1.6. POLYIMIDE (PI)

Polyimide is yellow in colour, transparent, soft, thermoplastic polymer. It has a high tensile strength, excellent thermal stability, good dielectric properties and excellent mechanical strength. The presence of imide groups and aromatic rings in the backbone results in heat resistance and stability of PI to ionising radiations. The structure of the polymer is given below.

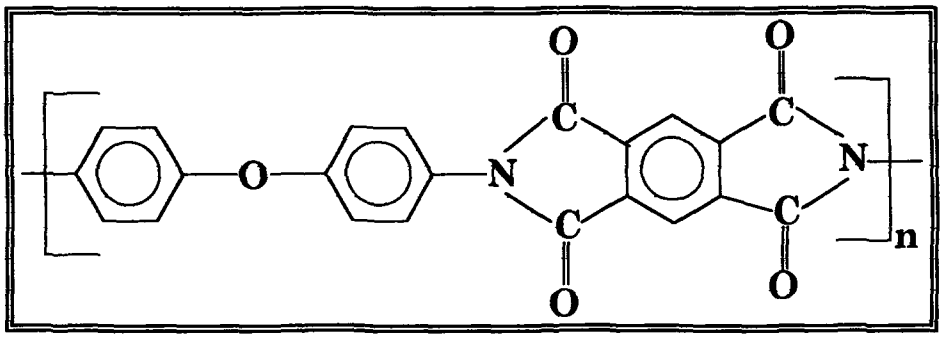

It can withstand a temperature of 425°C without undergoing any degradation. Ion beam irradiation on Polyimides leads to modifications in their electronic properties by production of graphitic nanoparticles, thus, converting it to a conducting polymer. Creation of free static volume by ion irradiation in PI leads to modification in diffusion property [42]. It is used in the insulation coating of

electromagnetic wirings, surface coatings in supersonic aircraft, backings and windows in many nuclear physics experiments, microfilters, IC fabrication, passivations and multilayer interconnections in microelectronics, etc. [43]. Loss of imide structures by pyrolysis with depletion of oxygen and nitrogen containing groups, leads to a modification in the electrical properties of Polyimide from initial insulating ($\rho = 10^{16}$ Ωcm), to semiconducting ($\rho < 10^{2}$ Ωcm) at 700 °C, to metallic ($\rho = 10^{-2}$ Ωcm) at 900 °C. When Polyimide is heated between 800°C to 850°C, the increase in conductivity has been reported, due to formation of dense heterocyclic carbon ring networks in the polymer [44]. Electrical conductivity in PI has also been reported on increasing the dose of Argon ion [45]. Ion beam irradiation in PI leads to the formation of alkynes and cyanates [39]. Increase in hardness and wear resistance has been found in ion irradiated PI [17].

2.1.7. POLYTETRAFLUORO ETHYLENE (PTFE)

PTFE also known as Teflon is one of the most stable polymers. It may be visualised as polyethylene with all its hydrogen atoms substituted by Fluorine.

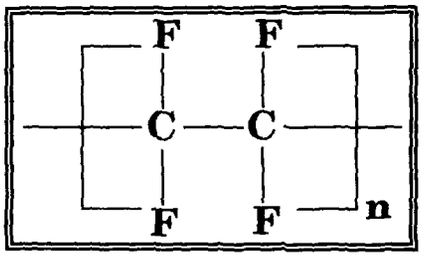

The monomer is a gas at room temperature with boiling point of -76°C. PTFE molecule has a highly regular structure with a configuration leading to a $1\ 3_6$ helix. It is also a linear polymer with practically no branching. This is because branching requires the breakage of the strong C-C bond, which is quite unlikely under the polymerisation conditions. It is smooth, transparent and a thermoplastic polymer. It can withstand temperatures up to 400°C, without undergoing degradation. Its high thermal stability can be attributed to the very high dissociation energy (452 $kJ.mol^{-1}$) of the C-F bonds. Besides, the highly electronegative nature of Fluorine protects the C-C bond in Teflon from an external attack. PTFE is highly crystalline and has a very low dielectric constant. It has a very high mechanical strength (from -100°C to +350°C). It does not dissolve in any of the strong acids and is resistant to corrosive alkalis and known organic solvents. It finds extensive applications in domestic and industrial appliances, pump valves, pipes, homogeneous and

chemically resistance articles, non-lubricated bearings, belts, filter cloth, etc.

Ion irradiation in PTFE leads to scission of bonds, formation of stable radicals and cross-linking [46]. Irradiation in presence of oxygen leads to rapid deterioration of PTFE. Electron irradiation leads to dissociation of C-C and C-F bonds, formation of oligomers and a decrease in thermal resistance [47].

2.1.8. POLYALLYLDIGLYCOL CARBONATE (PADC)

PADC is a highly cross-linked polymer produced by polymerisation of a liquid monomer diethyleneglycol bis(allyl carbonate). PADC is manufactured by Homalite Corporation and is popularly known as Columbia Resin-39 (CR-39). The structure of PADC is given below.

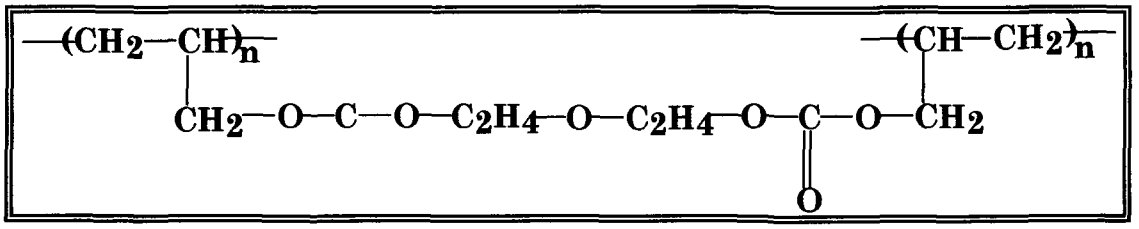

It is a transparent and thermosetting polymer having good uniformity. It is hard, amorphous, homogeneous and isotropic in nature. Its light weight, flexibility and excellent radiation sensitivity makes it a useful Solid State Nuclear Track Detector. It is used for observation of heavy nuclei in cosmic radiation, neutron dosimetry,

measurement of Uranium content, aeroplane and marine windows, opthalmic lens, industrial gas mask lens, biological test chambers, X-ray equipment and accessories, computer tape reels, watch crystals, etc. Ion irradiation of PADC leads to modification in the refractive index. Refractive index was found to be an increasing function of dose in case of gamma rays and 200 keV proton beams [19]. A modification in track registration properties of PADC on gamma irradiation has been observed [48-55].

Table 2.1. Some of the physical and chemical properties of the Polymers used.

Properties	POLYMERS							
	PET	PTFE	PP	MFN	PI	TTN	TBN	PADC
Composition	$C_{10}H_8O_4$	C_2F_4	C_3H_6	$C_{16}H_{14}O_3$	$C_{22}H_{10}N_2O_5$	$C_{12}H_{16}O_8$	$C_{20}H_{32}O_5$	$C_{12}H_{18}O_7$
Chemical Name	Polyethylene terphthalate	Polytetrafluoro ethylene	Polypropylene	Polycarbonate	Polyimide	Cellulose triacetate	Cellulose acetate butyrate	Polyallyl diglycol carbonate
Density (g/ml)	1.41	2.20	0.90	1.23	1.40	1.15	1.20	1.32
Thickness (μm)	13	100	8	100	50	100	200	1500
Uniformity	Good	Fair	Good	Fair	Good	Fair	Fair	Good
Clarity	Good	Good	Good	Good	Good	Good	Good	Good
Colour	Colourless	Milky white	Colourless	Yellow	Yellow	Blue	Violet	Colourless
Mol. wt.	192	100	42	254	382	288	385	274

2.2. CHARACTERISATION TECHNIQUES OF IRRADIATED POLYMERS

In this section, the different techniques used in the present investigation to characterise the irradiated polymers are described briefly.

2.2.1. TRACK STUDY

The track technique is based on the principle that the passage of a positively charged particle through an electrical insulator knocks out the orbital electrons of the atoms lying in and around its trajectory. This results in the formation of positive ions, which repel one another thereby creating a narrow cylindrical zone (3-10 nm in diameter) under high strain. The charged particles penetrating the organic polymer break the long molecular chains by ionisation and excitation. Latent tracks or narrow paths of intense damage on an atomic scale are created, which can be developed and fixed into optically observable permanent tracks by chemical etching. The parameters determined in this study are described as follows.

(a) Bulk etch-rate (V_G)

The V_G is defined as the rate at which the undamaged portion of the detector is dissolved by the etchant under a given etching

condition. There are three different methods to determine the bulk etch-rate.

- *Track diameter method:* The etch-rate along the track is faster than that along the surface making the shape of the tracks conical. The bulk etch-rate can be given as the rate of increase of track diameter with the etching time. Thus the bulk etch-rate in μm/h is given by

  $V_G = (D / 2t) (\tan\theta + \sec\theta)$ (2.1)

  where, d is the diameter of the track in μm, t is the etching time in hours and θ is the cone angle.

  For cone angle less than 5°, the term (tanθ + secθ) may be approximated to unity and $V_G = (D / 2t)$ (2.2)

- *Thickness method:* The bulk etch-rate is calculated from the rate of decrease of thickness of the detector with etching time. It is given by: $V_G = (X_i - X_f) / 2t$ (2.3)

  where, X_i is the initial thickness of the detector and X_f is the final thickness after etching time t.

- *Gravimetric method:* This method is based on the measurement of the weight lost by a sample foil of known area after etching for a given time period at a particular etching temperature. If m grams

is the weight lost by the detector of density 'ρ' (g/cm^3) and surface area 's' (cm^2) after etching time 't' then

$$V_G = \Delta m / 2s\rho t \times 10^4 \quad (2.4)$$

(b) True track-length

The true track length includes the observed track length (under microscope) and some correction factors. It is given by Dwivedi and Mukherji [56],

$$L = (l / \cos\varphi) + (V_G t / \sin\varphi) - V_G (t - t_C) \quad (2.5)$$

where, l is the projected track length on the surface plane,

φ is the angle of irradiation,

$V_G t_c / \sin\varphi$ is the bulk etching correction,

t_c is the complete etching time for complete revelation of track,

V_G is the bulk etch-rate,

$V_G (t - t_C)$ is the over etching correction.

(c) Track etch-rate (V_T)

Track etch-rate is defined as the rate of increase of track length with etching time. Assuming that over a small portion of the track, V_T remains constant, the track etch-rate can be determined by measuring the small increase in track length ΔL (μm) in a short interval of etching time Δt (hours) from the equation:

$V_T \cong \Delta L / \Delta t$ (μm/h) (2.6)

(d) Activation energy for etching (E_a)

Activation energy for etching is defined as the minimum energy provided by the etchant which is required to activate the molecules of the detector. It is given by,

$E_a = (-2.303)\ kT\ (\log V_G - \log A)$ (2.7)

where, E_a is the activation energy for bulk etching ($kJ.mol^{-1}$),

k is the Boltzman's constant,

T is the etching temperature in absolute units,

V_G is the bulk etch-rate,

A is a constant.

If m is the numerical value of the slope of the plot of log V_G versus 1/T, then the above equation is reduced to [57]

$E_a = 19.165\ m$ (2.8)

2.2.2. X-RAY DIFFRACTION STUDY (XRD)

X-rays can be used for chemical analysis in three different ways:

- The first method uses the fact that the X-rays emitted by an excited element have a wavelength characteristic of that element and the intensity proportional to the number of excited atoms. The excitation can be caused by direct bombardment of the target material with electrons (*direct emission analysis* and *electron probe*

microanalysis) or by irradiation of material with X-rays of shorter wavelength (fluorescent analysis).

- The second method utilises the differing absorption of X-rays by different materials (absorption analysis).
- The third method involves the diffraction of X-rays by crystals having geometrically periodic arrangement of atoms separated by distance comparable to X-ray wavelengths (diffraction analysis). This method is widely used for qualitative identification of crystalline phases. The condition for diffraction of a beam of X-rays from a crystal is governed by the Bragg equation:

$$2d\sin\theta = n\lambda \qquad (2.9)$$

where, d is the interplanar spacing, λ is the wavelength of X-rays used and θ is the angle of incidence of the X-rays.

2.2.3. UV-VIS ABSORPTION SPECTROSCOPY

Absorption methods involve determination of the reduction in power suffered by a beam of radiation as a consequence of passing through the absorbing medium. When an electromagnetic radiation in UV-Vis region (200 - 800 nm) falls on the target material, a part of the incident radiation is absorbed by the atoms leading to the transition of the orbital shell electrons. The amount of energy absorbed at each wavelength of UV-Vis region, is measured by a spectrophotometer.

The ratio of radiant power transmitted by the sample (P) to the radiant power incident on it is the transmittance, i.e.,

$$T = P/P_0 \qquad (2.10)$$

Information about the change in the optical band-gap (E_g) is attainable from the shift of the absorption edge of the UV-Vis spectra. It can be correlated by the Tauc's expression [58]:

$$\omega^2 \varepsilon_2 (\lambda) = (\hbar\omega - E_g)^2 \qquad (2.11)$$

where, $\varepsilon_2 (\lambda)$ is the optical absorbance at wavelength λ and ω is the frequency. The values of $\sqrt{\varepsilon_2}/\lambda$ are to be plotted against $1/\lambda$ to find out the gap-wavelength (λ_g) from the intersection of the extrapolated curve with the abscissa. The band-gap is then derived by the equation,

$$E_g = hc/ \lambda_g \qquad (2.12)$$

Further, the compounds having double- or triple-bonds and phenolate or quinonic structures favour cluster formation under suitable ion irradiation.

2.2.4. FOURIER TRANSFORM INFRA-RED (FT-IR) SPECTROSCOPY

Infra red spectroscopy is one of the most powerful analytical technique which offers the possibility of chemical identification. It involves the twisting, bending, rotating and vibrational motions of

atoms in a molecule. Upon interaction with the IR radiation, some portion of the incident radiation is absorbed at particular wavelengths. The multiplicity of vibration occuring simultaneously produces a highly complex absorption spectrum, which is uniquely characteristic of the functional groups comprising the molecule and of the overall configuration of the atoms as well.

For IR absorption to occur, two major conditions must be fulfilled.

- The energy of radiation must coincide with the energy difference between the excited and the ground state of the molecule. The radiant energy will then be absorbed by the molecule, increasing its natural vibration.
- The vibration must entail a change in the electrical dipole moment.

The infra-red spectra of a compound is essentially the superposition of absorption bands of specific functional groups. No two compounds will have same infra red spectra (except optical isomers). Thus, infra-red spectra is regarded as the fingerprint of a molecule. The higher frequency portion of the infra red spectra (4000-1300 cm^{-1}) is called the functional group region which shows the absorption arising from stretching vibrations and are useful for identification of the functional groups. The absorption pattern in the region 1400-650 cm^{-1} is unique for a particular compound and hence called the

fingerprint region. Both the stretching and bending modes of vibration give rise to absorption in this region.

2.2.5. ELECTRON SPIN RESONANCE (ESR) SPECTROSCOPY

Electron spin resonance, also called Electron Para Magnetic Resonance (EPR) and electron magnetic resonance (EMR) spectroscopy is based upon the splitting of magnetic energy levels produced by the action of a static magnetic field on an unpaired electron contained in an ion, a molecule or an atom. ESR spectrum results due to transitions between these magnetic energy levels by absorbing radiations of microwave frequency. The frequency capable of causing these transitions between the magnetic energy levels is a function of magnetic field strength. The main interest of ESR spectroscopy lies in the detection of paramagnetism. This technique is useful in studying the transition metal complexes and identification of free radicals.

2.2.6. THERMOGRAVIMETRIC ANALYSIS (TGA)

Thermogravimetric analysis provides the analyst with a quantitative measurement of any weight change associated with a transition. It can directly record the loss in weight with time and temperature. These weight changes are due to rupture and/or formation of various physical and chemical bonds at elevated

temperatures that lead to the evolution of volatile products or formation of heavier reaction products. Thermograms are characteristic for a given compound or a system because of the unique sequence of physico-chemical reactions which occur over definite temperature ranges and at rates that are a function of the molecular structure.

2.2.7. DIFFERENTIAL SCANNING CALORIMETRY (DSC)

In differential scanning calorimetry, the sample and the reference material are both subjected to a closely controlled program temperature. In case of a transition in the sample, thermal energy is added to or subtracted from the sample or reference containers in order to maintain a constant temperature. Since this energy input is precisely equivalent in magnitude to the energy absorbed or evolved in the particular transition, a recording of this balancing energy yields a direct calorimetric measurement of the transition energy. The parameters derived from DSC studies are:

- The melting point (denoted by endotherm in DSC tehrmograms) of a polymer is more properly termed as the melting range, since single specimen consists of more than one molecular weight and more than one crystal size. It is characterised by abrupt change in specific

volume (first order transition), disappearance of opacity and polymer orientation.

2.2.8. SCANNING ELECTRON MICROSCOPY (SEM)

Scanning electron microscopy opens up a world of 3-dimensional structures. Samples to be scanned are given a conductive coating, which provides a low resistance path to the electrons and conducts beam-induced heat away from the specimen. Samples are bombarded by a well-collimated and highly focused electron beam produced by thermionic emission from a tungsten filament. The emitted electrons from the target are collected by a detector, which converts them into an electrical signal. This signal contains a variety of informations about a single point on the sample surface. The beam is systematically moved point-by-point and the collection of whole data forms an image, which can then be magnified as desired.

2.2.9. ATOMIC FORCE MICROSCOPY (AFM)

AFM is used to investigate the topographical properties of the samples. The cantilever of AFM, made of Silicon nitride, is used to sense the force between the tip and the surface. It is capable of measuring or imaging the electromagnetic forces between the surfaces on a length scale of 10^{-11} to 10^{-7} m. The most commonly measured forces include van der Wall's forces, electrostatic and magnetic forces,

friction and adhesion. The probe is brought into continuous or intermittent contact with the sample and raster scanned with the help of piezoelectric scanners to obtain topographic images. 3-dimensional images are formed by plotting the local height versus horizontal probe tip position.

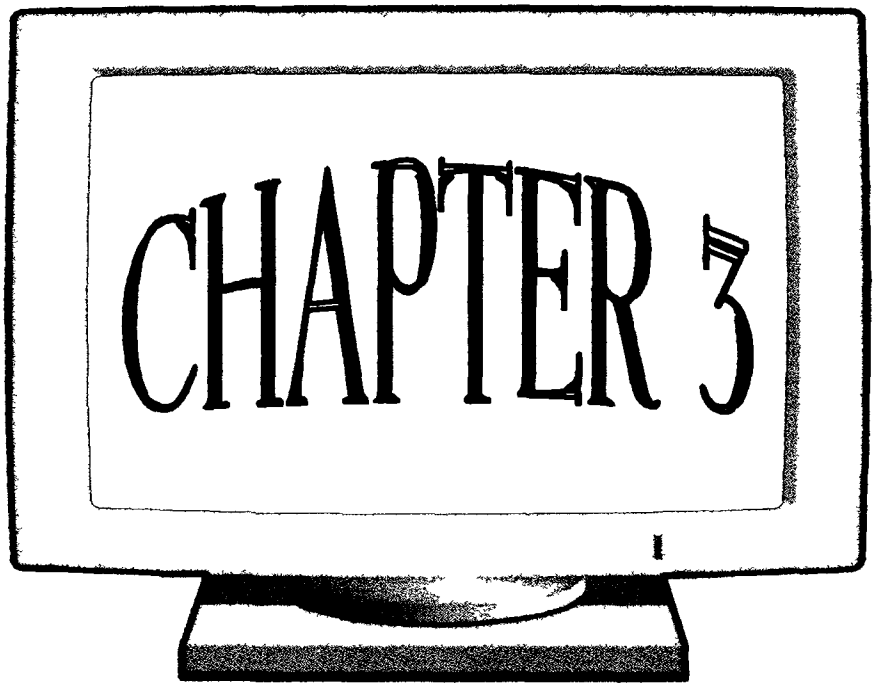
CHAPTER 3

CHAPTER 3

EXPERIMENTAL TECHNIQUES

In the present investigation eight different polymers viz. PADC, PP, PET, PTFE, PI, MFN, TTN and TBN have been used. A detailed description of these polymers including their structure, composition, density and utilities is given in Chapter 2.

3.1. THICKNESS MEASUREMENT

The thickness of these polymers were measured by a sensitive Heidenhain device. The gauze (CT-60) measuring length of the device had a glass scale with DIADUR line grating (grating with pitch 1.0 μm). The glass scale had a rigid connection to the plunger. The scale grating was photo-electrically scanned. The measuring gauze was connected to a digital VRZ-210 display unit. The thickness of the samples was measured at 10-15 different places chosen at random. These were found to be 200 μm, 8 μm, 50 μm, 13 μm, 100 μm, 200 μm, 100 μm and 1500 μm for PTFE, PP, PI, PET, MFN, TBN, TTN and PADC respectively as shown in Table 2.1. The accuracy in thickness measurement by this device was ± 0.1 μm.

3.2. TARGET PREPARATION

Four pieces of PADC and fourty pieces of each of PTFE, PI, PP, PET, MFN, TTN and TBN of size (1x1) cm^2 were cut from commercially available sheets. These were washed thoroughly by soap solution and deionised water. The cleaned samples were then dried inside a vacuum desiccator.

Four polymer stacks were prepared each having one piece of PADC and 10 foils each of PTFE, PI, PP, PET, MFN, TTN and TBN, covered at both ends by radiation sensitive Polyvinylacetate (PVA). PVA was used to check the uniformity of the impinging beam by its colour change. All the four target stacks were prepared in the same sequence (Fig. 3.2.1). The four target stacks were marked as S1, S2, S3 and S4 for proton irradiation.

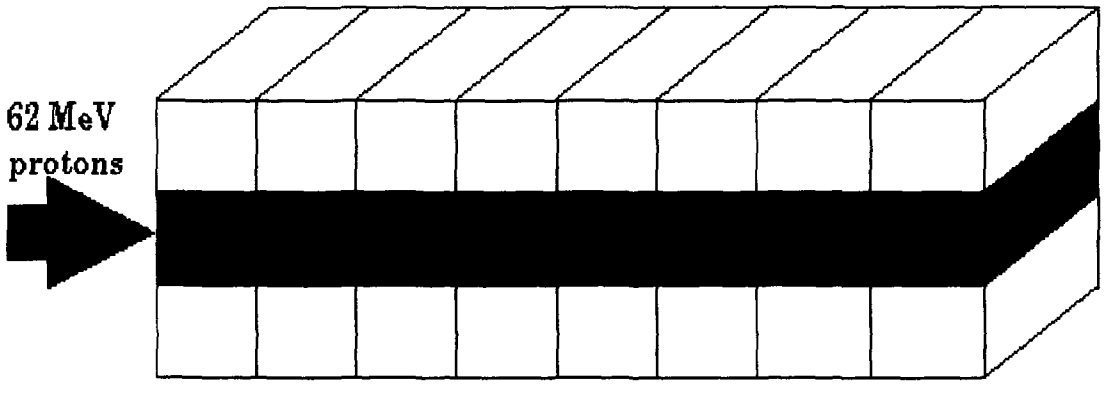

Fig.3.2.1. Arrangement of polymers in Stacks S1, S2, S3, S4.

Another stack of 4 PADC foils sandwiching 1mm thickness of Fullerene layer between 2nd and 3rd foils as shown in Fig. 3.2.2. {PADC / PADC / C_{60} / PADC / PADC} with Polyvinylacetate at both ends was prepared and referred to as S5.

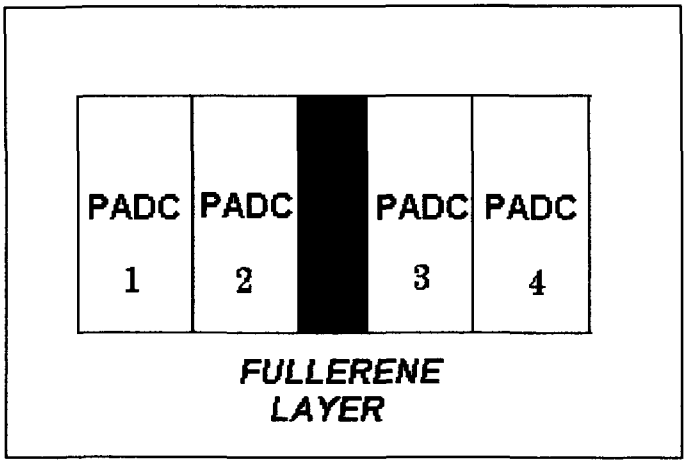

Fig.3.2.2. Arrangement of Fullerene layer in Stack S5.

Again two other stacks of PADC samples, one sandwiching aluminium foils (15μm) and the other sandwiching gold foils (3μm) were prepared (in the sequence shown in Fig. 3.2.3) and were referred to as S6 and S7 respectively. The details of the irradiation of different stacks are given in Table 3.2.1.

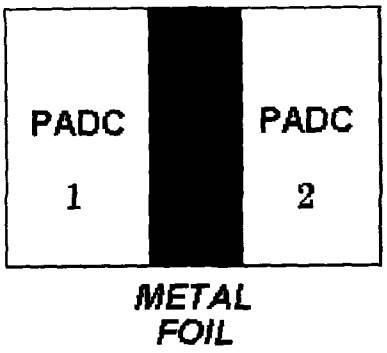

Fig.3.2.3. Partial arrangement of Stack S6 and S7.

Table 3.2.1. Irradiation doses and details of additional irradiation of different target stacks.

TARGET STACKS	PROTON DOSE (kGy)	FLUENCE (cm^{-2})	ADDITIONAL IRRADIATION
S1	10	4.3×10^{12}	^{252}Cf
S2	30	1.3×10^{13}	^{252}Cf
S3	60	2.6×10^{13}	^{252}Cf
S4	80	3.4×10^{13}	^{252}Cf
S5	10	4.3×10^{12}	^{252}Cf
S6	10	4.3×10^{12}	^{28}Si
S7	10	4.3×10^{12}	^{28}Si

3.3. PROTON IRRADIATION

The target stacks were irradiated by different doses of 62 MeV protons from the heavy ion accelerator of the Ion Beam Laboratory

"ISL" at the Hahn Meitner Institute (HMI), Berlin. Irradiations were done in the presence of air. The collimated proton beam was allowed to fall perpendicularly onto each target stack. As the beam size was 3mm x 1cm, the target stack was adjusted in such a way that the proton beam passed through the centre of the stack, which was indicated by decolourisation of the methylene blue dopant of the PVA foils at that particular area. The irradiated target stacks were allowed to cool for about 24 hours to allow the induced radioactivity to fall below the safe limits of handling. The samples were then separated, marked and preserved in plastic boxes.

3.4. CHARACTERISATION OF POLYMER STACKS (S1, S2, S3 AND S4)

The characterisation of the pristine and the irradiated samples of the stacks S1, S2, S3 and S4 were done by different spectroscopic techniques (UV-Vis spectroscopy, Fourier Transform IR spectroscopy, Electron spin resonance spectroscopy), thermal techniques (Thermogravimetric Analysis, Differential Scanning Calorimetry), Structural analysis technique (X-ray diffraction), Chemical analysis (Track technique) and Topographical analysis (Scanning Electron

Microscopy and Atomic Force Microscopy). The instrumental set up and the experimental conditions are described below.

i) UV-Vis Spectroscopy

UV-Vis spectroscopy for the pristine and the first foil of each polymer from each stack were done by Beckman DU-650 spectrophotometer. All the spectra were taken with the pristine as reference. The scanning speed of the apparatus was 1200 nm/min in the wavelength range of 200 nm to 800 nm. The wave-length range of absorption edges were found to be within 200-345 nm for PTFE, 400-550 nm for PI, 300-325 nm for PET, 200-255 nm for PP, 275-310 nm for MFN, 280-320 nm for TTN, 290-400 nm for TBN and 325-375 nm for PADC. The optical band-gap was calculated using eqn. (2.11) and (2.12) of Chapter 2. The maximum probable error in determining the energy band-gap can be attributed to $\pm$ 0.1 eV.

ii) Fourier Transform Infra-red Spectroscopy (FT-IR)

The FT-IR spectra of the pristine as well as the first foil of each polymer of each stack were recorded in transmission mode using Fourier transforming instrument (model NICOLET, IMPACT 410) keeping air as reference. The measurements were done in the wavenumber range of 4000 to 400 cm^{-1} and the transmittance (or absorbance) spectra of the polymers were obtained (transmittance %

or absorbance as a function of wavenumber). The variation of transmittance(%) for the pristine and irradiated polymers were compared and the peak analysis was done to study the disappearance of some existing bands, emergence of new ones and the structural changes which includes the alteration in position and intensity of the characteristic bands with an accuracy better than ± 1% to ± 3%.

The errors, while recording the spectra, might be due to stray radiation, zero setting of the instrument, noncontinuous sample, atmospheric absorption, slit width, scan speed, etc.

iii) Electron Spin Resonance Spectroscopy

A Varian (E-109, X-band) spectrometer with 100 kHz field modulation was used for the ESR spectral analysis. The samples were cut into (0.5x0.5) cm^2, placed in a quartz tube and the spectra were recorded at room temperature. The frequency used for this instrument was 9.6 GHz. The instrumental setup was:

Field set: 3382 Gauss, Scan range: 1000 Gauss, Time constant: 0.25 sec, Scan time: 4 minutes, Modulation amplitude: 0.5, Receiver gain: $6.3x10^4$, Microwave power: 2 mW.

iv) Thermogravimetric Analysis (TGA)

TGA was done for the pristine and the irradiated polymer using a simple automatic Perkin Elmer Delta series Thermal Analysis

system. The samples were cut into very small pieces, crimped in small aluminium pans and weighed in a micro balance. The micro balance operates as a high gain electromechanical system, which permits the measurement of weight changes as small as 0.1μg. The standard furnace in the instrument is a platinum wound microfurnace, which functions both as a heater and a resistance thermometer, detecting its own temperature and supplying power to heat the sample. The samples were heated up to 600°C-800°C at a pre-determined rate of 20°C/min. The 3700 data station attached to the instrument controls the scanning rate and keeps a record of the weight loss continuously and simultaneously. The thermograms, a plot of weight percent (ordinate) as a function of temperature (abscissa) were obtained indicating the decomposition manner of the samples. This weight loss in a sample due to constant supply of heat energy at a pre-determined rate can be attributed to the chemical reactions, decomposition, solvent and water evolution, oxidation etc. The error in recording the TGA thermogram was ± 2°C.

v) Differential Scanning Calorimetry (DSC)

DSC analysis of the pristine and the irradiated polymers were done using a Perkin Elmer Delta-series Thermal analysis system. The samples were cut into small pieces, hermetically sealed in aluminium

pans and weighed in thermobalance as above in TGA. Heat power was adjusted to maintain a constant temperature in the sample and the reference. Nitrogen was used as the flushing gas for the measurements. The thermograms were obtained with heat flow in the sample (ordinate) as a function of temperature (abscissa). The scan rate was maintained at 20°C/min. In the instrument, the temperature-measuring probe is connected to the sample pan, so the thermal peaks pointing upwards represent the endothermal reactions and those pointing downwards represent the exothermic reactions undergone by the sample due to application of heat. The error in recording the DSC thermogram was ± 2°C.

vi) <u>X-ray Diffraction (XRD)</u>

XRD patterns of the pristine and the irradiated polymers were recorded using the Cu - Kα (λ = 1.54 Å) radiation with 8.04 keV energy from Rigaku θ - 2θ X-ray spectrometer at Inter University Consortium, Indore, India. A rotating anode source and a Sodium Iodide scintillation detector was used in the system. The samples were fixed in the sample holder and placed in the XRD chamber, having entrance slit dimension of 0.2 mm. The value of 2θ ranged from 3° to 90° and the step size was 0.04 mm.

vii) ***Atomic Force Microscopy (AFM)***

The Atomic Force Microscopy of the pristine and the irradiated samples were done at Inter University Consortium, Indore, India using a Digital instrument, Nanoscope E, in contact mode. The pristine and irradiated samples were cleaned, glued down to the sample puck using cyanoacrylate glue (superglue). The sample puck was placed on the top of the scanner tube. The instrument consists of a microscopic force sensor (cantilever) made of silicon nitride that is used to sense the force between the sample and the tip while scanning the sample surface. The laser spot is positioned on to the cantilever. The photodiode is then positioned to maximise the signal and the spot is fine-adjusted on to the very tip of the cantilever. The deflection of the cantilever as well as the local height of the sample was recorded during the course of scanning. Three-dimensional images of the surface scanned were then obtained. Further, the surface roughness of the samples was measured at 10-15 different places on the sample surface at random and the mean was taken as the surface roughness of the sample.

viii) ***Track etch method***

The irradiated polymers PET, PI, TTN, TBN and MFN along with their pristine were further exposed to ^{252}Cf having a half-life of

2.65 years with an activity of 5.7×10^3 fission/minute, at an angle of 90° for 30 minutes. The samples were fixed in the sample holder, kept at a distance of 1cm from the source and then irradiated inside a desiccator in the presence of air. The samples were washed in soap solution to remove all greasy substances and contamination from the sample surfaces. These samples were then dried between the layers of the soft filter paper (Whatman 42) and later in a vacuum desiccator. The irradiated polymers were chemically etched to convert the latent tracks into optically visible tracks. The etchant for the polymers as well as the etching temperatures used are tabulated in Table 3.4.1.

The fission-fragment track diameters were measured by the Leitz optical microscope at 625x magnification at regular intervals of etching time till they are completely etched. The bulk etch-rate (V_G) were determined by the track diameter method as discussed in Chapter 2. The bulk etch-rate (V_G) was then derived from the slope of the plot of the etching time versus the track diameter curve as shown in equation (2.2) of Chapter 2. The activation energy for bulk etching was determined (by using equation (2.7) and (2.8) of Chapter 2) for PET, PI, TTN, TBN and MFN by plotting log V_G against the reciprocal of the etching temperature. The track diameters were measured to an

accuracy of ±1.12μm and the errors associated with etch-rate measurements lay between 0.3 to 0.6μm/h.

Table 3.4.1. Etchants and the etching temperatures of the polymers used.

POLYMERS	ETCHANT	ETCHING TEMPERATURE (°C)
Polyethylene terephthalate	6N NaOH	50, 55, 60, 65, 70
Polyimide	NaOCl	50, 55, 60, 65
Triafol-BN	6N NaOH	60, 65, 70, 75
Triafol-TN	3N NaOH	60, 65, 70, 75
Makrofol-N	6N NaOH	55, 60, 65, 70, 75
Polyallyldiglycol carbonate	6N NaOH	55

3.5. POLYMER CHARACTERISATION OF FULLERENE EMBEDDED STACK (S5)

Out of four pieces the first three pieces of PADC samples of the stack S5 (Fig.3.2.2) were analysed in different ways as described below.

- The first piece of PADC was divided into two parts. The first part was etched in 6 N NaOH at 55°C for different etching times upto

330 minutes and was observed under Scanning Electron Microscope (SEM).

Scanning Electron Microscopy: SEM of the etched samples was done at Regional Sophisticated Instrumentation Centre, N.E.H.U., Shillong, India. The etched samples were gold plated to make the polymer surface conducting and was then cooled for some time. This was done by Ion Sputter JFC-1100 for 15 minutes under vacuum at 10mA and 1kV conditions. Scanning was done by the JSM-35 CF Scanning Electron Microscope at a magnification of 3000x, under complete vacuum conditions. The surface damages were analysed from the photo-micrographs of the samples.

- The second part was exposed to ^{252}Cf for 15 minutes and was etched in similar conditions for different etching times ranging from 60 minutes to 300 minutes. The fission track diameters was measured by the Leitz optical microscope at 625x magnification.
- In the second piece of PADC, the back surface was coated with fullerene and then both the surfaces (back and front) were irradiated to proton. This sample was etched in 6N NaOH at 55°C up to 300 minutes. SEM of the two surfaces was done in the same way as mentioned above. The two surfaces were compared using

SEM micrographs to observe the surface modification caused by fullerene destruction.

- In the third piece of PADC, the front surface was coated with fullerene and the back surface was left blank. Both the surfaces were irradiated by proton. The samples were etched under similar etching conditions for 120 minutes. The samples were analysed by scanning electron microscopy following the same procedure.

The samples for the optical microscopy were first irradiated by ^{252}Cf for 15 minutes and then etched up to 300 minutes followed by the measurement of the fission track diameters using the Leitz Optical microscope at a magnification of 625x.

3.6. POLYMER CHARACTERISATION OF METAL FOIL EMBEDDED STACKS (S6 AND S7)

(i) Irradiation by 140 MeV ^{28}Si

The surfaces adjacent to the gold and the aluminium foils of the first pieces of PADC of stacks S6 and S7 and also another piece of pristine PADC were again irradiated by 140 MeV ^{28}Si ions at an angle of 45°, depositing particles of the order of 10^{12} ions/sec in the 20° port of the General Purpose Scattering Chamber (GPSC) at Nuclear

Science Centre, New Delhi, India. After irradiation, the samples were allowed to cool and then stored in plastic boxes.

(ii) Chemical Treatment

These irradiated samples were washed thoroughly in luke-warm water and etched in 6N NaOH at 55°C. Succesive etchings were done for 3 hours till the tracks were completely etched. The etched samples were washed in running water and dried in filter paper inside a vacuum dessicator.

(iii) Measurement of track parameters

The surfaces were scanned by the Leitz optical microscope at a magnification of 625x to measure the track lengths and track diameters. The bulk etch-rates were calculated from the slope of the plot between ^{28}Si track diameters versus etching time. The maximum etchable track lengths were calculated from the projected values of track lengths, which were measured after every successive etching.

(iv) Scanning Electron Microscopy (SEM)

SEM was done for the etched samples at 1000x magnifications by the JSM-35 CF Scanning Electron Microscope after gold coating the samples for 15 minutes in the Ion Sputter JFC-1100. Photomicrographs were taken to study the surface damage.

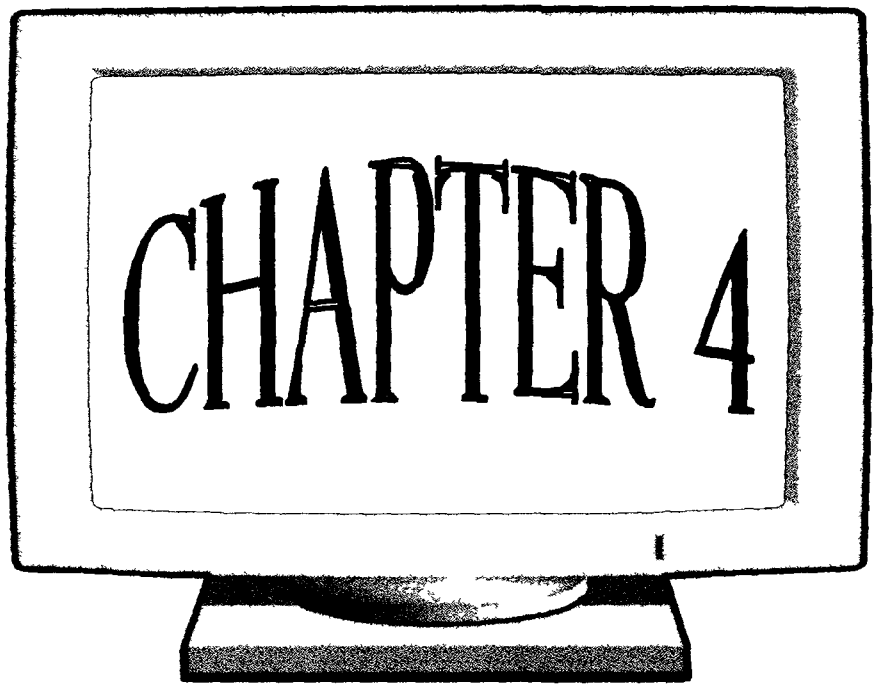
CHAPTER 4

CHAPTER 4

RESULTS AND DISCUSSION

In this chapter, the results derived from all the experiments described earlier in chapter 3 are presented. This chapter is divided into eight parts to explain the results of eight polymers separately and exclusively.

4.1. MAKROFOL-N (MFN)

The pristine and the irradiated polymers at four different doses were characterised through track studies, spectroscopic and thermal techniques.

4.1.1. Track Studies

The track study was done after proper chemical treatment of the pristine and irradiated samples. The track diameters of the fission fragments were measured and plotted against the corresponding etching times to determine the bulk etch-rate (V_G). The log of V_G was plotted against the reciprocal of different etching temperatures (Fig.4.1.1) to calculate the activation energy (E_a) of etching. The values calculated are given in Table 4.1.1. V_G was found to be the same for the lower two doses (10kGy, 30kGy) which was about 15-25%

higher than that of the pristine. The V_G increased by about 50-75% for the higher doses (60kGy and 80kGy). The activation energy (E_a) for etching was found to be decreasing with increase in dose (Fig.4.1.1), signifying the degradation of the polymer with proton irradiation.

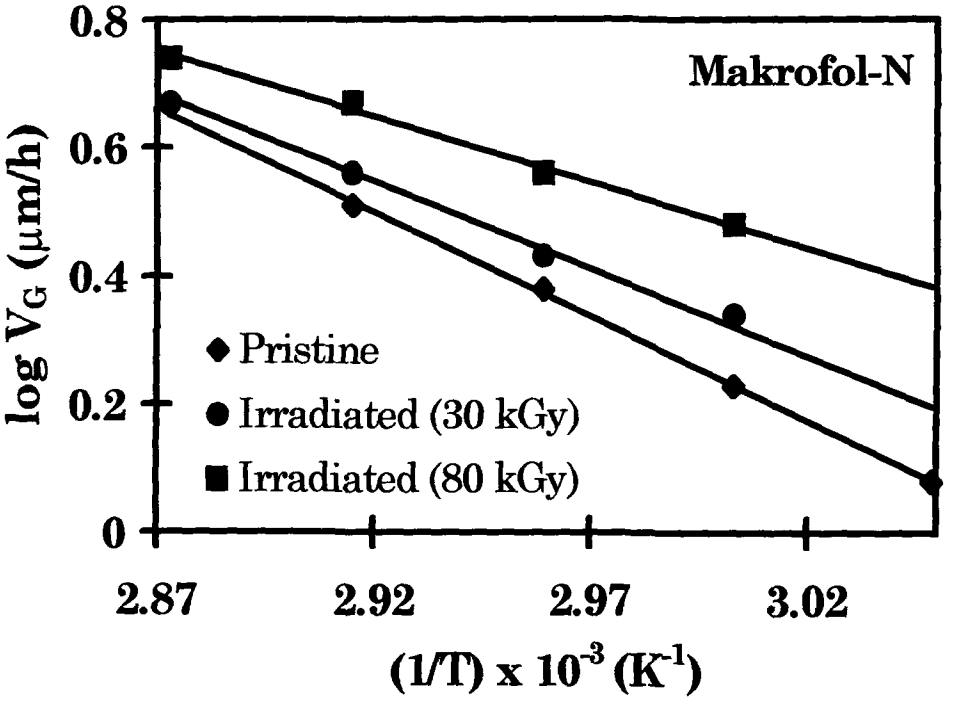

Fig.4.1.1. The plot of log V_G versus the inverse of etching temperature of pristine and proton irradiated MFN at two different doses (30 and 80 kGy).

Table 4.1.1. The bulk etch-rate (V_G) at different etching temperatures (T_{etch}) and the activation energy of etching (E_a) of the pristine and the MFN irradiated to 62 MeV protons (10, 30, 60, 80 kGy).

	T_{etch} (°C)	Dose (kGy)				
		0	10	30	60	80
V_G (μm/h)	55	1.2	-	-	-	-
	60	1.7	2.1	2.2	2.7	3.0
	65	2.4	2.7	2.7	3.3	3.6
	70	3.2	3.6	3.6	4.2	4.7
	75	-	4.7	4.7	5.2	5.5
E_a (kJ.mol^{-1})		62.0	52.1	52.1	42.8	39.3

4.1.2. Spectral Analysis

Three spectroscopic techniques (UV-Visible, Fourier Transform Infra-red and Electron spin resonance) were used to characterise the pristine as well as the irradiated MFN films.

(i) UV-Visible Spectroscopy

The spectra are obtained from UV-Vis spectroscopy to observe the shift of the absorption edges from UV to visible side and to calculate the wavelength-gaps (λ_g) and the energy band-gaps (E_g) using the equations given in chapter 2. The energy band-gap (E_g) for

the pristine MFN was found to be 4.1±0.1 eV which remained unchanged up to a dose of 30 kGy and then reduced to 4.0±0.1 eV at the higher two doses (60, 80 kGy) of proton irradiation.

(ii) Fourier Transform Infra-red Spectroscopy

The spectra of the pristine and the irradiated MFN samples are shown in Fig.4.1.2 and the wavenumbers for the characteristic peaks along with their interpretations are given in Table 4.1.2.

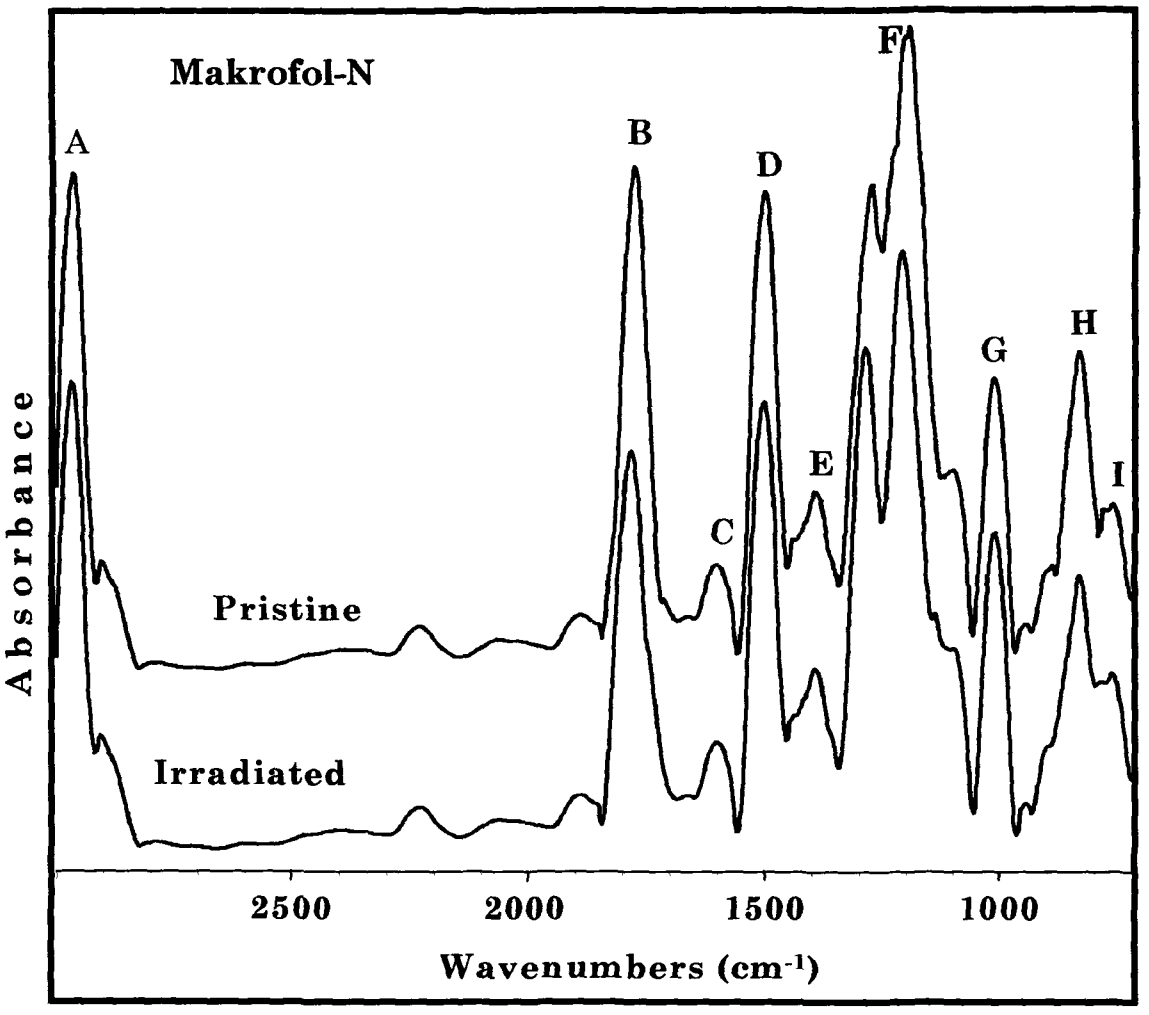

Fig.4.1.2. FT-IR spectra of pristine and proton irradiated MFN (80 kGy) in the range of 3000-750 cm^{-1}.

The IR spectra of the pristine and irradiated MFN shows that even at the highest dose of proton irradiation there was no new band formation, rather the transmittance of most of the bands decreased showing that degradation is the dominant phenomena resulting from proton irradiation. This is in accordance with the IR results obtained by 250 keV proton irradiation on MFN reported by Gagnadre et al. [59].

Table 4.1.2. Identification of absorption bands in MFN corresponding to their wavenumbers ($1/\lambda$).

Peak	$1/\lambda$ (cm^{-1})	Identification
A	2968	CH_3 stretching vibrations
B	1776	C=O vibrations
C D	1600 1500	C=C phenyl ring stretching vibration
E	1391	Symmetric in-plane bending of CH_3 group
F G	1191 1107	Anti-symmetric stretching of C-O-C links
H	831	C-H out-of-plane bending vibrations
I	760	C-H & C-C vibrations

The peak positions remained almost fixed denoting less impact of proton irradiation on corresponding groups. A little variation in peak positions might be from contribution of Fermi and Coriollis type of interactions [60].

(iii) Electron Spin Resonance Spectroscopy

Formation of free radicals, as expected from heavy ion irradiation, could not be traced from the ESR spectral analysis of the irradiated MFN. Since the irradiated samples were kept at room temperature for a few months after irradiation, any free radicals formed, if at all, would have been annihilated during that time.

4.1.3. Thermal Studies

Thermogravimetric analysis and Differential scanning calorimetry were done to characterise the pristine and the irradiated polymers.

(i) Thermogravimetric analysis

The decomposition behaviour of the polymers was examined by this technique. Fig.4.1.3 represents the thermograms of the polymers. The results obtained are shown in Table 4.1.3. The pristine MFN remained stable up to 172°C and decomposed completely at 518°C without leaving any residue. But the stability of the irradiated

polymers was reduced to a maximum of about 24% at the highest irradiation dose. The slow decomposition zone, in all the cases, was accompanied by a weight loss of about 10%. The fast decomposition zone was accompanied by a weight loss of about 90% for the pristine and 65-70% for irradiated samples. The irradiated polymers underwent a degradation leading to the formation of residue of about 15-25% of the total weight of the polymer, whose decomposition temperatures also decreased from 701°C to 634°C with the increase in dose. This indicated that more residue was formed at the lower doses of the proton irradiation. The decomposition of the polymer in other zones (i.e. stable, slow and fast decomposition zones) was also an inverse function of the dose of the proton beam.

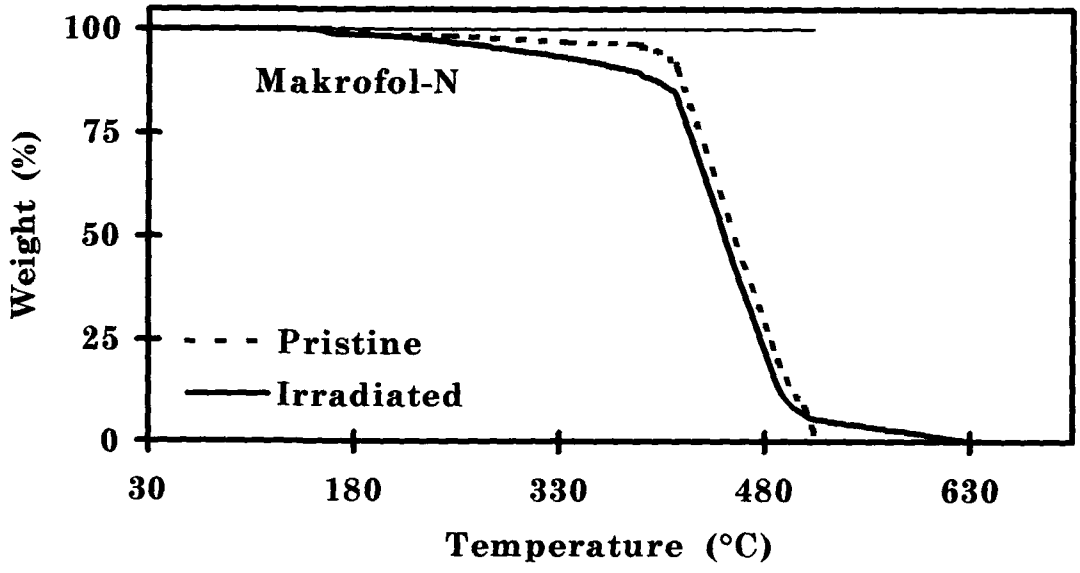

Fig.4.1.3. TGA thermograms of the pristine and the proton irradiated MFN (80 kGy).

Table 4.1.3. Thermal decomposition temperatures at different zones for the pristine and the MFN samples irradiated to different doses (10, 30, 60, 80 kGy).

Dose (kGy)	Stable zone (°C)	Slow decomposition zone (°C)	Fast decomposition zone (°C)	Residual decomposition zone (°C)
0	30-172	172-416	416-518	-
10	30-160	160-410	410-515	515-701
30	30-157	157-410	410-511	511-701
60	30-130	130-390	390-490	490-660
80	30-130	130-388	388-490	490-634

(ii) Differential scanning calorimetry

The thermograms are shown in Fig.4.1.4. The exotherms indicating the temperature of crystallisation (T_c) were not clear for the pristine and for the polymers irradiated at lower doses (up to 30 kGy). It appeared at 188°C for the MFN irradiated to 60 kGy and at 180°C for the one irradiated to 80 kGy (A). The melting temperature (denoted by endotherm) for the pristine MFN was found to be at 260°C (B_0), which remained almost constant up to the dose of 30 kGy and then reduced to 200°C (B_1) for the sample irradiated to 60 kGy and 80 kGy of 62 MeV protons. This may be attributed to the degradation caused by irradiation, which corroborates the results of track study.

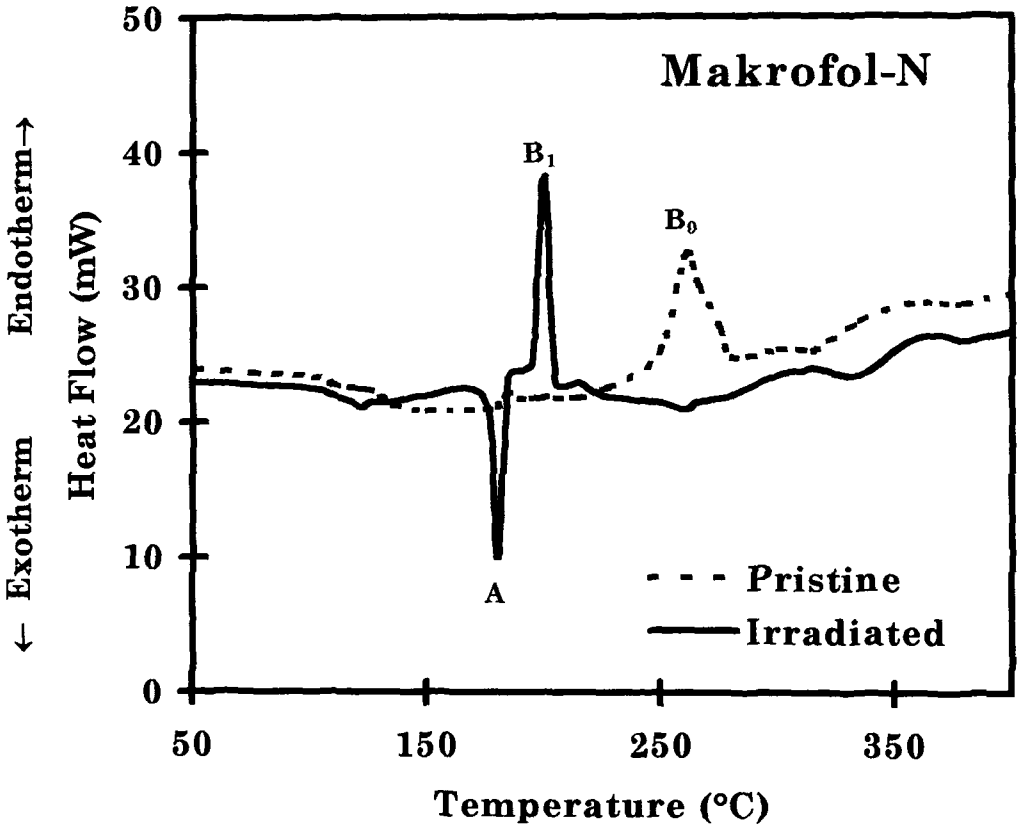

Fig.4.1.4. DSC thermograms of the pristine and the proton irradiated MFN (80 kGy).

4.2. TRIAFOL-TN (TTN)

The pristine and the irradiated polymers at four different doses were characterised through track studies, spectroscopic and thermal techniques.

4.2.1. Track Studies

The fission fragment track diameters were measured and plotted against the corresponding etching times to determine the bulk etch-rate (V_G). The log of V_G was plotted against the reciprocal of

different etching temperatures (Fig.4.2.1) to calculate the activation energy (E_a) of etching. The values calculated are given in Table 4.2.1. The bulk etch-rate (V_G) and the activation energy (E_a) remained almost the same for the pristine and the irradiated polymers. The parallel lines in Fig.4.2.1 revealed that the E_a was not modified under different doses of proton irradiation. However, the polymer irradiated to the highest dose of proton (80 kGy) was etched faster than other polymers and became brittle, rough and it crumpled after 1 hour of etching time.

Table 4.2.1. The bulk etch-rate (V_G) at different etching temperatures (T_{etch}) and the activation energy of etching (E_a) for the pristine TTN and the TTN irradiated to 62 MeV proton (10, 30, 60, 80 kGy).

	T_{etch} (°C)	Dose (kGy)				
		0	10	30	60	80
V_G (µm/h)	60	1.7	1.8	1.8	1.8	1.9
	65	2.3	2.3	2.3	2.4	2.5
	70	3.1	3.2	3.2	3.2	3.3
	75	4.0	4.2	4.2	4.2	4.3
E_a	(kJ.mol^{-1})	53.4	53.4	53.4	53.4	53.0

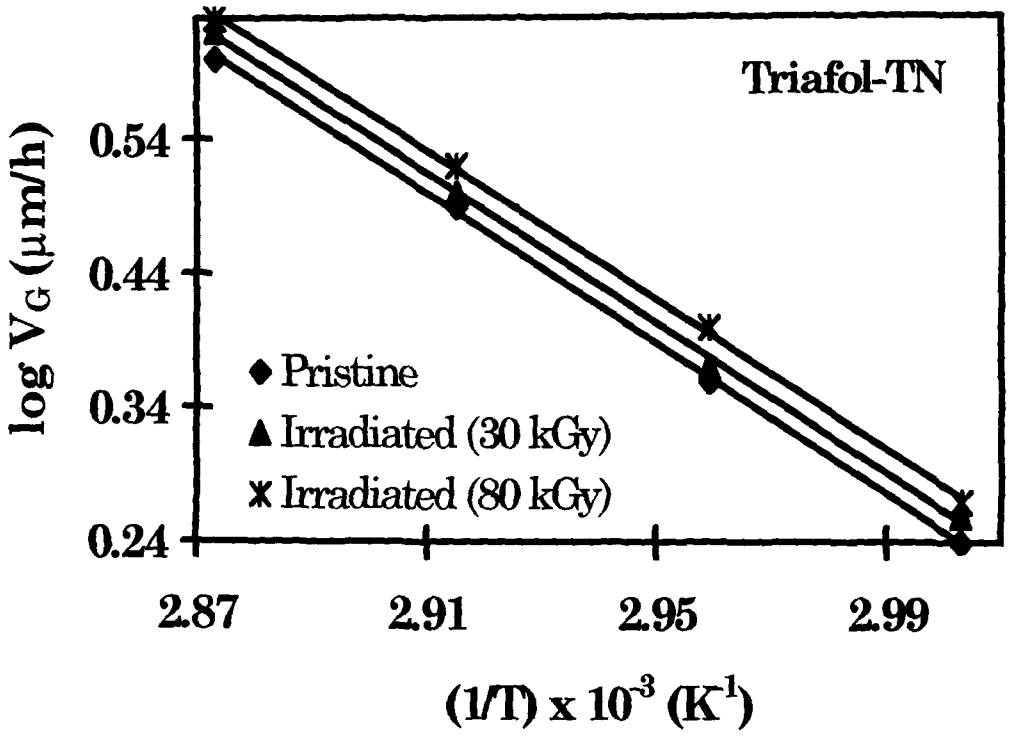

Fig.4.2.1. The plot of log V_G versus the inverse of etching temperature of pristine and proton irradiated TTN at two different doses (30 and 80 kGy).

4.2.2. Spectral Analysis

Spectral studies were done using three different techniques viz. UV-Visible, Fourier Transform Infra-red and Electron spin resonance, to identify any structural characteristic changes due to proton irradiation.

(i) UV-Visible spectroscopy

The spectra are shown in Fig.4.2.2. The absorbance values were used to obtain the tauc's plot for calculating the optical band-gap. The absorption edge of the irradiated TTN (80 kGy) shifted from UV

towards the visible side, thus, leading to a decrease in the band-gap due to proton bombardment. The energy band-gap (E_g) for the pristine was found to be 3.8 ± 0.1 eV which remained unchanged up to the dose of 60 kGy and then reduced to 3.5 ± 0.1 eV at the highest dose of irradiation (80 kGy).

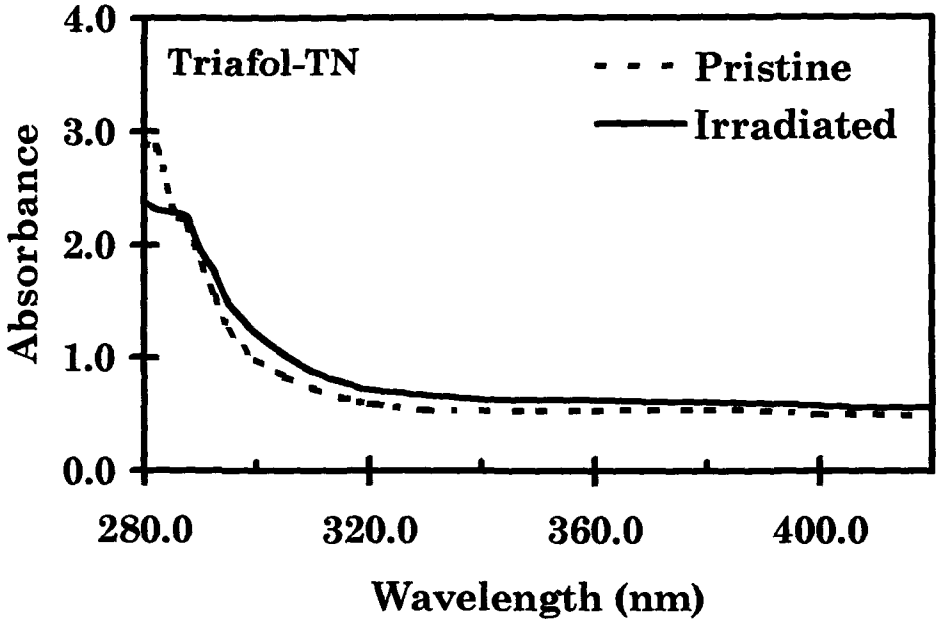

Fig.4.2.2. UV-Vis spectra of pristine and irradiated TTN (80 kGy).

(ii) Fourier Transform Infra-red spectroscopy (FT-IR)

The FT-IR spectra are shown in Fig.4.2.3. The identification of the absorbance peaks is presented in Table 4.2.2. No significant change in the vibrational frequencies was observed, which implied that inter-chain separation is not affected much by proton irradiation. Most of the peak positions were found to be unshifted. Only the

absorbance or transmittance value of particular functional groups changed. This might be due to the result of decrease in concentration of the pre-existing bonds or groups. It was observed that the peak position at around 1187 cm^{-1} (F) due to stretching vibration of the main chain became intense for the sample irradiated to 80 kGy of 62 MeV proton.

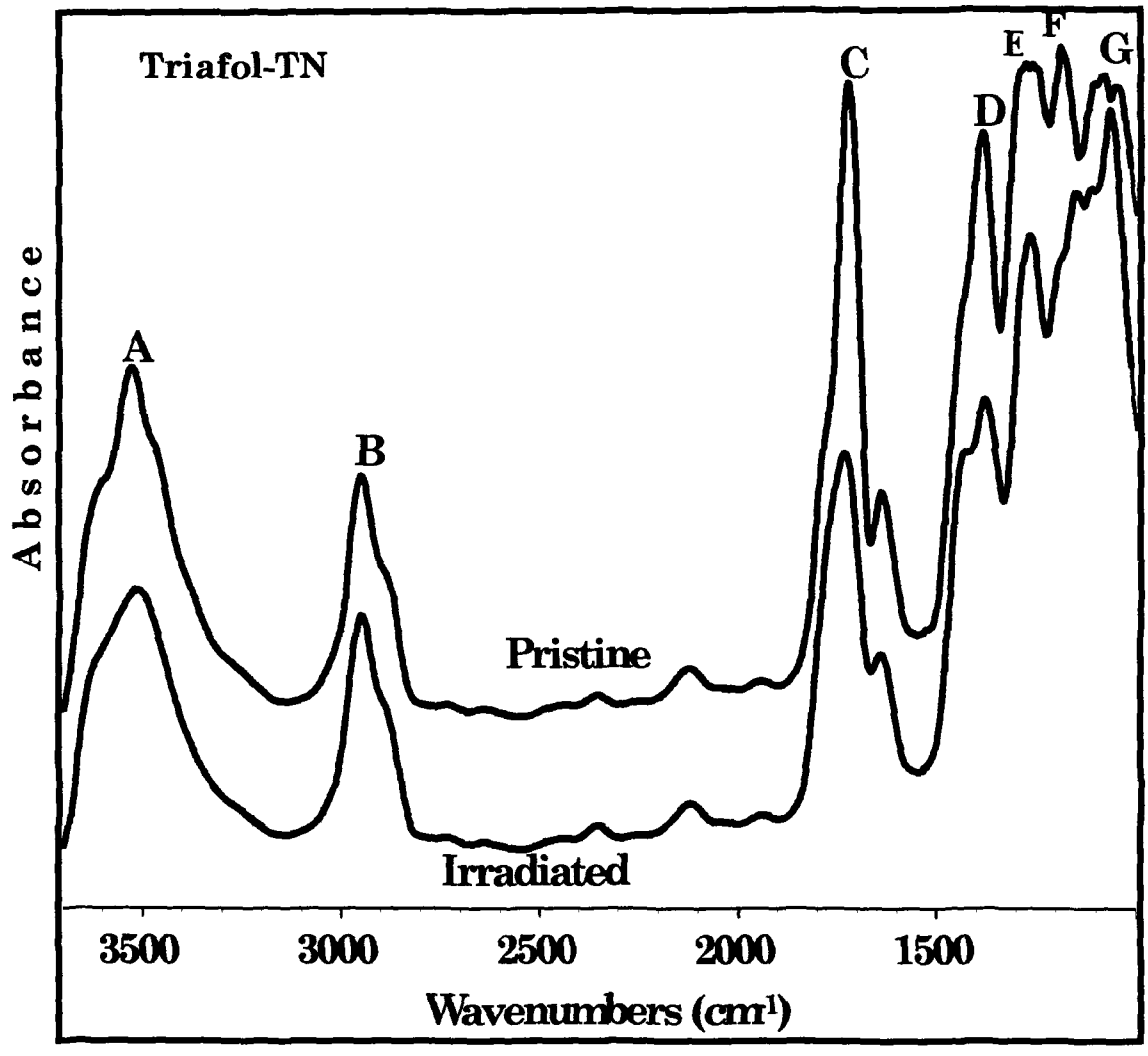

Fig.4.2.3. FT-IR spectra of the pristine TTN and the proton irradiated TTN (80 kGy) in the range of 3700-1000cm^{-1}.

Table 4.2.2. The identification of the absorption bands in TTN corresponding to their wavenumbers (1/λ).

Peak	1/λ(cm^{-1})	Identification[61]
A	3530	COOH (or OH)
B	2951	C-H stretching
C	1723	C=O stretching from ester
D	1386	CH2-O scissors
E	1276	C-O-C stretching from ester
F	1187	Stretching vibration of the main chain
G	1080	C-O-C stretching from ester

(iii) Electron Spin Resonance Spectroscopy

Formation of free radicals, as expected from heavy ion irradiation, could not be traced from the ESR spectral analysis of the irradiated TTN. Since the irradiated samples were kept at room temperature for a few months after irradiation, any free radicals formed could have been annihilated during that time.

4.2.3. Thermal Studies

The response of the pristine and the irradiated TTN samples was verified by two techniques, viz. (i) Thermogravimetric analysis and (ii) Differential Scanning Calorimetry.

(i) Thermogravimetric analysis

Fig.4.2.4 represents the theremograms and the results are shown in Table 4.2.3.

Table 4.2.3. Thermal decomposition temperatures at different zones for the pristine and the TTN samples irradiated to different doses (10, 30, 60, 80 kGy).

Dose (kGy)	Stable zone (°C)	Slow decomposition zone (°C)	Fast decomposition zone (°C)	Residual decomposition zone (°C)
0	-	30-300	300-410	410-515
10	-	30-297	297-409	409-515
30	-	30-297	297-405	405-518
60	30-169	169-295	295-400	400-600
80	30-170	170-304	304-400	400-625

It can be seen from the table that, the lower doses (up to 30 kGy) could not produce any significant change in decomposition behaviour of the polymer. The pristine and the irradiated samples at two lower doses (10, 30 kGy) underwent slow decomposition up to around 300°C without having a stable zone. It might be due to decomposition of the dye. At the higher two doses (60, 80 kGy), the polymer remained stable up to around 170°C, where the dye was already evaporated due

to ion irradiation then underwent a slow decomposition up to around 300°C as is in case of the rest of the TTN films.

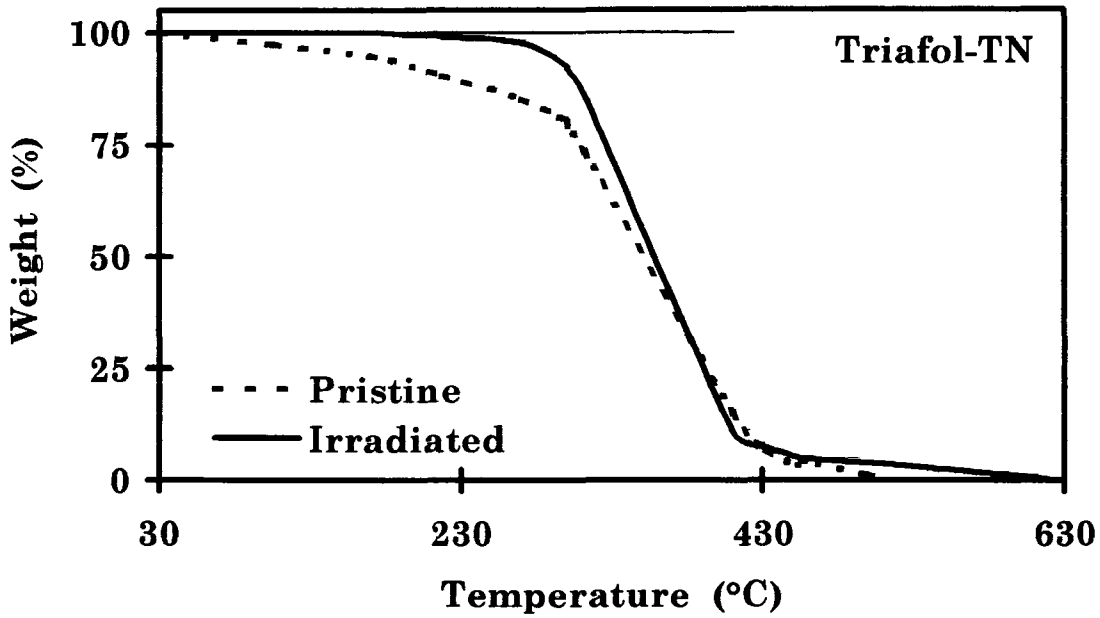

Fig.4.2.4. TGA thermograms of pristine and proton irradiated TTN (80 kGy).

The slow decomposition zone in all the cases involved a weight loss of about 5-12%. The fast decomposition zone accompanied by a weight loss of about 80% continued up to 410°C (for pristine) but reduced to 400°C for the sample irradiated by highest dose (80 kGy). The temperature of residual decomposition increased from 515°C (for pristine) to 625°C (80 kGy) associated with a weight loss of 7-11%.

(ii) Differential Scanning Calorimetry

The derived results from the thermogram (Fig.4.2.5) are tabulated in Table 4.2.4. The exothermal peak (crystallisation)

appeared at 279°C (A) for the pristine TTN, which shifted towards lower temperature with increase in proton dose and vanished for the sample irradiated to the highest dose (80 kGy). All the samples melted at around 315°C (B) (within the instrumental error of ±2°C).

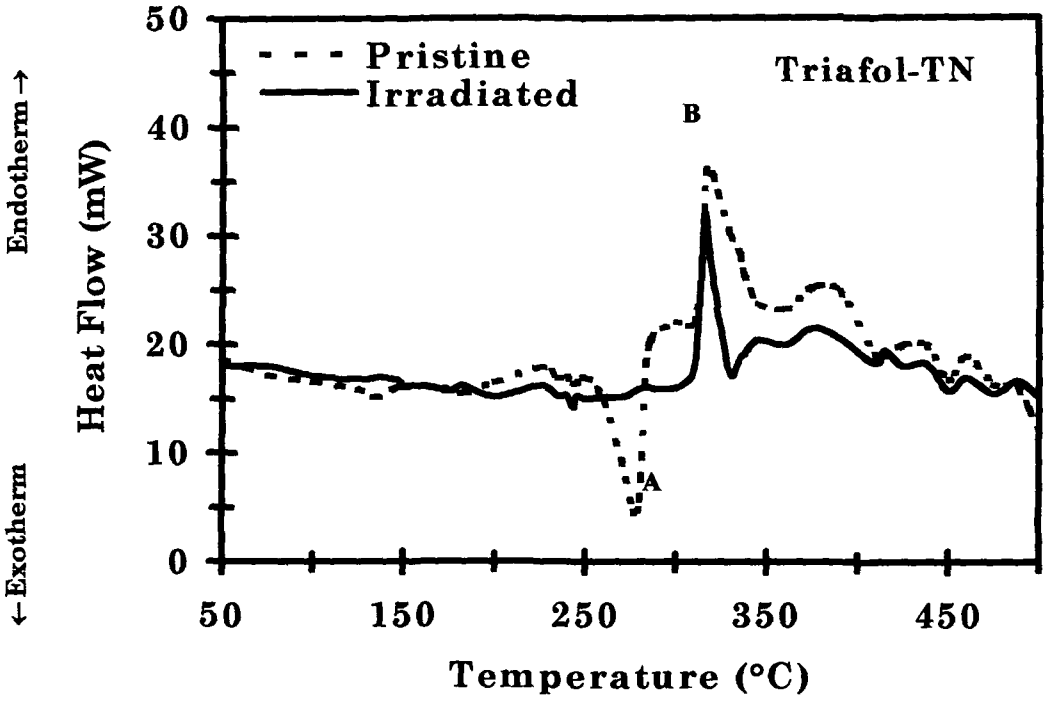

Fig.4.2.5. DSC thermograms of the pristine and the proton irradiated TTN (80 kGy).

Table 4.2.4. The temperature of crystallisation (T_c) (exothermal transition) and melting (T_m) (endothermal transition) in pristine and proton irradiated TTN at different doses (10, 30, 60, 80 kGy).

Doses (kGy)	0	10	30	60	80
T_c (°C)	279	265	265	260	-
T_m (°C)	316	315	318	314	315

4.3. POLYETHYLENE TEREPHTHALATE (PET)

The proton irradiated PET samples were characterised by track studies, surface studies, X-ray diffraction analysis, spectroscopic and thermal techniques.

4.3.1. Track Studies

The fission fragment track diameters were plotted against different etching times to determine the bulk etch-rate (V_G) of pristine PET and that irradiated to different doses of proton. The log V_G was plotted against the reciprocal of different etching temperatures (Fig.4.3.1) to calculate the activation energy (E_a) of etching.

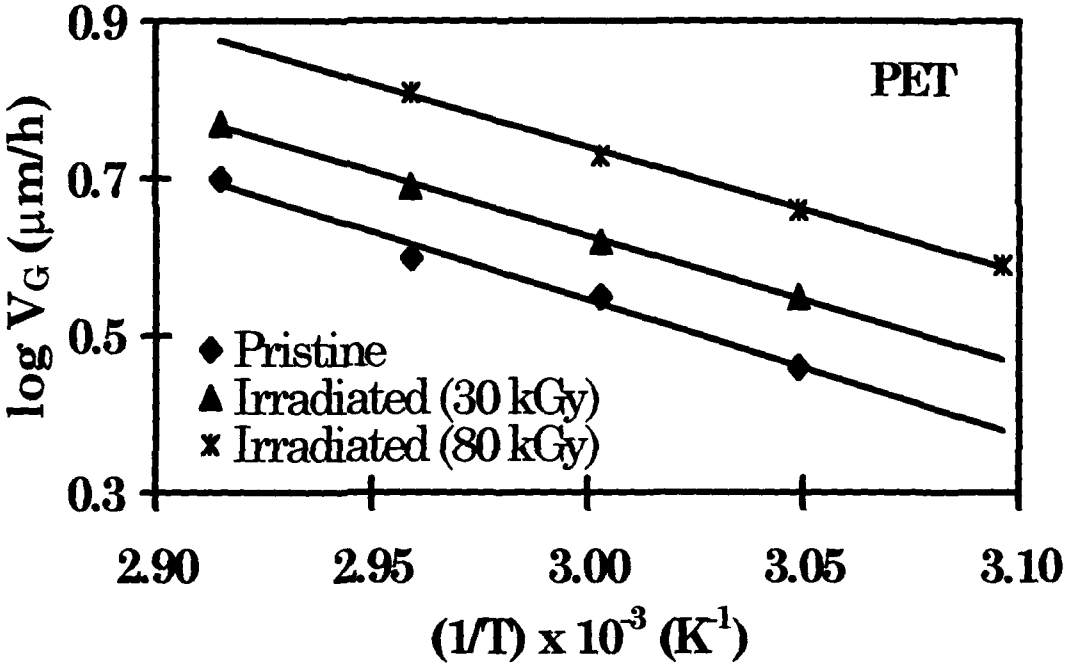

Fig.4.3.1. The plot of log V_G versus the inverse of etching temperature of pristine and proton irradiated PET at two different doses (30 and 80 kGy).

The values obtained are given in Table 4.3.1. The V_G was found to be increasing thereby decreasing the activation energy (E_a) of etching with the increase in proton dose. V_G increased by about 5-15%, 15-25%, 33-40% and 50-60% for PET irradiated to 10 kGy, 30 kGy, 60 kGy and 80 kGy doses of proton respectively than that of the pristine.

Table 4.3.1. The bulk etch-rate (V_G) at different etching temperatures (T_{etch}) and the activation energy of etching (E_a) for pristine and proton irradiated PET at different doses (10, 30, 60, 80 kGy).

	T_{etch} (°C)	Dose (kGy)				
		0	**10**	**30**	**60**	**80**
V_G (µm/h)	50	-	-	-	3.4	3.9
	55	2.9	3.4	3.6	4.0	4.6
	60	3.6	3.8	4.2	4.8	5.4
	65	4.0	4.6	4.9	5.6	6.5
	70	5.0	5.6	5.9	-	-
E_a	**(kJ.mol^{-1})**	33.1	31.8	31.4	31.0	30.6

The proton irradiation made the polymer easily etchable. The PET irradiated to highest dose (80 kGy) became hard before dissolving slowly at higher etching temperatures (60°C, 65°C). After etching, the portion of the polymer where the ions passed slowly became opaque

and rough as it often happens with heavy ion surface treatment. This indicates a growth of anti-reflectivity in the polymer. The track study here suggested a degradation of the polymer due to irradiation of energetic protons.

4.3.2. Surface Studies

Atomic force microscopy was done to study the surface of the pristine and the irradiated PET to the highest dose (80 kGy) of 62 MeV proton. The AFM images showing the surface topography are presented in Fig.4.3.2. The surface roughness (R_q), averaged over 20 different fields over the polymer surface, were found to be 4.9 ± 0.5 nm for the pristine and 5.1 ± 0.5 nm for the irradiated one. The proton irradiation at the highest dose enhanced the surface roughness of the polymer slightly by about 4%.

4.3.3. X-ray Diffraction Analysis

The XRD spectra of the pristine and proton irradiated PET (80 kGy) are shown in Fig.4.3.3 and the parameters assigned with the peaks are given in Table 4.3.2. The result shows that the intensity of the main peak (C) at $2\theta=26.26°$ for the pristine increased and shifted to $2\theta=25.92°$ after irradiation with the highest dose (80 kGy) of proton.

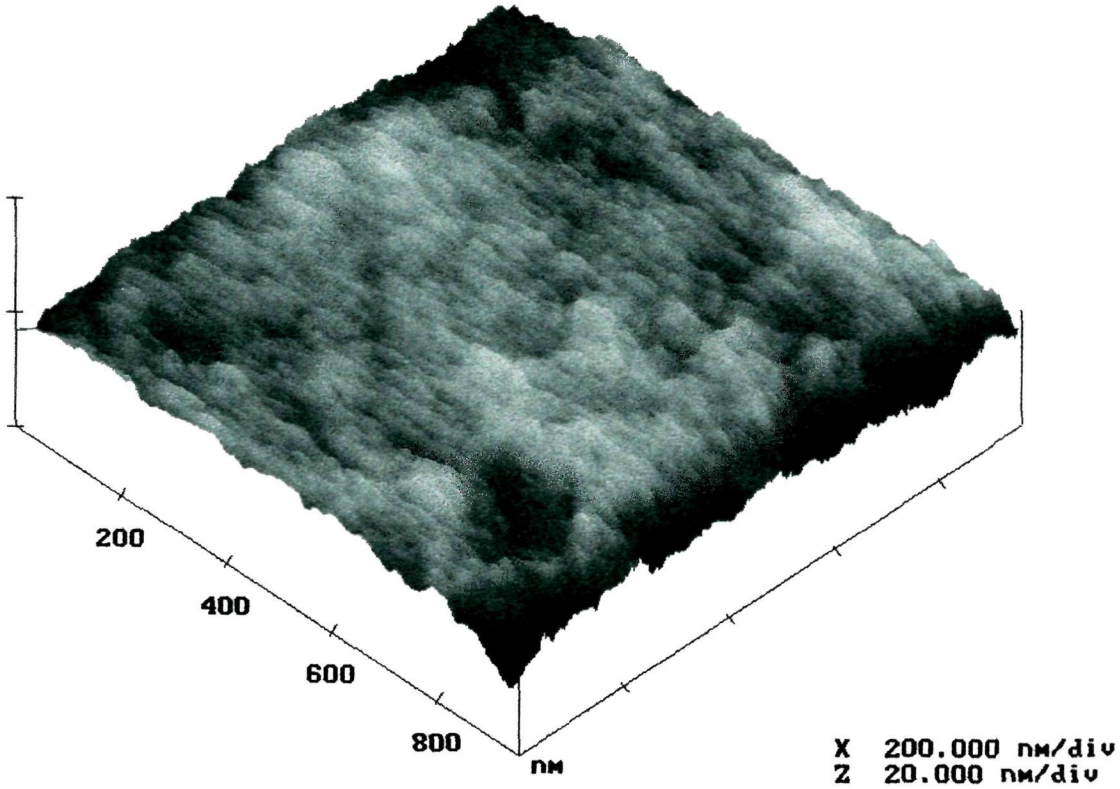

Fig.4.3.2.(i). AFM image of the Pristine PET.

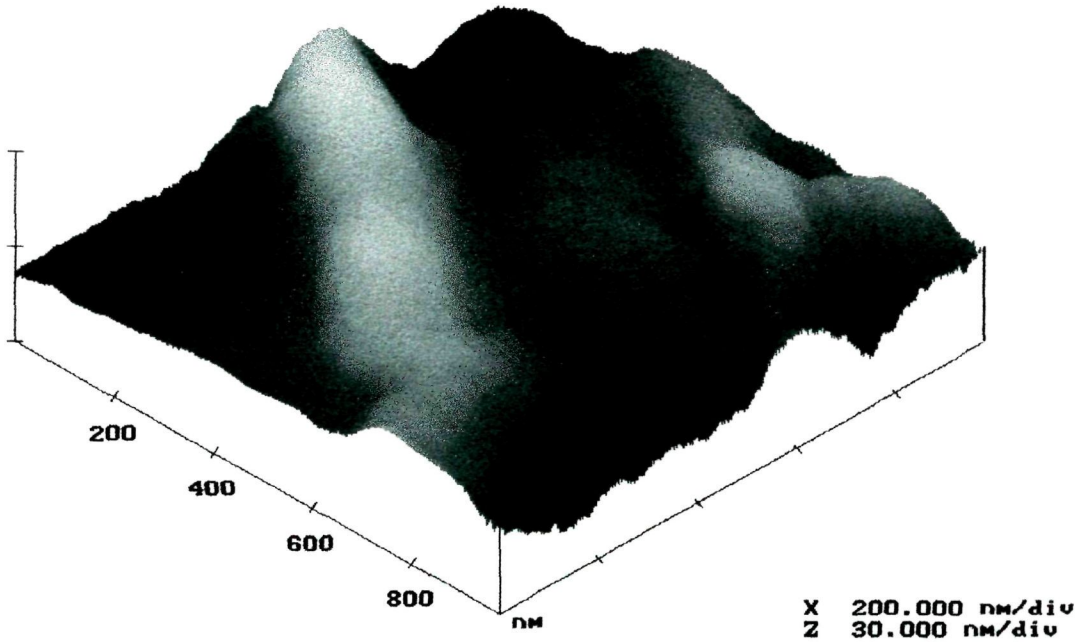

Fig.4.3.2.(ii) AFM image of the irradiated PET (80 kGy)

This change can be attributed to the differences in density of the pristine and irradiated zones arising out of the restoration of the crystal structure due to the increasing strain on the irradiated PET. Three new peaks (A, B, D) emerged at 2θ = 9.45°, 13.18° and 28.63° after irradiation, which might be due to the newly formed fine polymer crystallites in the amorphous zone of PET, not present in the pristine polymer.

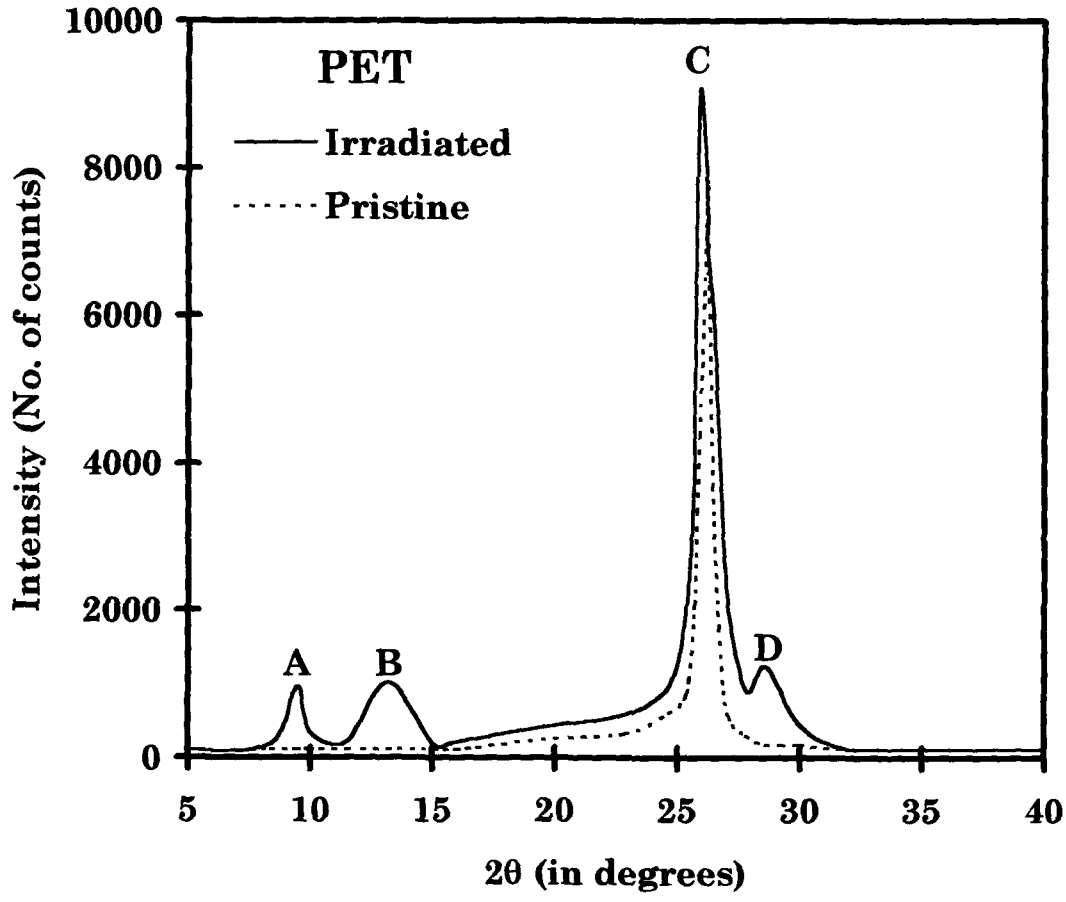

Fig.4.3.3. XRD spectra of the pristine and the proton irradiated PET (80 kGy).

Since the diffraction pattern depends upon the internal structure of the polymer, the observed changes in the X-ray diffraction spectra represent the growth in orderliness of the original lamella (crystalline) structure of PET, thus, leading to a considerable increase in its crystallinity after proton irradiation at the dose of 80 kGy.

Table 4.3.2. Position (2θ), Intensity (I) and full width half maximum (FWHM) of the XRD peaks of the pristine (P) and proton irradiated PET (80 kGy).

Peak	2θ (degree)		I_{rel}		I (CPS)		FWHM (degrees)	
	P	80kGy	P	80kGy	P	80kGy	P	80kGy
*A	-	9.46	-	11	-	967	-	0.13
*B	-	13.18	-	18	-	909	-	3.40
C	26.26	25.92	100	100	7825	7303	0.50	0.70
*D	-	28.63	-	14	-	1247	-	1.20

* New peaks formed after irradiation.

4.3.4. Spectral Analysis

Three spectroscopic techniques, viz. (i) UV-Visible (ii) Fourier Transform Infra-red and (iii) Electron spin resonance are used to characterise the pristine and the irradiated PET samples.

(i) UV-Visible Spectroscopy

UV-Vis spectroscopy was done to observe the shift of the absorption edges from UV to visible side and to calculate the wavelength-gap (λ_g) and the energy band-gap (E_g) from the equation 2.11 and 2.12 given in chapter 2. The energy band-gap for the pristine PET was found to be 3.9 ± 0.1 eV, which remained unchanged even after the highest does (80 kGy) of proton irradiation. Though there was a possibility of cluster formation due to the presence of the aromatic group in the backbone structure of the polymer, yet the energy deposition could not possibly be sufficient to initialise the process. Rather, the phenolic group, which is resistive to radiation, has delocalised the excitation energy.

(ii) Fourier Transform Infrared Spectroscopy

The spectra of the pristine and irradiated PET (80 kGy) are shown in Fig.4.3.4. Here, the change in most of the characteristic peak positions denotes the deformation of the structure. The simultaneous change of all IR lines indicate that the irradiation-affected regions are distributed randomly all over the polymer molecules. The absorption bands obtained from the spectra are interpreted in Table 4.3.3. No new band was observed at 3294 cm^{-1}, which was basically assigned to

the alkyne group. This was in contrast with the result obtained by Steckenreiter et al. [32] regarding the alkyne group formation after heavy ion irradiation. However, for the highest dose, the increase in absorbance at 730 cm^{-1} implied the possible recrystallisation after proton irradiation but the increase in absorbance at 873 cm^{-1} implied some amorphisation of the newly formed crystals.

Table 4.3.3. The identification of the absorption bands in PET corresponding to their wavenumbers ($1/\lambda$).

Peak	**$1/\lambda(cm^{-1})$**	***Identification* [61, 32]**
A	2975	CH stretching of CH_2 group
B	1723	C=O stretching vibration
C D E	1373 1273 1203	C-C stretching of phenyl ring, Vibration band of para substituted benzene rings
F G	1123 1013	C-O-C stretching of ester
H	862	CH deformation of phenyl ring,Vibration band of para substituted benzene rings
I	732	Ring deformation of phenyl ring, Bending vibration of CH_2 group

This kind of simultaneous behaviour was possible when the pristine polymer was partly crystalline. Increase in absorbance of the band at 1471 cm^{-1} indicated a loss of crystallinity of the polymer.

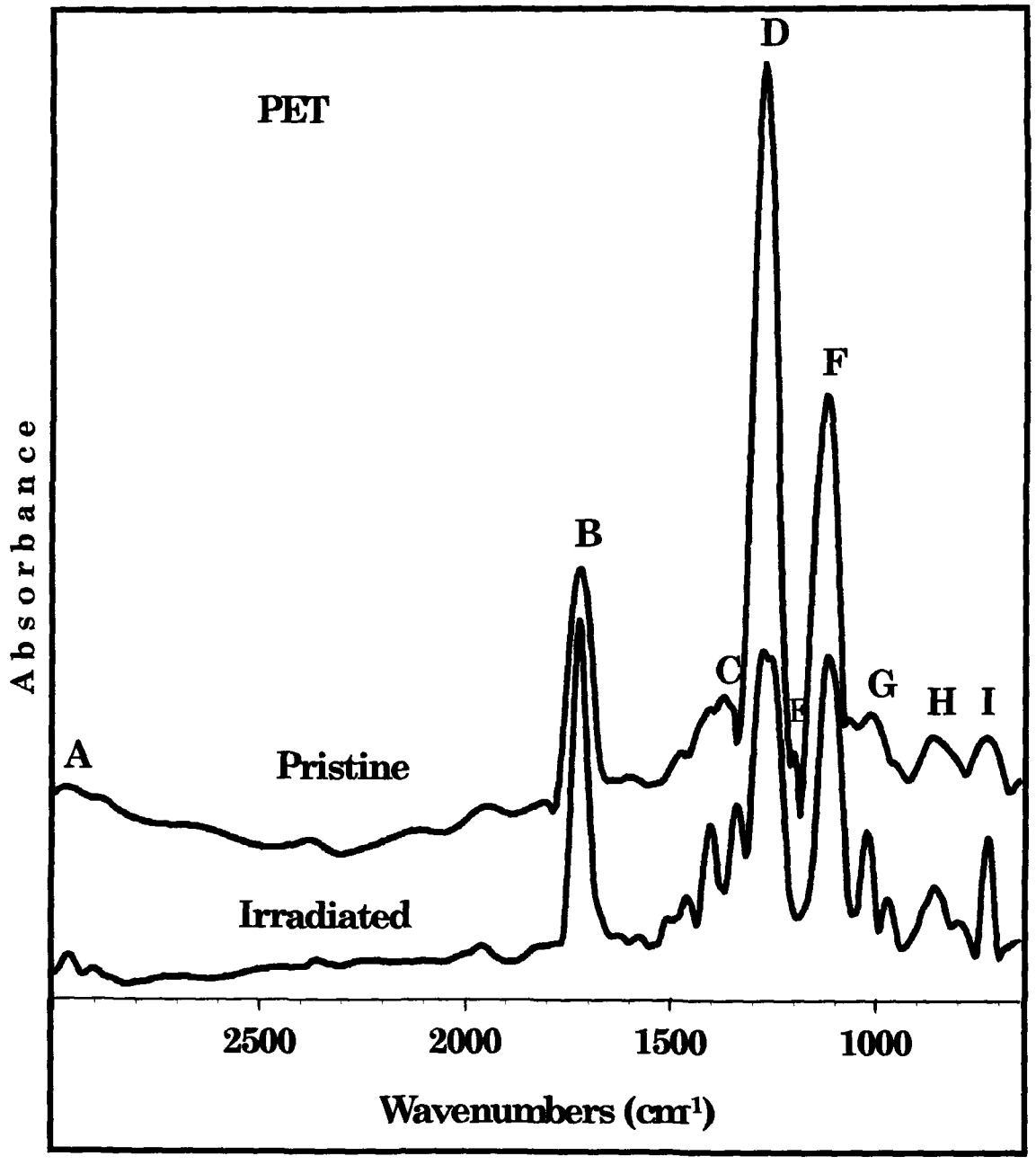

Fig.4.3.4. FT-IR spectra of the pristine and the proton irradiated PET (80 kGy) in the range of 3000-650 cm^{-1}.

Amorphisation process was further enhanced because of the irradiation of the polymer in presence of air. Increase in absorbance of para- substituted benzene ring bands at the highest dose indicated the stability of the aromatic unit. Similarly, there are instances when the polymer underwent degradation without affecting the whole structure of the polymer.

(iii) Electron Spin Resonance Spectroscopy

Formation of free radicals, as expected from heavy ion irradiation, could not be traced from the ESR spectral analysis of the irradiated PET. Since the irradiated samples were kept at room temperature for a few months after irradiation, the free radicals formed, if any, would have been annihilated during that time.

4.3.5. Thermal Studies

The thermal response of the polymers was studied by following two techniques viz. Thermogravimetric analysis and Differential scanning calorimetry.

(i) Thermogravimetric analysis

The decomposition behaviour of the pristine and the irradiated polymers were studied by this technique. The thermograms are shown in Fig.4.3.5 and the temperatures for different zones are given in

Table 4.3.4. As depicted from the figure, the stable zone disappeared for the irradiated polymers, which was up to 165°C for the pristine PET. The irradiation made the polymer to undergo a slow decomposition from the moment of application of heat. This slow decomposition zone continued up to 410°C involving only about 10% of weight loss for the pristine, whereas a weight of about 20-25% was lost in case of the irradiated ones at a lower temperature (346-390°C).

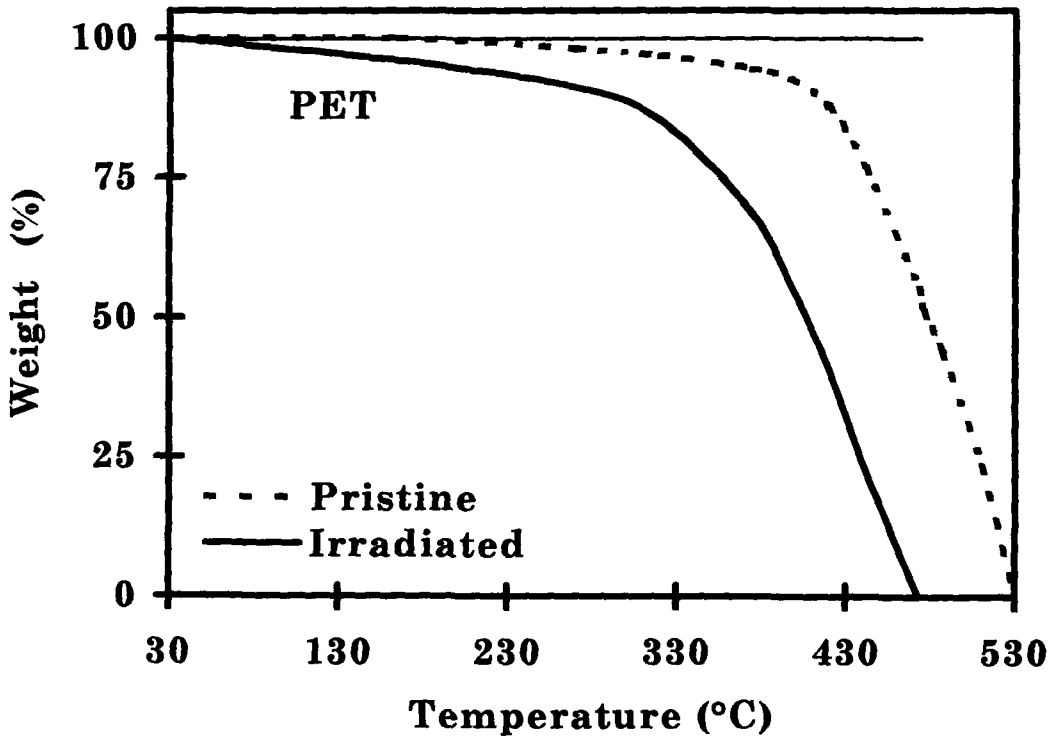

Fig.4.3.5. TGA thermograms of the pristine and the proton irradiated PET (80 kGy).

Similarly, the fast decomposition zone went up to 530°C involving a weight loss of about 90% for the pristine and up to 460-

475°C for the irradiated polymers associated with a weight loss of about 75-80%. From the data, it is observed that the decomposition nature of the polymer depended upon the dose of the proton beam irradiation, i.e., the more the dose, the less the thermal stability. This denotes a degradation of the polymer matrix under proton beam irradiation making it to decompose earlier than the pristine PET.

Table 4.3.4. Thermal decomposition temperatures at different zones for the pristine and the PET samples irradiated to different doses (10, 30, 60, 80 kGy).

Dose (kGy)	Stable zone(°C)	Slow decomposition zone(°C)	Fast decomposition zone(°C)
0	30-165	165-410	410-530
10	-	30-390	390-475
30	-	30-390	390-475
60	-	30-377	377-465
80	-	30-346	346-460

(ii) Differential scanning calorimetry (DSC)

The DSC thermograms of the pristine and the proton irradiated PET is shown in Fig.4.3.6. The error in temperature recording was ±2°C. It was observed that the exotherms denoting the temperature of crystallisation (T_c) appeared at around 208°C (A_0 in pristine, A_1 in

irradiated) in all the cases. But the endotherms denoting the melting temperatures (T_m) underwent a change after proton irradiation. The endotherm is sharp for the pristine PET appearing at about 229°C (B_0), but continuous endothermal distortions were found in all the irradiated PET samples, spreading over a temperature range (up to 450°C), the starting point of which was around 224°C (B_1).

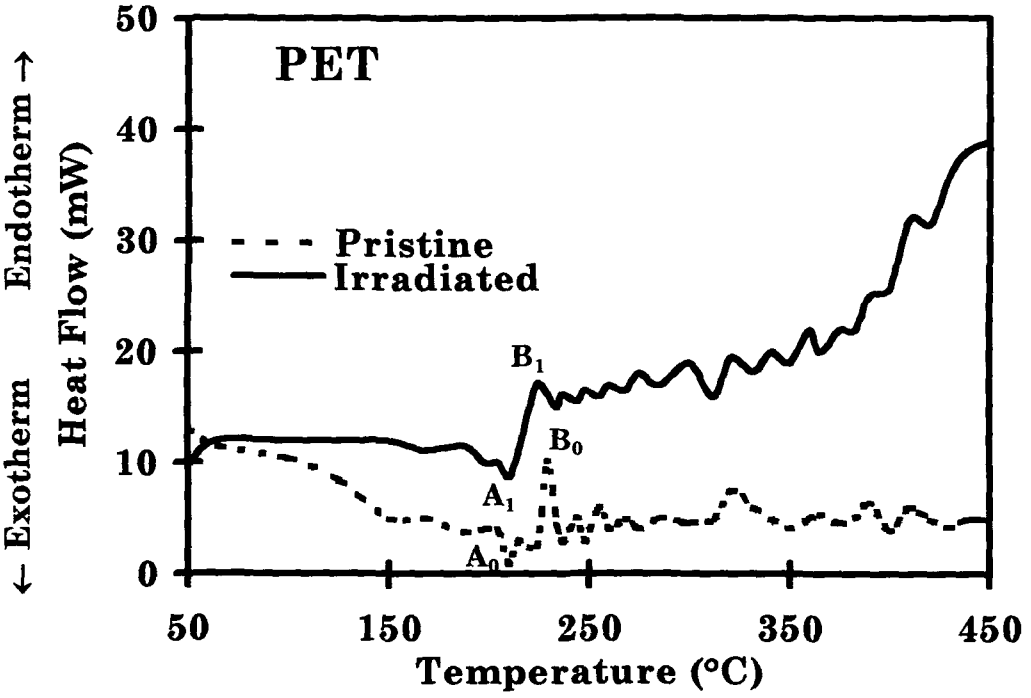

Fig.4.3.6. DSC thermograms of the pristine and the proton irradiated PET (80 kGy).

4.4. TRIAFOL-BN (TBN)

The pristine and the irradiated polymers at four different doses are characterised by track studies, spectroscopic and thermal techniques.

4.4.1. Track Studies

The track diameters were measured and plotted against the corresponding etching times to determine the bulk etch-rate (V_G). The log of V_G was plotted against the reciprocal of different etching temperatures (Fig.4.4.1) to calculate activation energy (E_a) of etching.

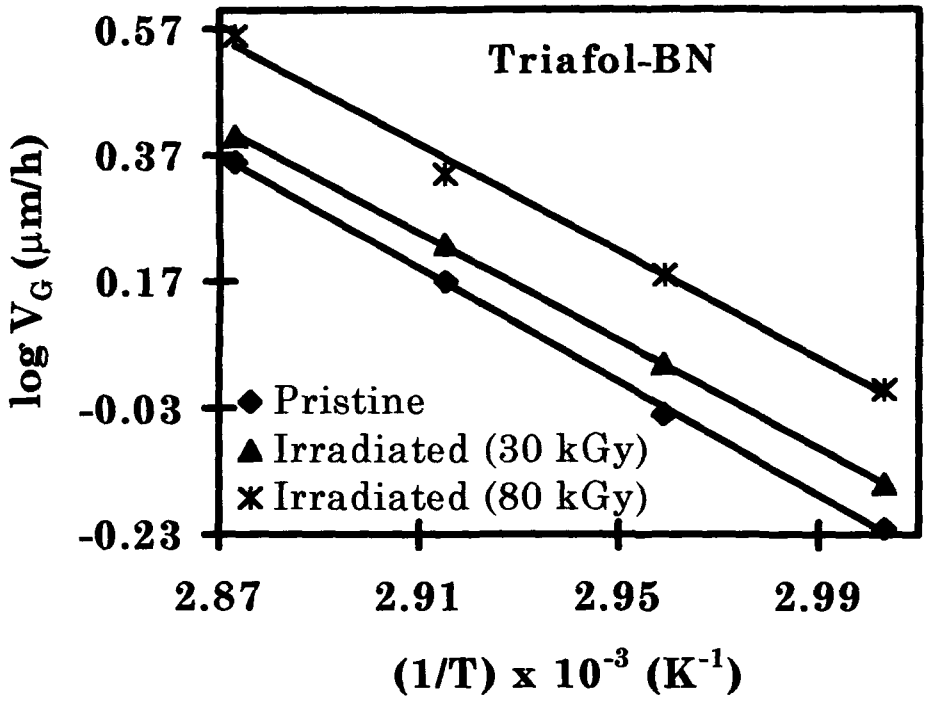

Fig.4.4.1. The plot of log V_G versus the inverse of etching temperature of pristine and proton irradiated TBN at two different doses (30 and 80 kGy).

The measured values of V_G are given in Table 4.4.1. There is no significant increase in V_G up to the dose of 30 kGy. It increased by about 30% for the polymer irradiated to 60 kGy and by about 50% for the one irradiated at 80 kGy of 62 MeV proton. The parallel lines in

Fig.4.4.1 show that, the activation energy for bulk etching was not modified under different doses of proton irradiation even though the etch-rates were increasing.

Table 4.4.1. The bulk etch-rate (V_G) at different etching temperatures (T_{etch}) and the activation energy of etching (E_a) of the pristine TBN and the TBN irradiated to 62 MeV proton (10, 30, 60, 80 kGy).

	T_{etch} (°C)	Dose (kGy)				
		0	10	30	60	80
V_G (µm/h)	60	0.6	0.7	0.7	0.8	1.0
	65	0.9	1.0	1.0	1.2	1.5
	70	1.5	1.7	1.7	1.9	2.2
	75	2.3	2.5	2.6	2.9	3.6
E_a (kJ.mol^{-1})		81.1	81.3	81.3	81.2	81.2

4.4.2. Spectral Analysis

Spectral studies were done using three different techniques viz. UV-Visible, Fourier Transform Infra-red and Electron Spin Resonance, to identify any structural characteristic changes due to proton irradiation.

(i) UV-Vis Spectroscopy

The spectra are shown in Fig.4.4.2. The absorbance values were used to obtain the tauc's plot for calculating the optical band-gap. The absorption edge of the irradiated TBN (80 kGy) shifted from the visible side towards the UV side, thus, leading to an increase in the band-gap due to proton bombardment. The energy band-gap (E_g) for the pristine TBN was found to be 2.1 ± 0.1 eV, which increased to 2.8 ± 0.1 eV after irradiation and did not vary further with increase in dose.

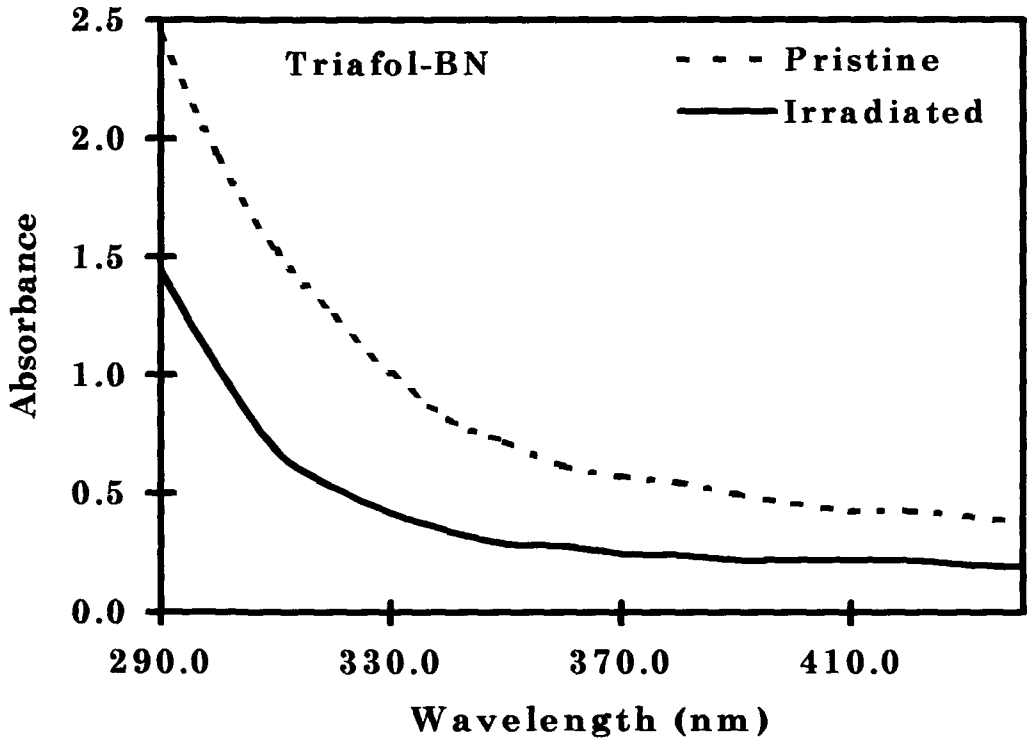

Fig.4.4.2. UV-Vis spectra of the pristine TBN and the proton irradiated TBN (80 kGy).

The energy band-gap (E_g) thus increased by about 33% after irradiation, which is in contrast with the results obtained for other

polymers. The increase in energy band-gap (by about 33%) suggests an enhanced insulating nature of the irradiated polymers.

(ii) Fourier transform Infrared spectroscopy

The FT-IR spectra are given in Fig. 4.4.3 and the identification of the absorption bands along with their wavenumbers are listed in Table 4.4.2. No significant change in the vibrational frequencies was observed, which implied that inter-chain separation is not affected much by proton irradiation. Most of the peak positions were found to be unshifted. It was observed that the peak position at around 1139 cm^{-1} (F) due to stretching vibration of the main chain became intense for the sample irradiated to 80 kGy of 62 MeV proton.

Table 4.4.2. The identification of the absorption bands in TBN corresponding to their wavenumbers ($1/\lambda$).

Peak	**$1/\lambda$(cm^{-1})**	**Identification [61]**
A	3517	COOH (or OH)
B	2909	C-H stretching
C	1716	R-C=O (ketone of ester)
D	1318	-C-O-C- (ether bonding)
E	1290	
F	1139	Stretching vibration of the main chain

A decrease in transmittance percentage was also observed. This was probably due to the chain-scissioning leading to degradation in the irradiated TBN samples. The change in absorbance or transmittance values of particular functional group may also be attributed to the decrease in concentration of the pre-existing bonds or groups. This study further clarified the increase in optical band-gap as obtained from the UV-Vis spectroscopy.

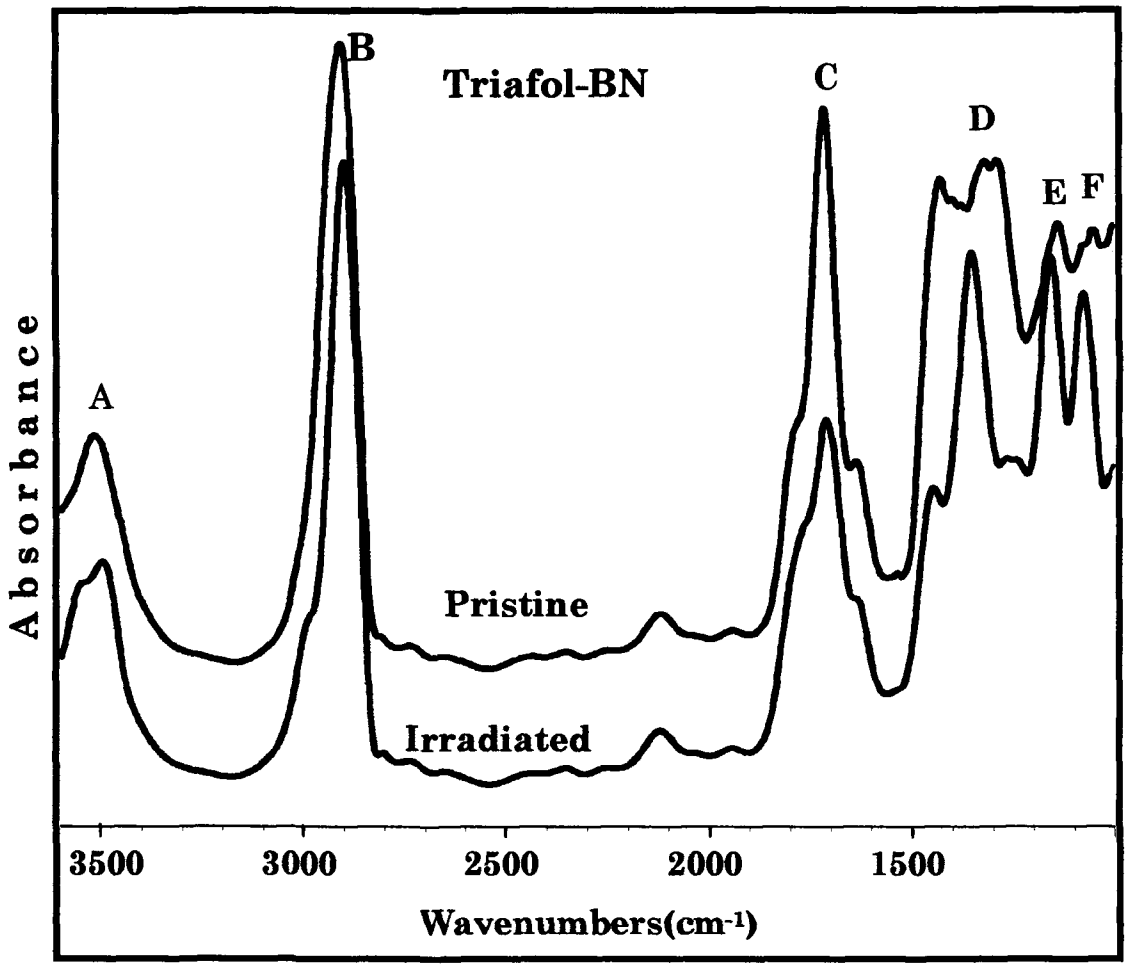

Fig.4.4.3. FT-IR spectra of pristine TBN and proton irradiated TBN (80 kGy) in the range of 3700-1000 cm^{-1}.

(iii) Electron Spin Resonance Spectroscopy

Formation of free radicals, as expected from heavy ion irradiation, could not be traced from the ESR spectral analysis of the irradiated TBN. Since the irradiated samples were kept at room temperature for a few months after irradiation, the free radicals formed, if any would have been annihilated during that time.

4.4.3. Thermal Studies

Thermogravimetric analysis and Differential scanning calorimetry were done to characterise the pristine and the irradiated TBN films.

(i) Thermogravimetric analysis

The decomposition behaviour of the polymers was examined by this technique. Fig.4.4.4 represents the thermograms of the polymers. The results obtained are shown in Table 4.4.3. As soon as the heat was applied, the pristine TBN started decomposing slowly up to 322°C. It might be due to decomposition of the dye. The irradiated samples remained generally stable up to 180°C and then underwent slow decomposition up to 322°C for the samples irradiated at 10, 30, 60 kGy and up to 290°C for the one irradiated to the highest dose (80 kGy). A weight loss of about 10% was associated with the slow

decomposition zone. The fast decomposition zone (up to 425°C for the pristine) accompanied by a weight loss of about 80% reduced up to about 405°C (for irradiated samples).

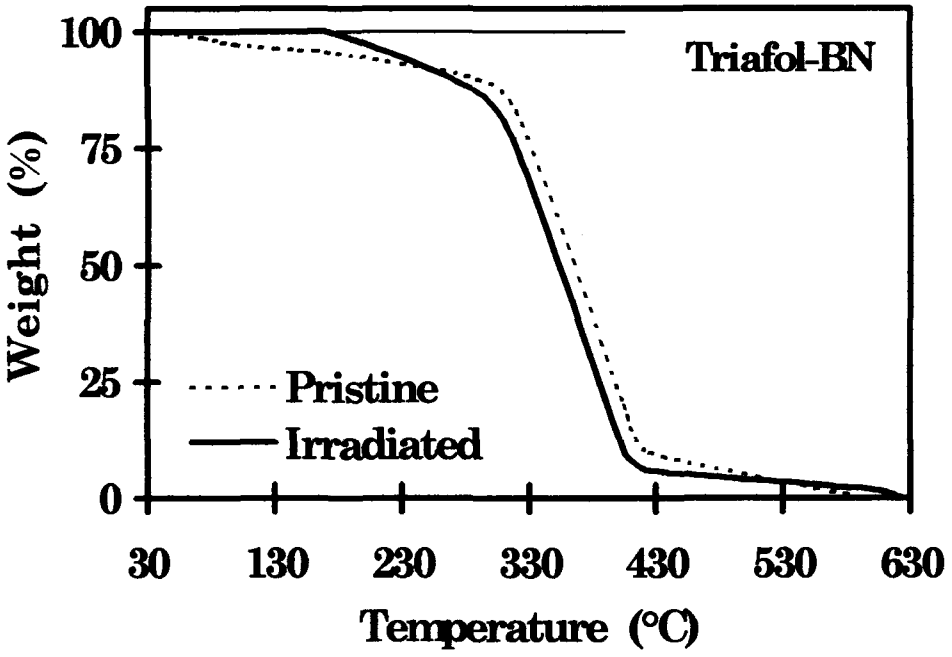

Fig.4.4.4. TGA thermograms of the pristine TBN and the proton irradiated TBN (80 kGy).

This suggested that the proton irradiation had reduced the thermal resistance of the polymer, even though the activation energy of etching was not affected. The temperature for the residual decomposition (about 5-10%) however increased from 593°C (pristine) to about 624°C (80 kGy).

Table 4.4.3. Thermal decomposition temperatures at different zones for the pristine and the TBN samples irradiated to different doses (10, 30, 60, 80 kGy).

Dose (kGy)	Stable zone (°C)	Slow decomposition zone (°C)	Fast decomposition zone (°C)	Residual decomposition zone (°C)
0	-	30-322	322-425	425-593
10	30-180	180-322	322-405	405-616
30	30-180	180-322	322-405	405-620
60	30-180	180-322	322-407	407-620
80	30-180	180-290	290-406	406-624

(ii) Differential scanning calorimetry

The DSC thermograms are characterised by the appearance of one endotherm peak denoting melting temperature of the samples. The melting temperature, as evident from the thermogram (Fig.4.4.5), for the pristine was found to be 334°C, which reduced to about 321°C for the irradiated polymers denoting bond cleavage in the molecule, which corroborated the results of TGA and the spectral studies.

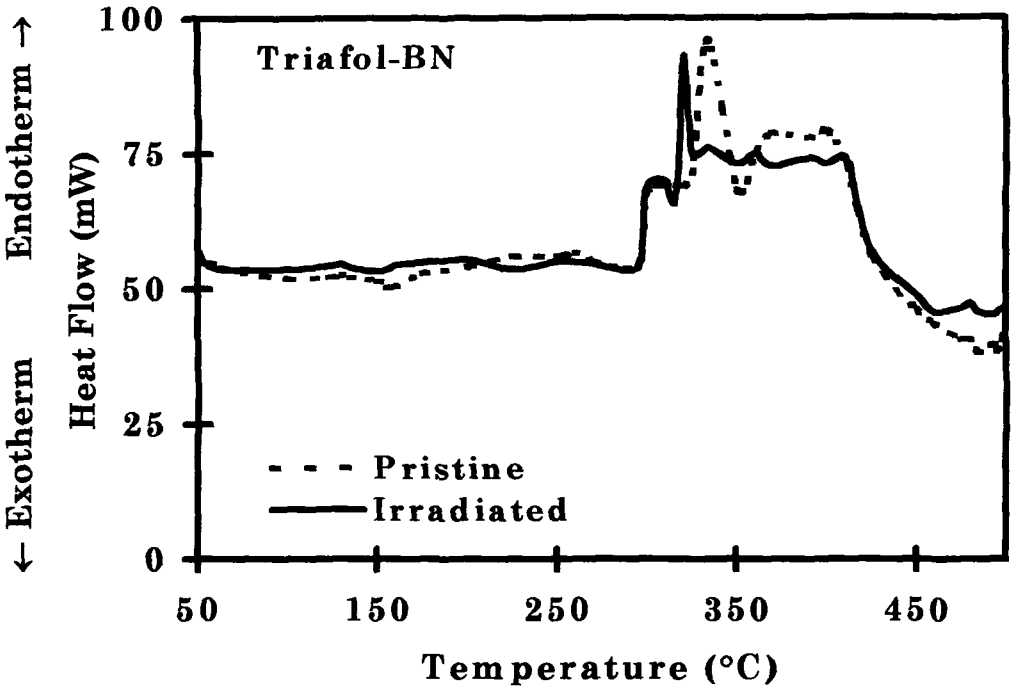

Fig.4.4.5. DSC thermograms of the pristine TBN and the proton irradiated TBN (80 kGy).

4.5. POLYPROPYLENE (PP)

The pristine and the irradiated polymers were characterised by surface studies, X-ray diffraction analysis, spectroscopic techniques and thermal techniques.

4.5.1. Surface Studies

The Atomic force microscopy was done to study the surface of the pristine PP and the PP irradiated to the highest dose (80 kGy) of 62 MeV proton. The micrographs are shown in Fig.4.5.1.

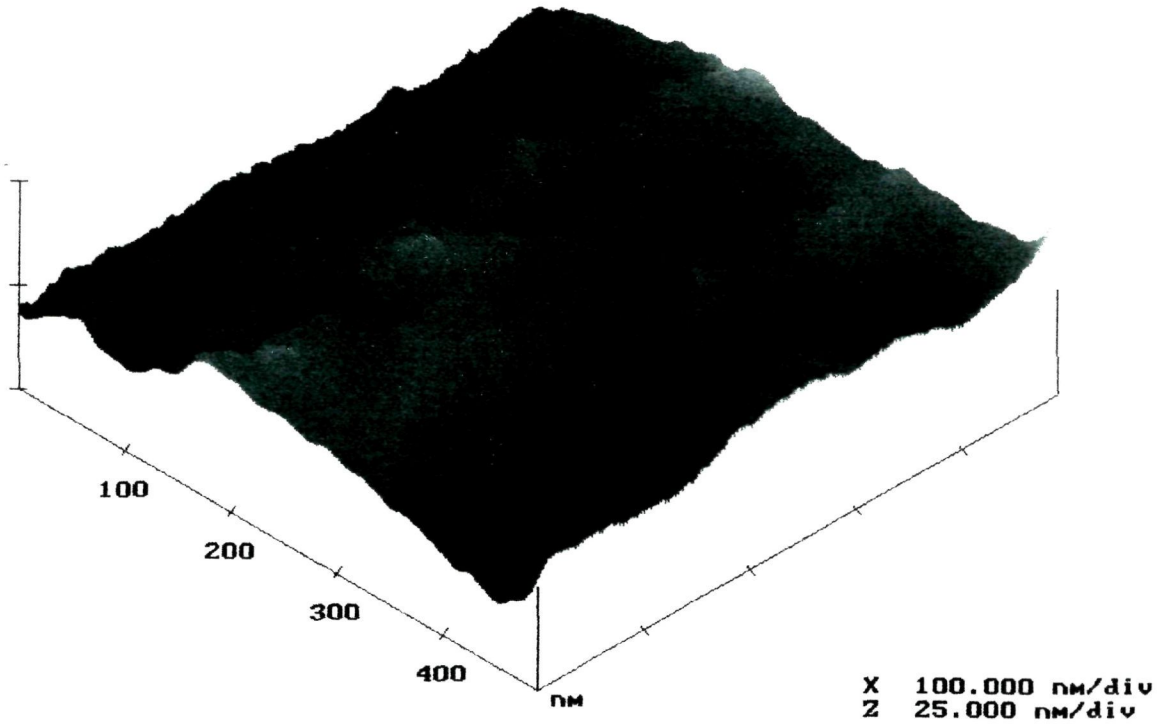

Fig.4.5.1(i). AFM image of the pristine PP.

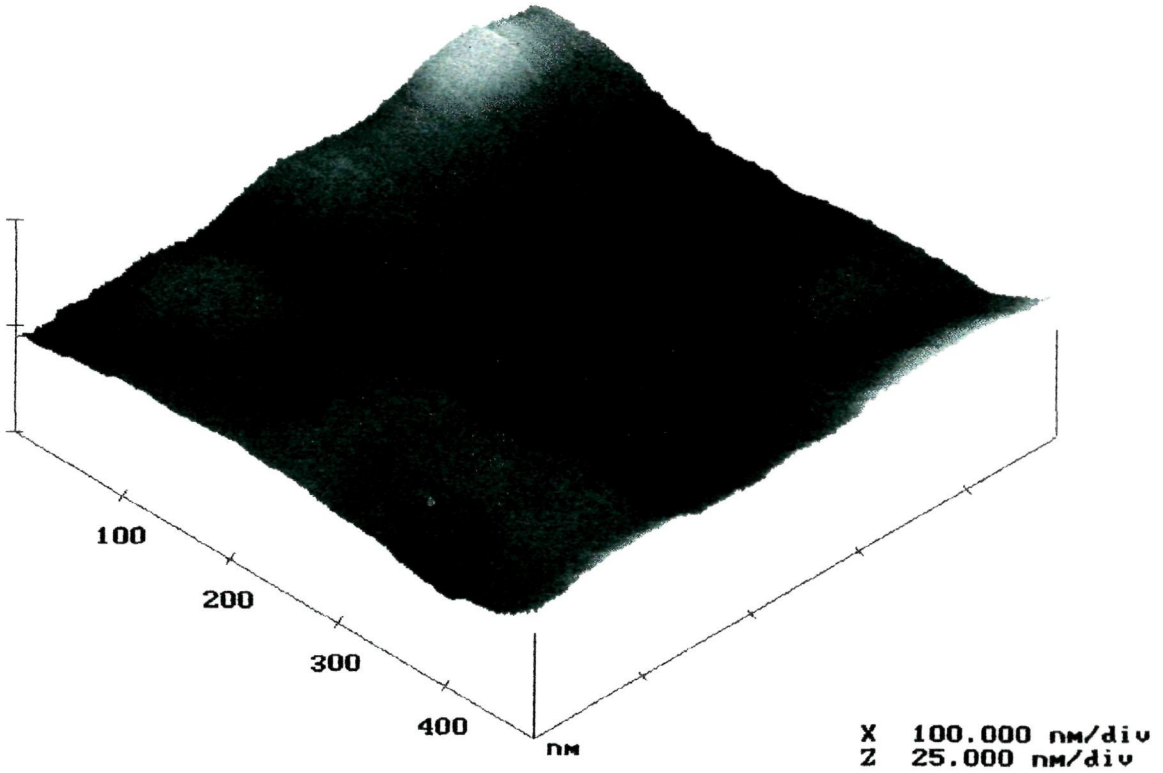

Fig.4.5.1(ii). AFM image of the irradiated PP (80 kGy).

The surface roughness (R_q), averaged over 20 different fields over the polymer surface, was found to be 7.2 ± 0.4 nm for the pristine and 5.0 ± 0.6 nm for the irradiated PP (80 kGy). The 80 kGy dose of 62 MeV proton irradiation reduced the surface roughness of PP by about 31% at nanoscopic level, which was in contrast with the results of the proton irradiated PET. This might be due to the production of defects and chemical modifications in the bulk and material ejection at the surface as is expected when the insulators are irradiated to energetic ions [62].

4.5.2. X-ray Diffraction Analysis

The XRD spectra of the pristine and the irradiated PP (80 kGy) are shown in Fig.4.5.2 and the various parameters assigned with the peaks are given in Table 4.5.1. The result showed that intensity of the main peak (C) at $2\theta = 18°$ for the pristine was enhanced and shifted to $2\theta = 16.9°$ after irradiation with the highest dose (80 kGy) of proton. The other peaks (B, D, F, G) suffered less shift in position with increased intensities. This change can be attributed to the differences in densities of the pristine and irradiated zones arising out of the cross - linking of the degraded molecules in the crystal structure due to the increasing strain on the irradiated PP.

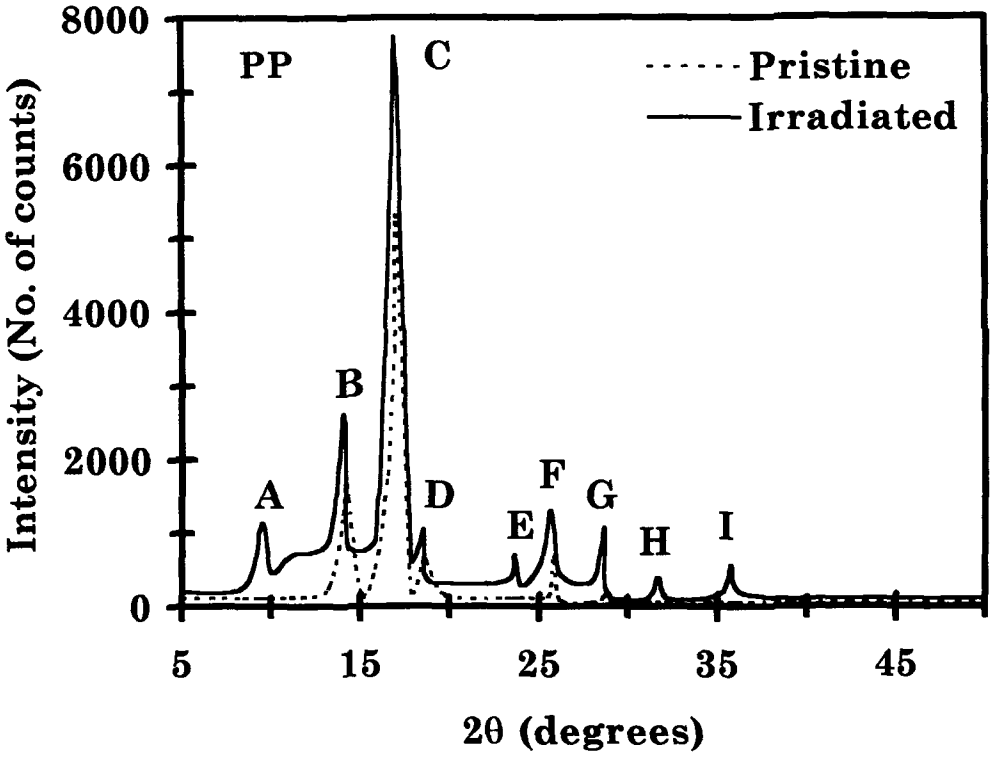

Fig.4.5.2. XRD spectra of pristine and proton irradiated PP (80 kGy).

Some new peaks (A, E, H, I) emerged after irradiation, which could have been due to the newly formed fine polymer crystallites in the amorphous zone of PP. Nevertheless, the observed changes in the X-ray diffraction spectra represented the restoration and increase in regularity of the original lamella (crystalline) structure of PP leading to an increase in crystallinity due to proton irradiation.

Table 4.5.1. Position (2θ), Intensity (I) and full width half maximum (FWHM) of the XRD peaks of pristine (P) and proton irradiated PP (80 kGy).

Peak	2θ (degree)		I_{rel}		I (CPS)		FWHM (degree)	
	P	80kGy	P	80kGy	P	80kGy	P	80kGy
A	-	9.45	-	15	-	1135	-	0.16
B	14.18	14.04	32	34	1658	2634	0.93	0.73
C	17.03	16.88	100	100	5225	7731	0.87	0.63
D	18.61	18.50	12	14	643	1048	1.29	1.25
E	-	23.59	-	9	-	702	-	2.44
F	25.63	25.56	13	17	684	1299	0.49	1.12
G	28.65	28.62	2	14	147	1077	0.92	0.27
H	-	31.65	-	5	-	399	-	4.40
I	-	35.73	-	7	-	571	-	0.24

4.5.3. Spectral Analysis

UV-Visible, Fourier Transform Infra-red and Electron Spin Resonance spectroscopy were done to identify any structural characteristic changes in PP due to proton irradiation.

(i) UV-Vis Spectroscopy

The UV-Vis spectra (Fig.4.4.3) showed a slight shift of the absorption edge for the polymer irradiated to highest dose (80 kGy)

leading to a small decrease in optical band-gap (E_g). The value of E_g for the pristine was 5.2 ± 0.1 eV, which remained constant for the proton irradiated PP up to a dose of 60 kGy, but only for the PP irradiated to a dose of 80 kGy, it was reduced to 4.9 ± 0.1eV.

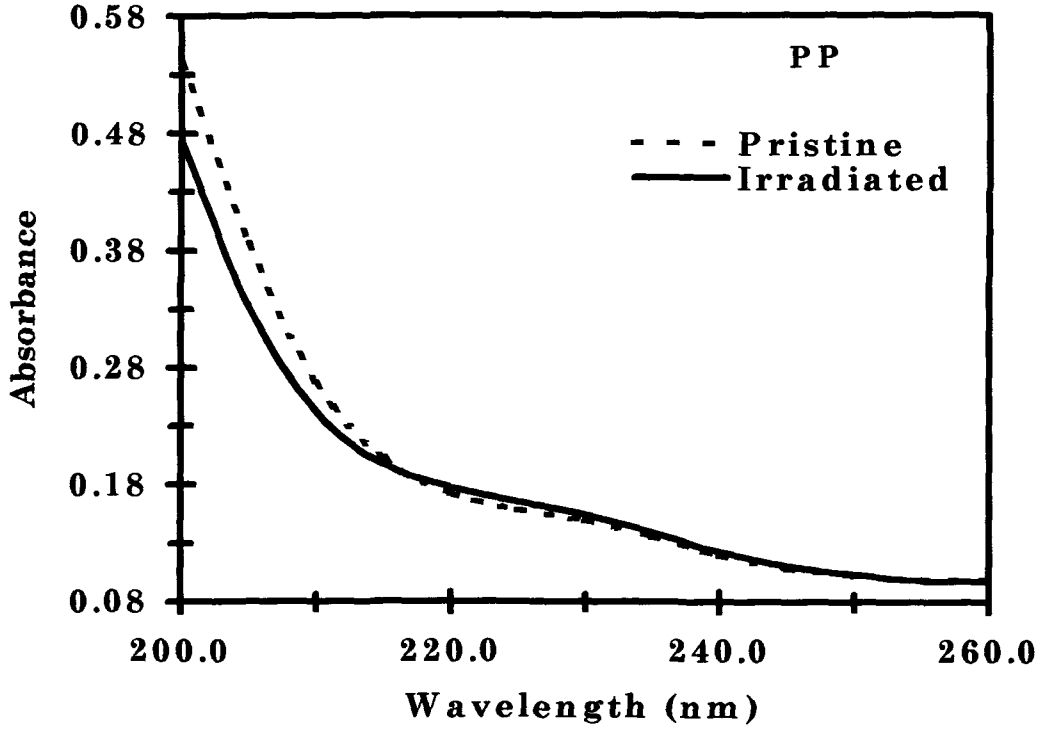

Fig.4.5.3. UV-Vis spectra of the pristine and the proton irradiated PP (80 kGy).

(ii) Fourier transform Infra-red Spectroscopy

The FT-IR spectra of the pristine and the proton irradiated PP (80 kGy) are shown in Fig.4.5.4 and the identification of the structural characteristic peaks [60] at the corresponding wavenumbers are given in Table 4.5.2.

Table 4.5.2. Identification of absorption bands in PP corresponding to their wavenumbers (1/λ).

Peak	1/λ (cm^{-1})	Identification
A	2956	CH_3 asymmetric stretching vibration
B	2918	CH_2 asymmetric stretching vibration
C	2875	CH_3 symmetric stretching vibration
D	2840	
E	2361	CO_2 from air? [61]
F	1456	CH_3 asymmetric scissor
G	1375	CH_3 symmetric scissors
H	1165	3/1 Helix structure
I	996	(isotacticity of the polymer)

The peak positions in the pristine and the irradiated PP samples remained almost constant indicating that the 3/1 helix structure of the polymer was not destroyed after proton irradiation. Hence, the isotactic nature of the polymer was not disturbed by proton bombardment. A little alternation in these peak positions might be due to the effect of the Fermi's or Corrriolis type of interactions. A slight increase in absorbance of the characteristic peaks (C, D) has been observed at 2875 cm^{-1} and 2840 cm^{-1}, which arose due to the CH_3

symmetric stretch. An increase in absorbance at all the wavenumbers demonstrated the change in the crystallinity matrix and corroborating the results obtained from XRD analysis.

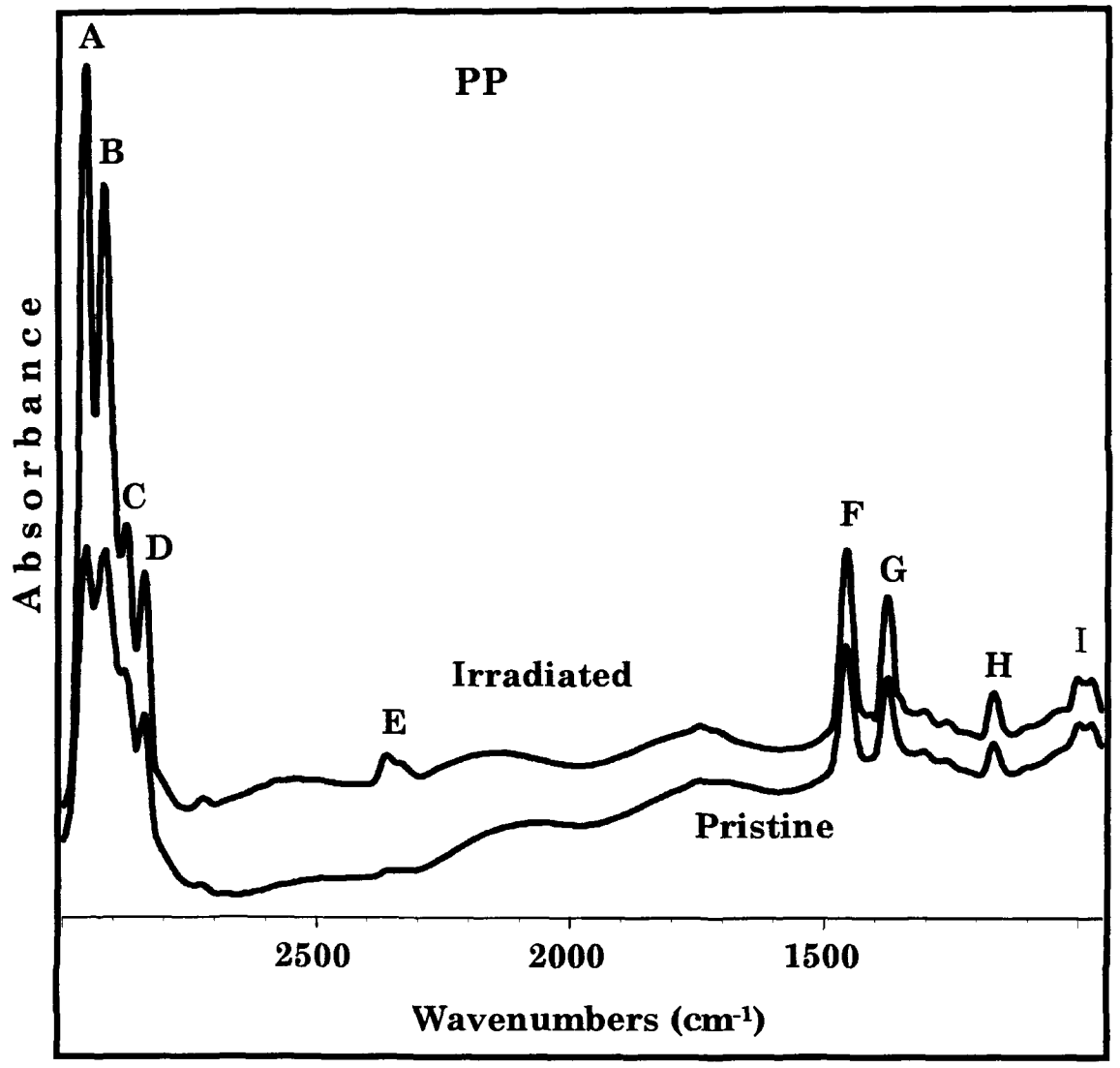

Fig.4.5.4. FT-IR spectra of pristine PP and proton irradiated PP (80 kGy) in the range of 3000-950 cm^{-1}.

(iii) Electron Spin Resonance Spectroscopy

Formation of free radicals could not be traced from the ESR spectral analysis of the irradiated PP. Since the irradiated samples were kept at room temperature for a few months after irradiation, free radicals formed, if any, would have been annihilated during that time.

4.5.4. Thermal Studies

Thermogravimetric analysis and Differential scanning calorimetry were done to characterise pristine and irradiated PP.

(i) Thermogravimetric analysis

The TGA thermograms for the pristine and proton irradiated PP (80 kGy) are shown in Fig.4.5.5. The temperatures corresponding to different decomposition zones are given in Table 4.5.3. The stable zone was found to increase from 102°C (pristine) to 145°C (at highest dose). This increase was linear (roughly) with the dose of the proton irradiation. In slow decomposition zone, only 6% of the total weight of the pristine PP was lost within the temperature range 102-266°C. In the slow decomposition zone of the irradiated PP samples, the weight loss was about 10% for the lower two doses and about 20% for the higher two doses. The terminating temperature of the fast

decomposition zone was found to be increasing from 374°C in pristine to 414°C in the PP irradiated to highest dose (80 kGy).

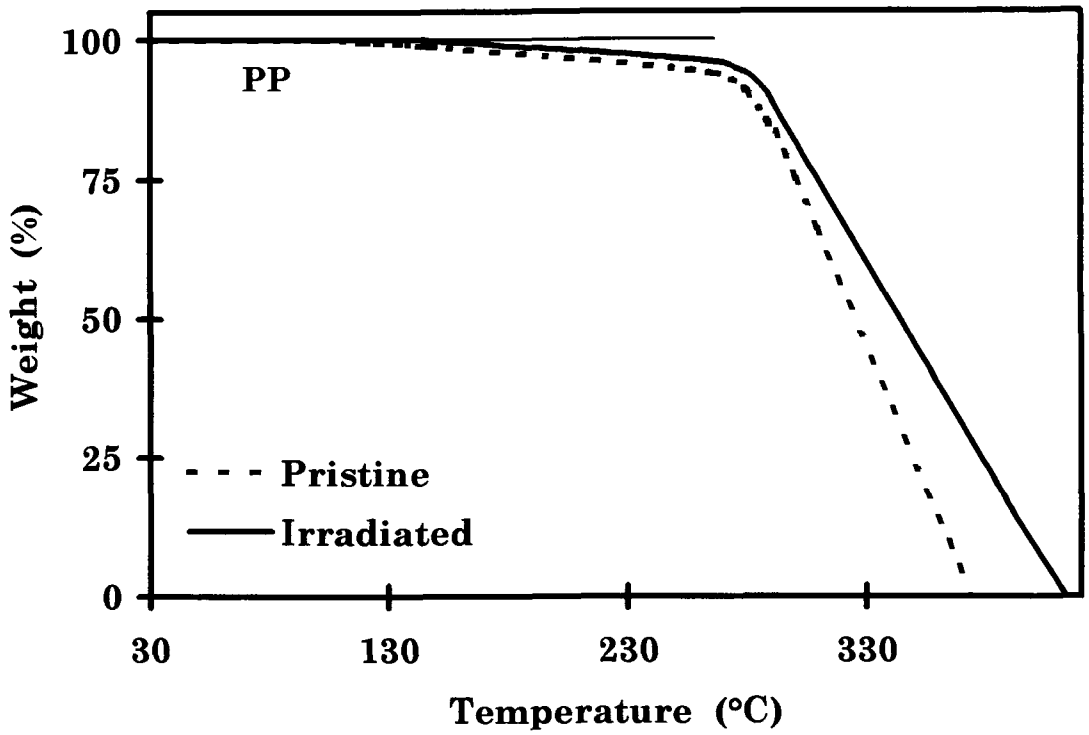

Fig.4.5.5. TGA thermograms of the pristine and the proton irradiated PP (80 kGy).

This overall increase in thermal stability of the polymer was attributed to the cross-linking effect caused by proton irradiation enhancing the crystallinity of the material. This dose dependent modification of the thermal property endorsed the findings of the XRD and FT-IR studies described earlier (section 4.5.2., 4.5.3.).

Table 4.5.3 Thermal decomposition temperatures at different zones for the pristine and the PP samples irradiated to different doses (10, 30, 60, 80 kGy).

Dose (kGy)	Stable zone (°C)	Slow decomposition zone (°C)	Fast decomposition zone (°C)
0	30-102	102-266	266-374
10	30-120	120-280	280-388
30	30-126	126-280	280-389
60	30-138	138-282	282-393
80	30-145	145-289	289-414

(ii) Differential scanning calorimetry

The DSC thermograms showing the exothermic and endothermic transitions in the pristine and the irradiated PP (80 kGy) are shown in Fig.4.5.6. The exothermic peaks exhibiting the temperature of crystallisation (T_c) were observed at 203°C (A_0) in the pristine PP. This exothermic peak suffered a shift in its position for the irradiated PP samples and is observed at around 175°C (A_1) for the proton irradiated PP samples. Similarly, the endothermic peak (B_0) denoting the melting temperatures (T_m) was observed at 212°C for the pristine PP.

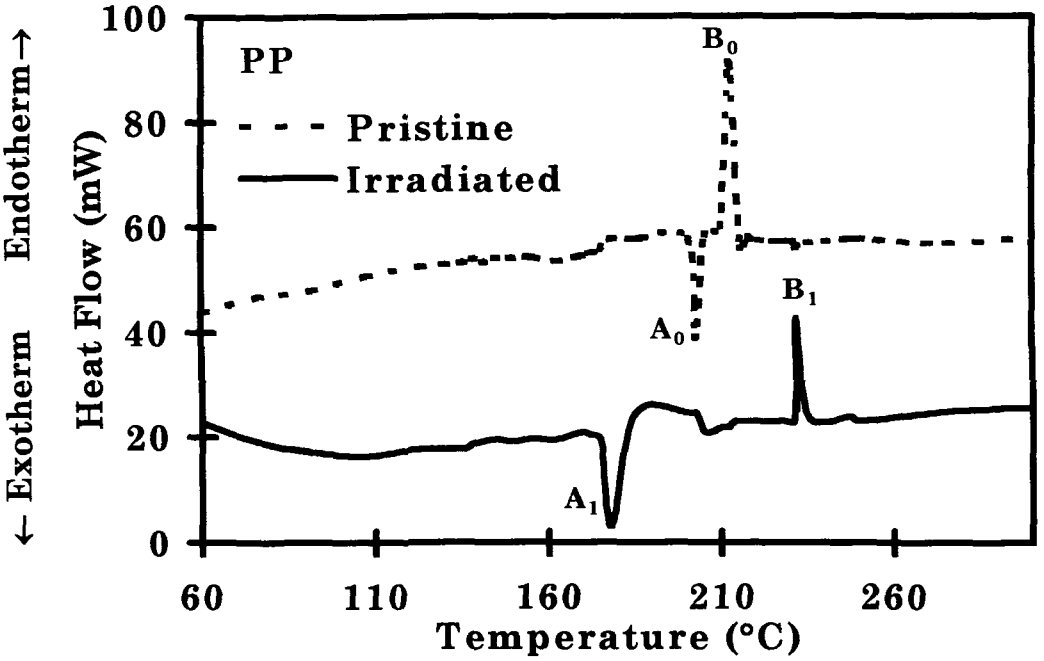

Fig.4.5.6. DSC thermograms of pristine and proton irradiated PP (80 kGy).

This melting temperature increased for the proton irradiated PP samples and was observed at 232°C (B_1) for the proton irradiated PP samples. The increase in melting temperature indicated the improvement in thermal behaviour of PP. This increase in T_m can be related to increase in crystallinity of the polymer as observed from the XRD spectral analysis. This effect can be explained in terms of thermal degradation as follows: The prolonged heating causes a random breaking of bonds and, sometimes, the detachment of low-molecular products. This is due to the reaction of side groups without any appreciable change in the initial molecular weight. The detached

molecular segments can migrate and cause disordered cross-linking of the macromolecules as well as the formation of branched and cross-linked structures. The initial deposition of energy by irradiation has favoured the segmental vibration thereby lowering the T_c values where as the increase in T_m can be attributed to the cross-linking effect thereby enhancing the thermal stability of the polymer [63].

4.6. POLYIMIDE (PI)

The pristine and the proton irradiated PI films at four different doses were characterised by track studies, surface studies, spectroscopic and thermal techniques as follows.

4.6.1. Track Studies

The track diameters were plotted against the corresponding etching times from the slope of which the bulk etch-rate (V_G) was calculated. The log of V_G was plotted against the reciprocal of different etching temperatures (Fig.4.6.1) to calculate the activation energy (E_a) of etching. The values calculated are given in Table 4.6.1. The bulk etch response of PI irradiated to lower doses (10, 30 kGy) was same, which increased slowly for the higher doses. The V_G increased by about 20-30% for the PI irradiated to the highest dose.

Table 4.6.1. The bulk etch-rate (V_G) at different etching temperatures (T_{etch}) and the activation energy of etching (E_a) of the pristine PI and the proton irradiated PI at different doses (10, 30, 60, 80 kGy).

	T_{etch} (°C)	Dose (kGy)				
		0	10	30	60	80
V_G (μm/h)	60	1.3	1.4	1.4	1.5	1.7
	65	1.9	2.0	2.0	2.1	2.3
	70	2.5	2.6	2.6	2.8	3.1
	75	3.4	3.6	3.6	3.8	4.3
E_a (kJ.mol^{-1})		60.6	59.4	59.4	59.0	59.1

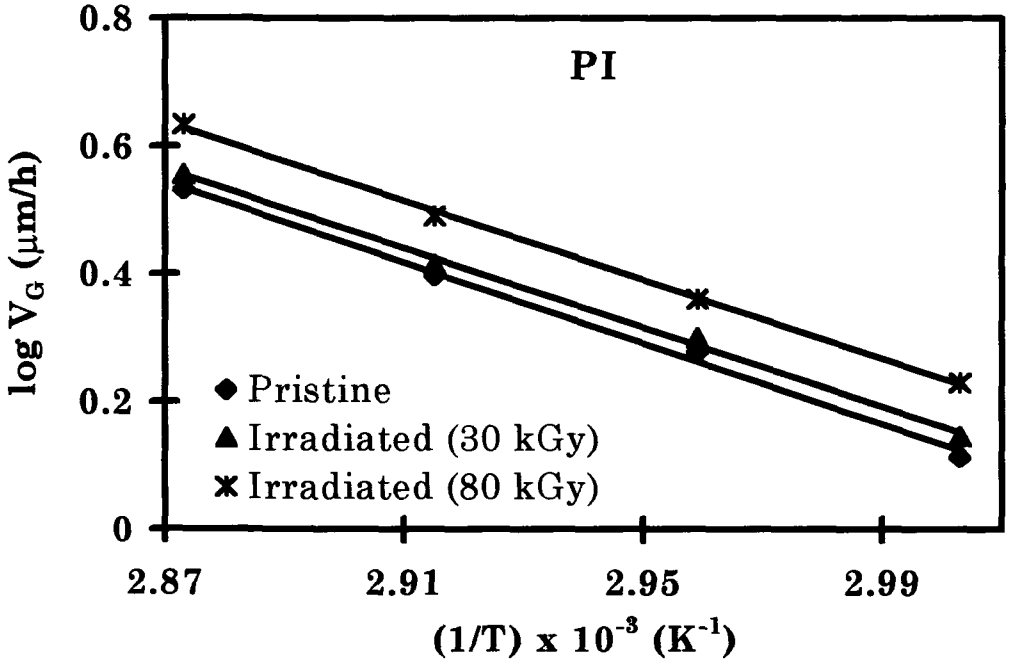

Fig.4.6.1. The plot of log V_G versus the inverse of etching temperature of pristine and proton irradiated PI at two different doses (30 and 80 kGy).

But the activation energy for etching (E_a) remained almost constant, as can be seen from Fig.4.6.1. This shows that the proton irradiation made the polymer easily etchable but the response of bulk material to etching rate at different temperatures remained invariant.

4.6.2. Surface Studies

The topographical analysis of the PI samples was done by Atomic force microscopy (AFM). Fig.4.6.2 represents the AFM micrographs of the pristine and the proton irradiated (80 kGy) PI. The surface roughness (R_q) averaged over 20 different fields were found to be 8.0 ± 0.3 nm for the pristine and 3.9 ± 0.5 nm for the irradiated one. This reduction of surface roughness by about 52% meant that, the proton irradiation had made the surface smooth at the nanoscopic level. This might be due to the production of defects and chemical modification in the bulk and material ejection at the surface as it expected when the insulators are irradiated to energetic ions [62]. This could also be due to a kind of splash mechanism that occurred due to the swelling of the nearby surface in atomic scale around the impinging ions.

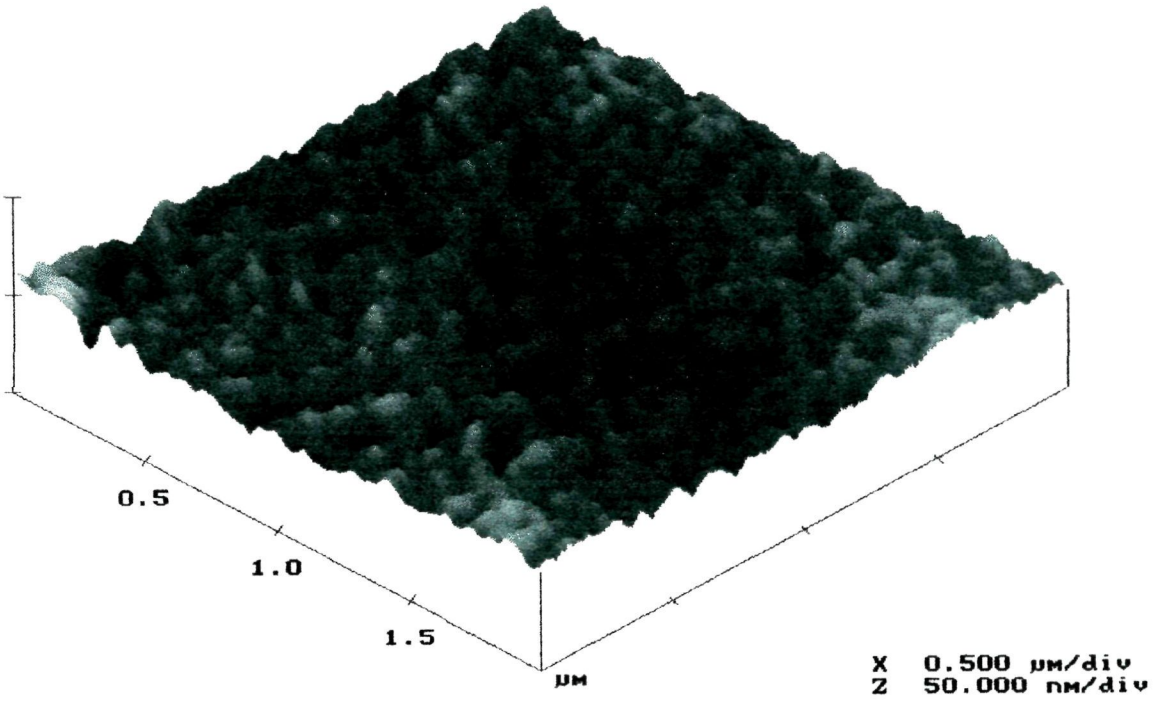

Fig.4.6.2(i) AFM image of the pristine PI.

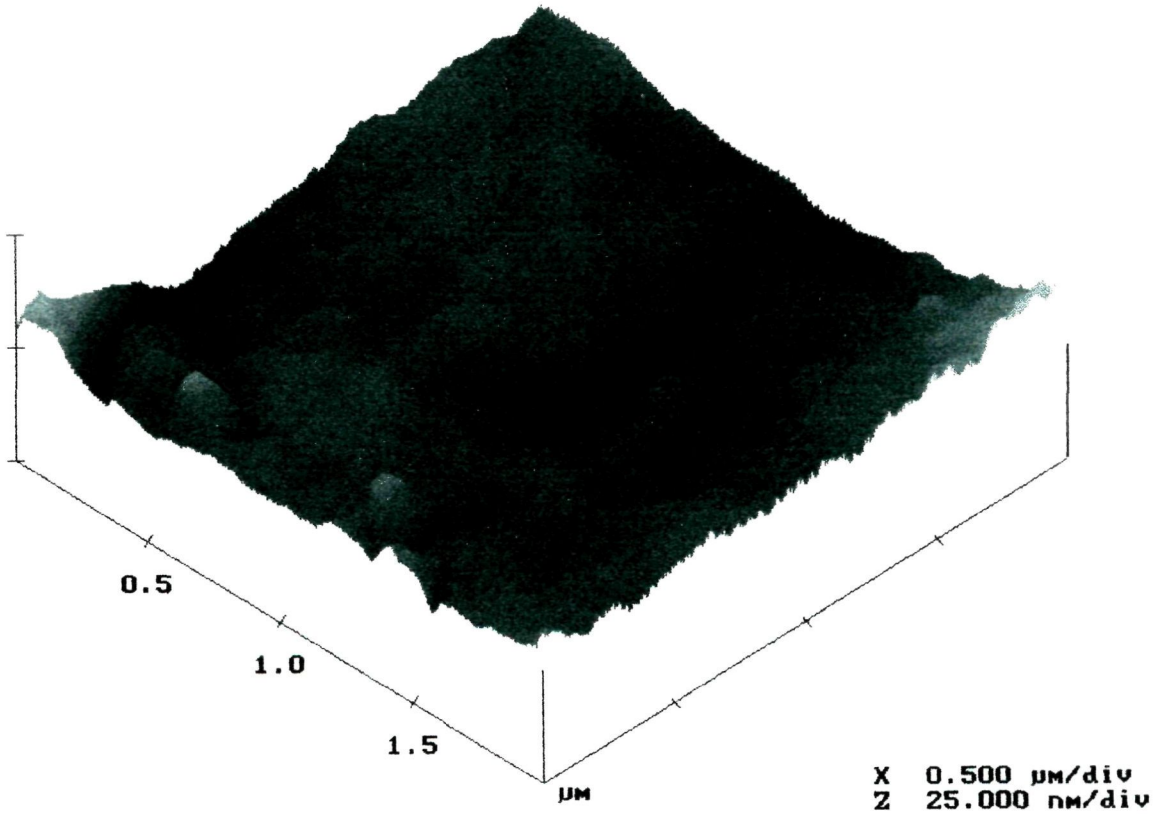

Fig.4.6.2(ii) AFM image of the irradiated PI(80 kGy).

4.6.3. Spectral Analysis

UV-Visible, Fourier Transform Infra-red and Electron Spin Resonance spectroscopy were performed to identify any structural characteristic changes in PI due to proton irradiation.

(i) UV-Vis Spectroscopy

The UV-Vis spectra of the pristine and the irradiated PI samples showed no considerable shifting in the absorbance edges. The optical band-gap in the pristine PI was calculated to be 2.2 ± 0.1 eV which remained constant even after proton irradiation at the highest dose (80 kGy). The aromatic groups present in the backbone structure of the polymer were responsible to delocalise the excitation energy making it radiation resistive. This corroborates the findings of the track study.

(ii) Fourier transform infrared spectroscopy

The FT-IR spectra (Fig.4.6.3) showed no significant shift in the peak positions. Only the absorbance or transmittance value of particular groups was altered. The identification of some absorption bands is given in Table 4.6.2. The increase in absorbance of the bands corresponding to phenyl groups, i.e., 939-602 cm^{-1} (C–H deformation), 1609 cm^{-1} and 1506 cm^{-1} (C–C stretching) was observed, which

indicated some degradation of the polymer due to the proton irradiation.

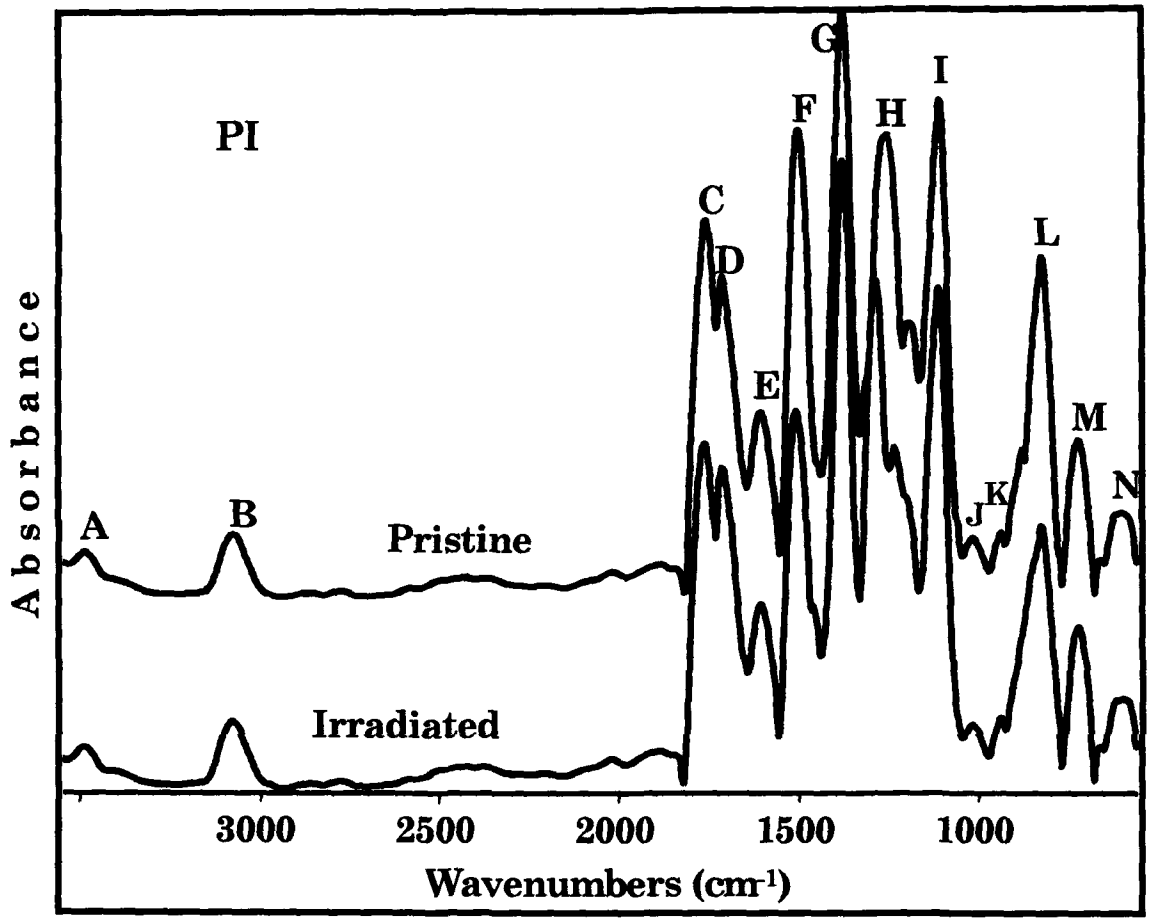

Fig.4.6.3. FT-IR spectra of pristine PI and proton irradiated PI (80 kGy) in the range of 3550-550 cm^{-1}.

It could occur even though aromatic groups present in the repeating units of polymer acted as stabilising elements against radiation induced degradation due to delocalisation of excitation energy in the aromatic units [61]. The characteristic absorbance bands corresponding to alkyne group and unsaturated carbon-nitrogen bonds were not observed even after irradiation by the highest dose. The

irradiation in the presence of air might have contributed to the degradation mechanism in the irradiated polymer.

Table 4.6.2. Identification of absorption bands in PI corresponding to their wavenumbers (1/λ).

Peak	1/λ (cm^{-1})	Identification
A	3490	N-H (normally weak)
B	3079	C-H (ring hydrogen)
C	1762	Aromatic anhydride(C=O)
D	1717	
E	1609	C-C stretching of Phenyl ring,
F	1506	Skeletal plane vibration
G	1381	C-N vibration of aromatic tertiary amines
H	1258	Vibration of aromatic ether group
I	1111	C-C-C stretching (ether)
J	1019	
K	939	
L	827	C-H deformation of phenyl ring
M	724	
N	602	

(iii) Electron Spin Resonance Spectroscopy

Formation of free radicals could not be traced from the ESR spectral analysis of the irradiated PI. Since the irradiated samples

were kept at room temperature for a few months after irradiation, free radicals formed, if any, would have been annihilated during that time.

4.6.4. Thermal Studies

Thermogravimetric analysis and Differential scanning calorimetry were done to characterise the pristine and the irradiated PI samples.

(i) Thermogravimetric analysis

The decomposition behaviour of the polymers was examined by this technique. The thermal stability of PI is known to be very high. The thermogram given in Fig.4.6.4 revealed that the stable zone for the pristine PI was up to 409°C, which slightly increased with increase in dose (up to 417°C for 80 kGy). There was no change in the slow decomposition zone. It was accompanied by a weight loss of about 10% of the total weight. But the terminating temperature for the fast decomposition zone was found to be increasing with the increase in dose as shown in the Table 4.6.3. This denotes that the proton irradiation had modified this polymer to be more thermally resistive. Moreover, the one irradiated to highest dose became so stable that it did not undergo complete decomposition within the recording temperature (800°C) leaving behind about 26% of the total weight

undecomposed. Due to instrumental limitation, the complete decomposition temperature for this sample could not be determined.

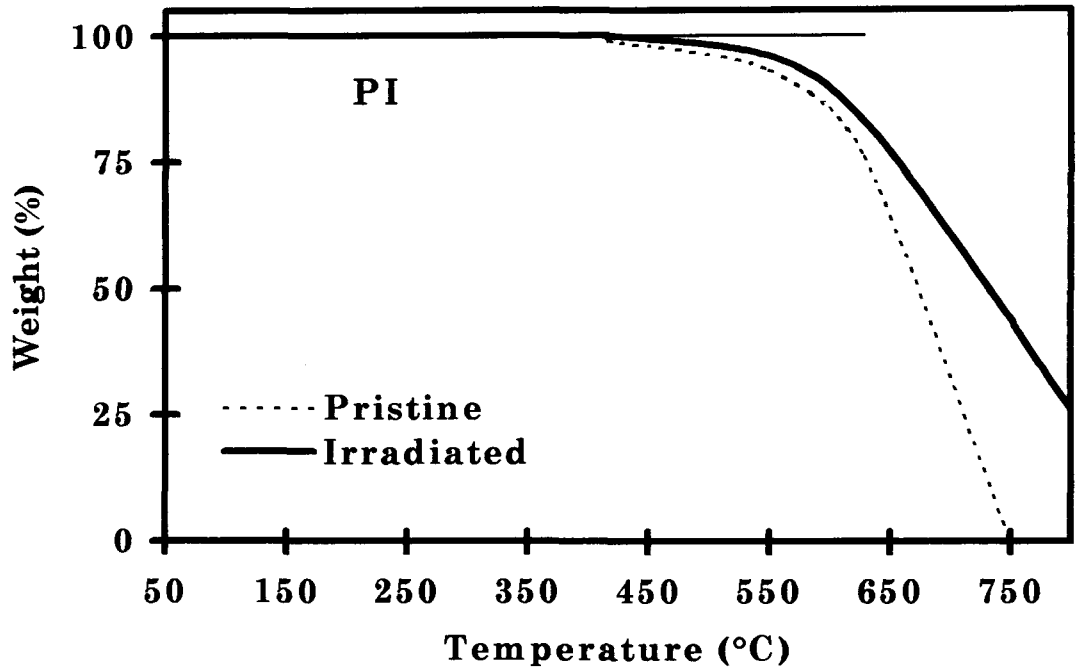

Fig.4.6.4. TGA thermograms of the pristine and the proton irradiated PI (80 kGy).

Table 4.6.3. Thermal decomposition temperatures at different zones for the pristine and the PI samples irradiated to different doses (10, 30, 60, 80 kGy).

Dose (kGy)	Stable zone (°C)	Slow decomposition zone (°C)	Fast decomposition zone (°C)
0	50-409	409-620	620-750
10	50-413	413-620	620-755
30	50-415	415-620	620-780
60	50-415	415-620	620-780
80	50-417	417-620	620 - *

* The complete decomposition temperature is beyond 800°C.

(ii) Differential scanning calorimetry (DSC)

The DSC thermograms of the pristine and proton irradiated PI (80 kGy) are shown in Fig.4.6.5. The exothermic transition (crystallisation) in the pristine PI occurred at around 298°C (A_0), followed by an endothermic peak at 316°C (B_0) denoting the melting temperature of the pristine PI. For the PI irradiated by the highest dose (80 kGy) the transition from exothermic to endothermic started at around 316°C (A_1) revealing the melting peak at about 324°C (B_1). A gradual increase in melting point of PI with increase in proton dose was recorded (Table 4.6.4.).

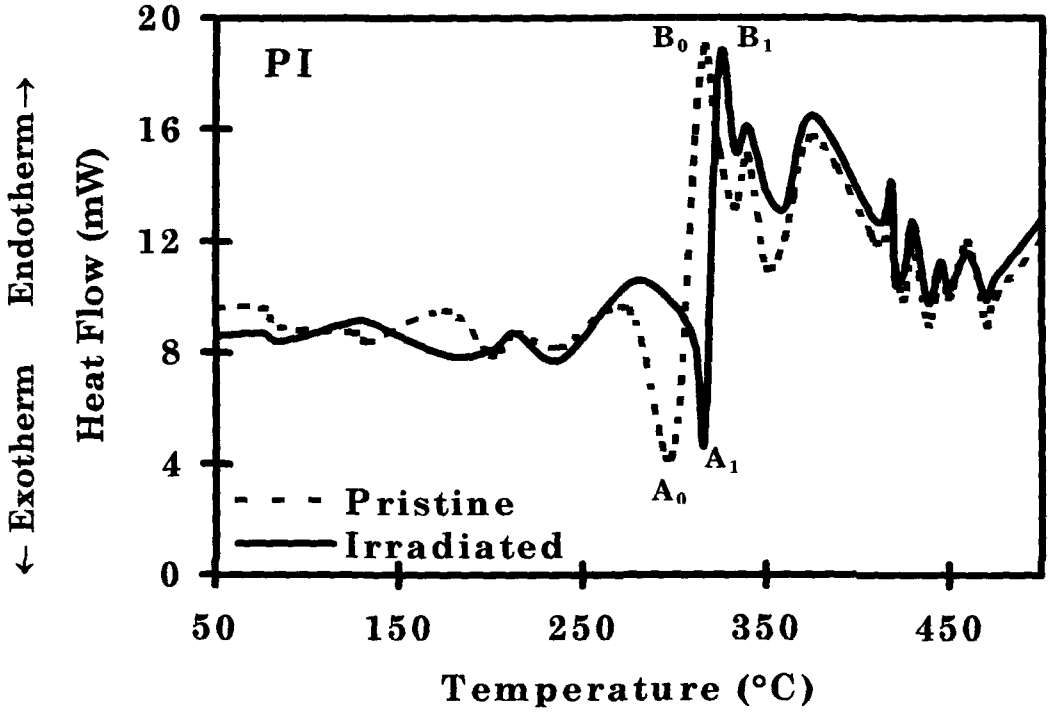

Fig.4.6.5. DSC thermograms of the pristine and the proton irradiated PI (80 kGy).

Table 4.6.4. The temperature of crystallisation (T_c) (exothermic transition) and melting (T_m) (endothermal transition) in pristine PI and proton irradiated PI at different doses (10, 30, 60, 80 kGy).

Dose (kGy)	0	10	30	60	80
T_c (°C)	298	307	307	309	316
T_m (°C)	316	319	320	322	324

4.7. POLYTETRAFLUORO ETHYLENE (PTFE)

The pristine PTFE and the proton irradiated ones were characterised by the following techniques. (1) Surface studies (Atomic Force Microscopy), (2) X-ray diffraction studies, (3) Spectral analysis (UV-Visible, Fourier Transform Infra-red, Electron spin resonance Spectroscopy) and (4) Thermal studies (Thermogravimetric analysis, Differential Scanning Calorimetry).

4.7.1. Surface Studies

The Atomic force microscopy was done to study the surfaces of the pristine and the PTFE irradiated at highest dose of proton (80 kGy). The micrographs are shown in Fig. 4.7.1. On comparing their surfaces, a decrease in surface roughness was found in case of the irradiated one.

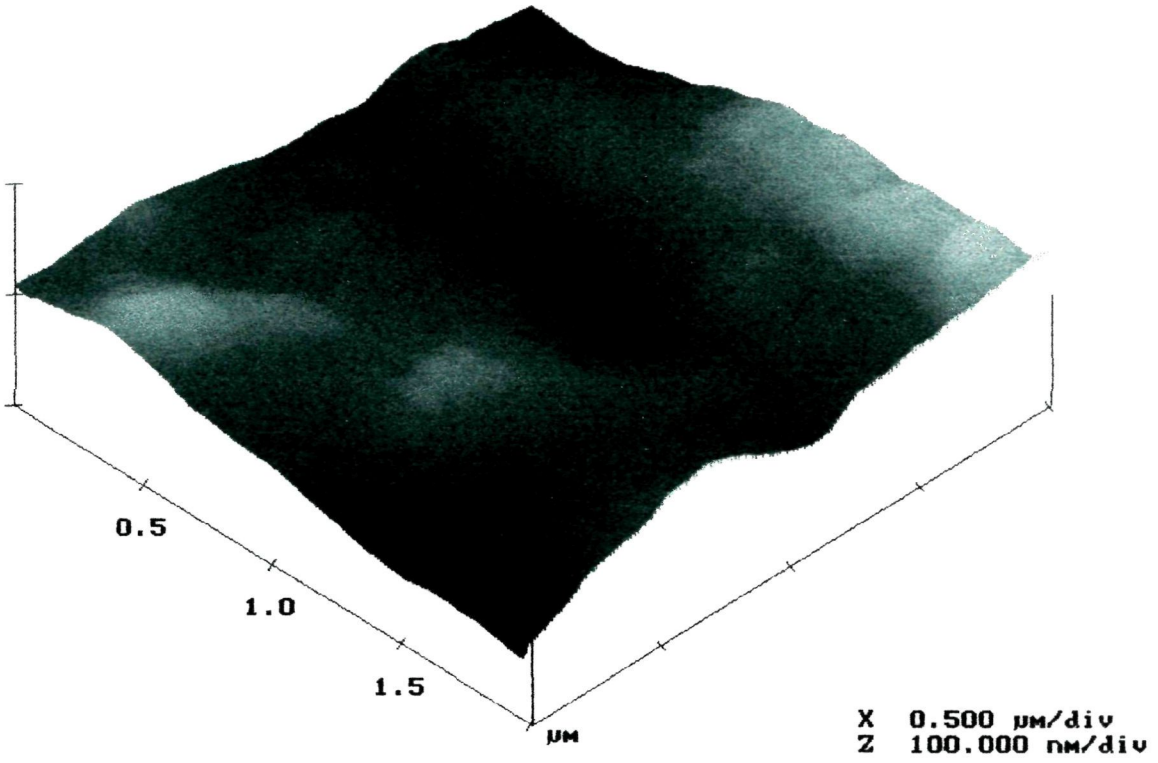

Fig.4.7.1(i) AFM image of the pristine PTFE.

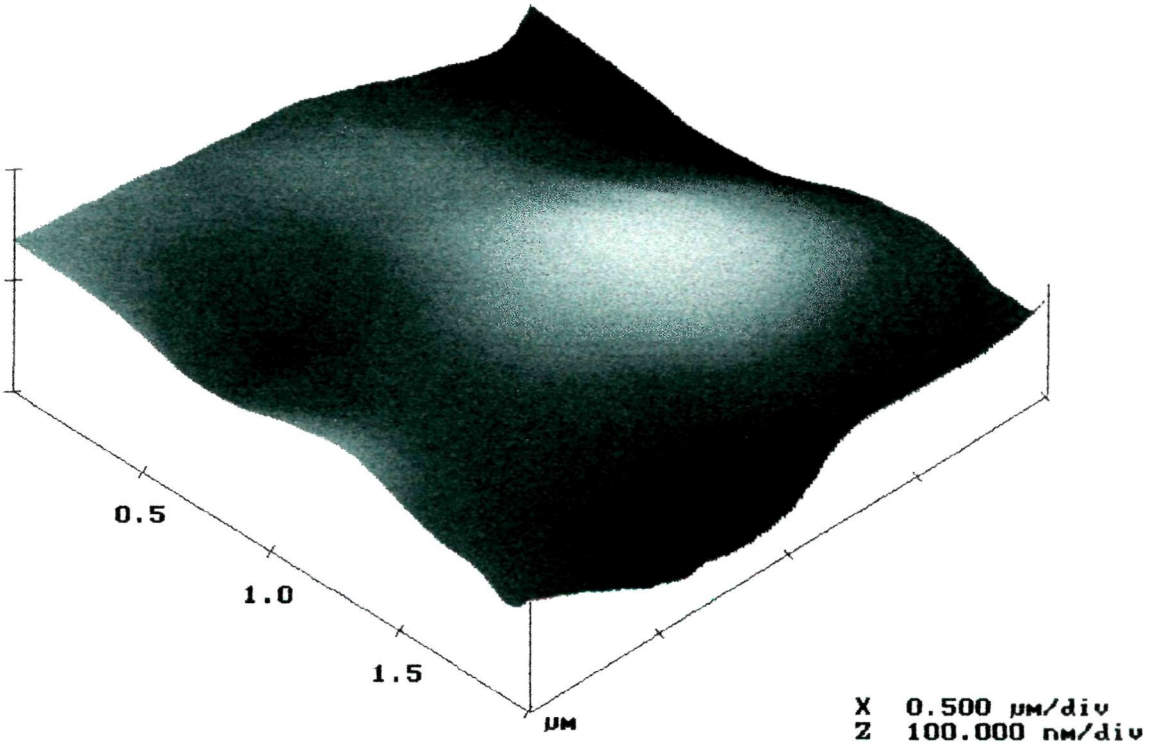

Fig.4.7.1(ii) AFM image of the irradiated PTFE (80 kGy).

Quantitatively, the roughness was found to be 19.4 ± 0.4 nm for the pristine and 9.2 ± 0.4 nm for the irradiated one. This considerable (53%) decrease in roughness could be explained as follows. This might be due to the production of defects and chemical modification in the bulk and material ejection at the surface as it expected when the insulators are irradiated to energetic ions [62].

4.7.2. X-ray Diffraction Analysis

The structures of the pristine (P) and the PTFE irradiated at the highest dose (80 kGy) were analysed by X-ray diffraction studies. The XRD spectra are shown in Fig.4.7.2 and the various parameters assigned with the peaks are given in Table 4.7.1. The result showed that intensity of the main peak (A) at $2\theta=21.79°$ for the pristine was reduced and shifted to $2\theta=17.9°$ for the PTFE irradiated to the highest dose (80 kGy) of proton. The intensity of the other two peaks (B and C) was also decreased after irradiation. The decrease in the main peak intensity and the intensities of the other peaks denoted some destruction of the orderliness of the original crystal structure due to proton irradiation.

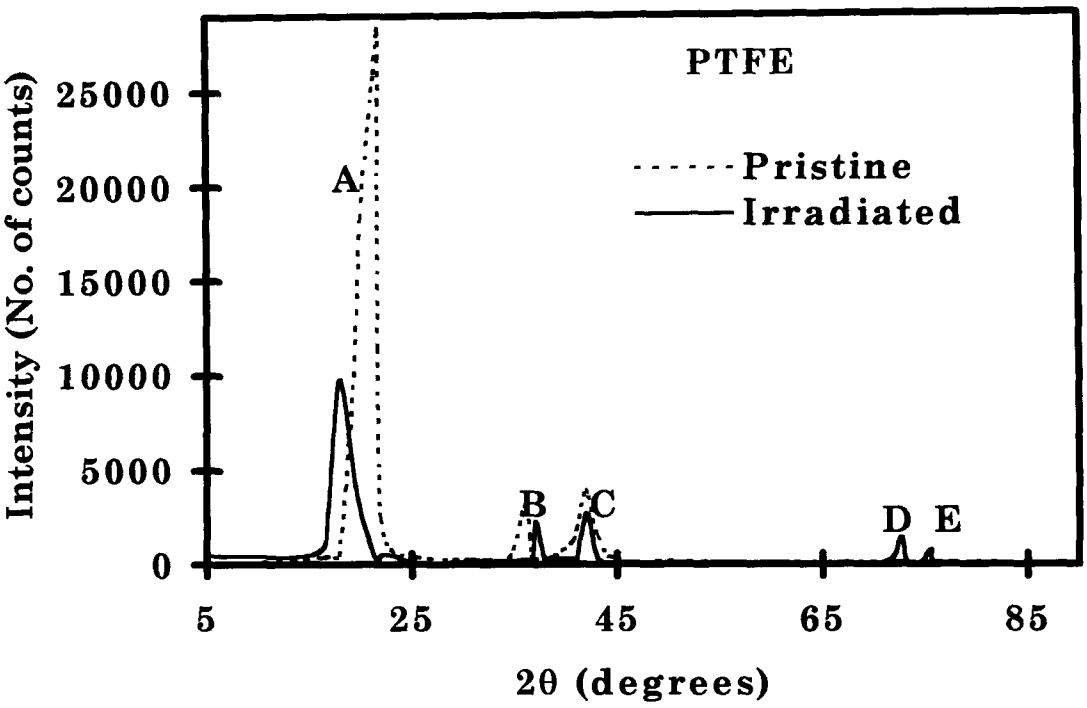

Fig.4.7.2. XRD spectra of the pristine and the proton irradiated PTFE (80 kGy).

Table 4.7.1. Position (2θ), Intensity (I) and full width half maximum (FWHM) of the XRD peaks of the pristine (P) and irradiated PTFE (80 kGy).

Peak	2θ (degree)		I_{rel}		I (CPS)		FWHM (degree)	
	P	80kGy	P	80kGy	P	80kGy	P	80kGy
A	21.79	17.9	100	100	28166	9796	2.60	2.00
B	36.00	36.99	8	23	3103	2281	0.40	0.30
C	42.00	42.00	4	7	3896	2747	2.90	0.29
D	-	72.57	-	15	-	1421	-	0.30
E	-	75.54	-	5	-	460	-	0.30

Some new peaks (D and E) also emerged at 2θ = 72.57° and 75.54° after irradiation (80 kGy). But these were of very low intensity, however at higher doses, these effects may be more pronounced.

4.7.3. Spectral Analysis

UV-Visible, Fourier Transform Infra-red and Electron Spin Resonance spectroscopy were performed to analyse any structural characteristic changes in PTFE due to proton irradiation.

(i) UV-Vis Spectroscopy

A shift of the absorption edge from UV towards visible side was observed in the UV-Vis spectra of PTFE with increase in proton dose. Fig.4.7.3 shows the UV-Vis spectra of the pristine and the PTFE irradiated to the highest proton dose (80 kGy). The optical band-gap (E_g) of PTFE was reduced from 1.1 ± 0.1 eV in pristine to about 0.8 ± 0.1 eV in PTFE irradiated to 80 kGy of proton (Table 4.7.2).

Table 4.7.2. Wavelength-gap (λ_g) and Optical band-gap (E_g) for the pristine and the proton irradiated PTFE at different doses (10, 30, 60, 80 kGy).

Dose (kGy)	0	10	30	60	80
λ_g (nm)	1141.5	1383.6	1370.7	1424.5	1468.2
E_g(eV)	1.1	0.9	0.9	0.9	0.8

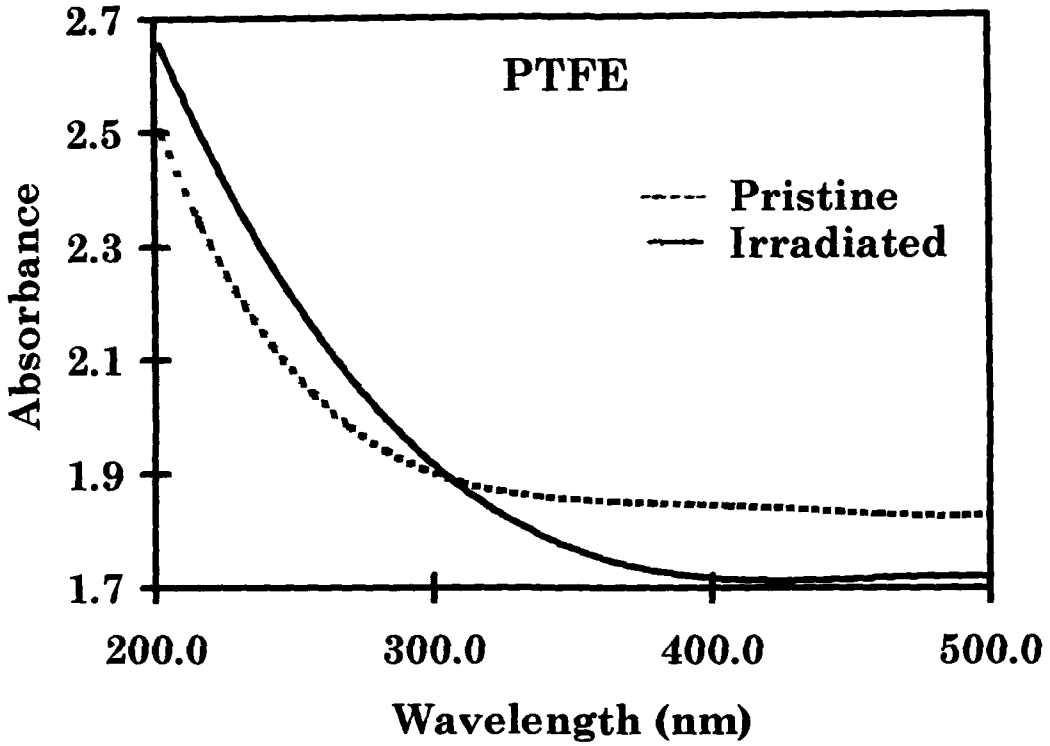

Fig.4.7.3. UV-Vis spectra of the pristine and proton irradiated PTFE (80 kGy).

(ii) Fourier transform Infra-red Spectroscopy

The FT-IR spectra of the pristine and the proton irradiated (80 kGy) PTFE are shown in Fig.4.7.4. The absorbance peaks from 1000 cm^{-1} to 1300 cm^{-1} (C) are contributions of the C-F stretching vibration [60]. Some new peaks emerged in case of the irradiated PTFE samples. The new peak at 1885 cm^{-1} (A) is originated from the carbonyl fluoride group (-COF) and that at 1795 cm^{-1} (B) is assigned to $CF=CF_2$ terminal double bond vibration [47, 64]. Here, the structure of the polymer (given in chapter 2, section 2.1.7) might be visualised as polyethylene with all its hydrogen atoms substituted by fluorine,

where C-F coupling was less covalent than C-C coupling due to more electronegativity of fluorine. This made the C-C bond relatively less probable towards cleavage.

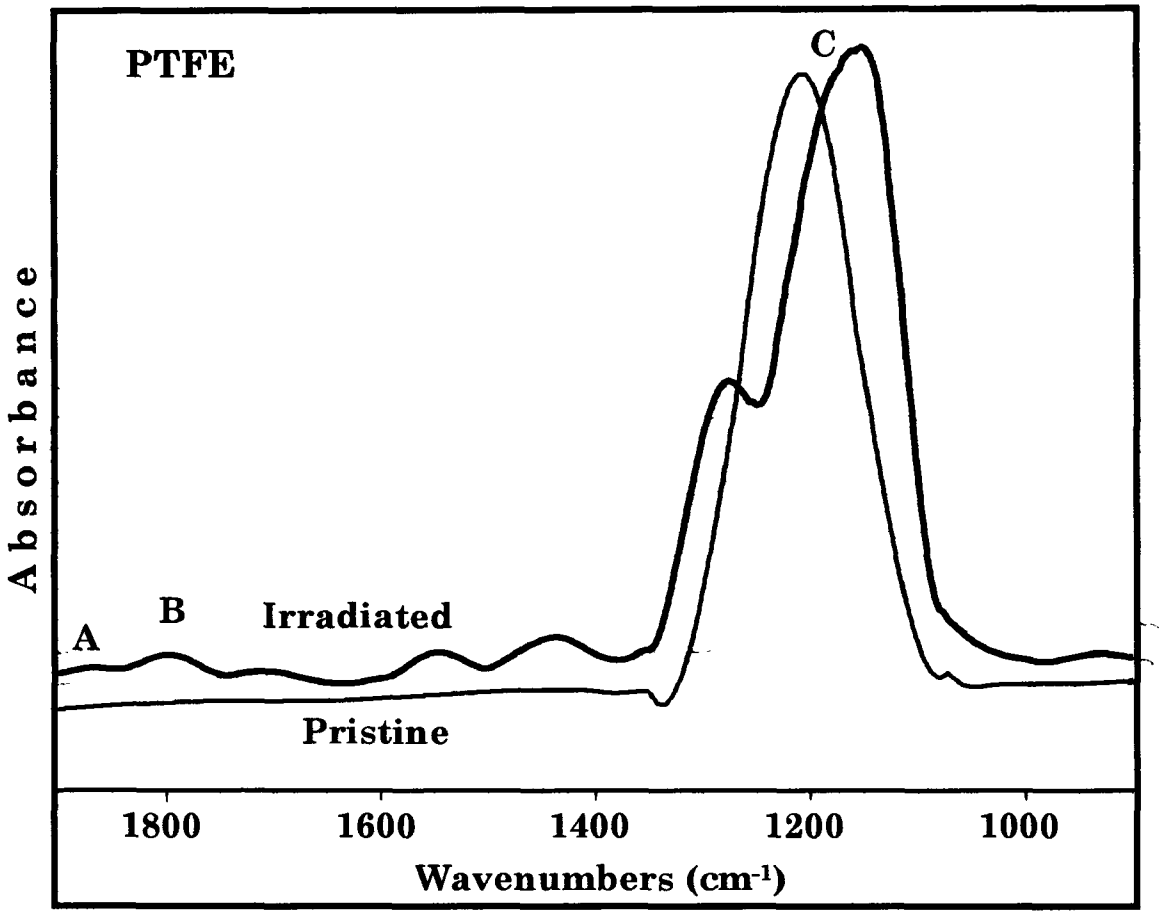

Fig.4.7.4. FT-IR spectra of the pristine and the proton irradiated PTFE (80 kGy) in the range of 1900-900cm^{-1}.

(iii) Electron spin resonance spectroscopy

The ESR spectrophotometer recorded a signal of free radical formation for the polymer irradiated to the highest dose. The spectra are shown in Fig.4.7.5.

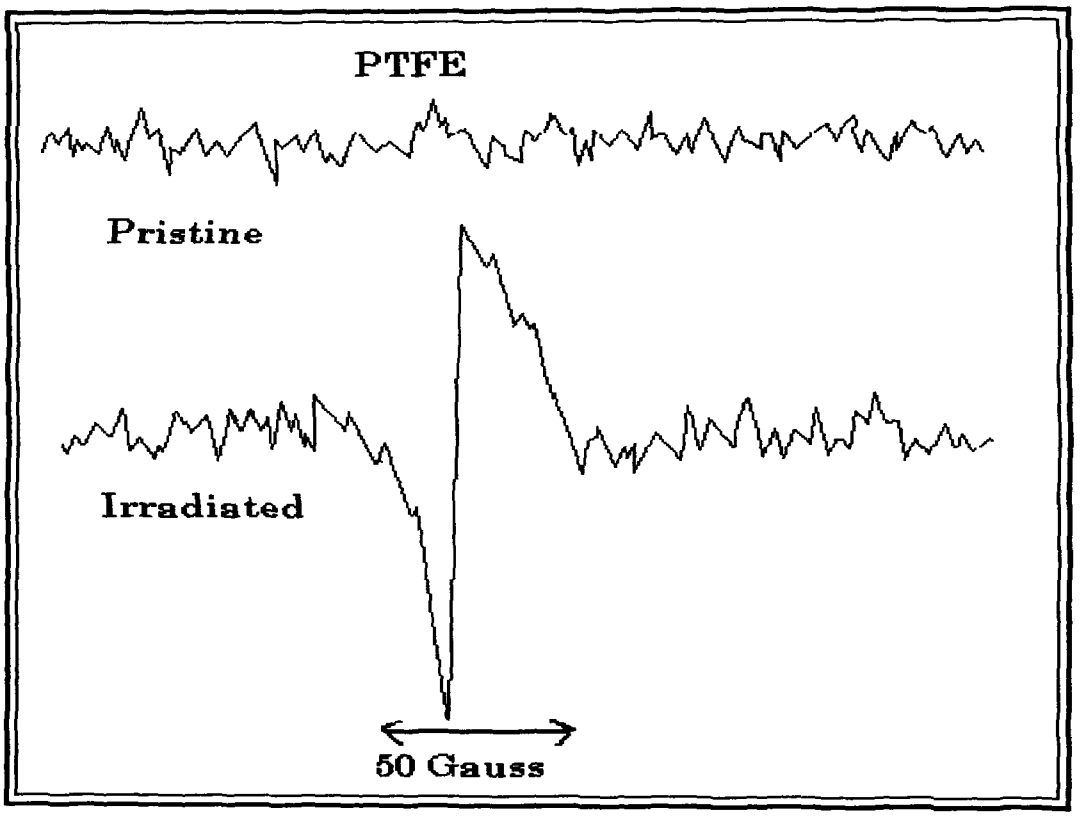

Fig.4.7.5. ESR spectra of the pristine and the proton irradiated PTFE (80 kGy) showing the free radical signal.

The width of the signal formed was around 50 Gauss, which was usually attributed to σ-bond. Since, the irradiation was done in the presence of oxygen, so a number of radiolysis products were formed (CF_4 and C_2F_6 in small amounts, high proportion of COF_2). These products were formed by random splitting of C-C bonds and C-F bonds to give radicals. Oxygen would add to organic radicals to give peroxy-radicals, which could react together to form alkoxy radicals as shown below [65].

$$—CF_2—CF_2^{\bullet} + O_2 \rightarrow —CF_2—CF_2O_2^{\bullet}$$

$$2\,—CF_2—CF_2O_2^{\bullet} \rightarrow 2\,—CF_2\,CF_2O^{\bullet} + O_2$$

Dissociation of alkoxy radicals produces carbonyl fluoride and a new organic radical by one -CF_2- unit as follows-

$$—CF_2—CF_2O^{\bullet} \rightarrow —CF_2^{\bullet} + COF_2$$

Formation of free radicals could not be traced from the ESR spectral analysis for the pristine and the irradiated PTFE at three lower doses (10 kGy, 30 kGy and 60 kGy) except for the highest dose (80 kGy). Since the irradiated samples were kept at room temperature for a few months after irradiation, the free radicals formed could have been annihilated during that time. The PTFE irradiated to 80 kGy dose of proton formed a relatively stable radical, which was detected by the instrument. This revealed that, the proton irradiation (80 kGy) in the polymer PTFE led to chain-scission resulting in the formation of free radicals. Increase in conductivity of PTFE irradiated by 80 kGy of proton as revealed by UV-Vis spectroscopy was possibly due to the formation of this free radical.

4.7.4. Thermal Studies

Thermogravimetric analysis and Differential scanning calorimetry were done to characterise the pristine and the irradiated PTFE films.

(i) Thermogravimetric analysis

The TGA thermograms of the pristine and the irradiated PTFE (80 kGy) are shown in Fig.4.7.6. The thermal stability was found to be decreasing with increase in proton dose. The temperature values for different decomposition zones are listed in Table 4.7.3.

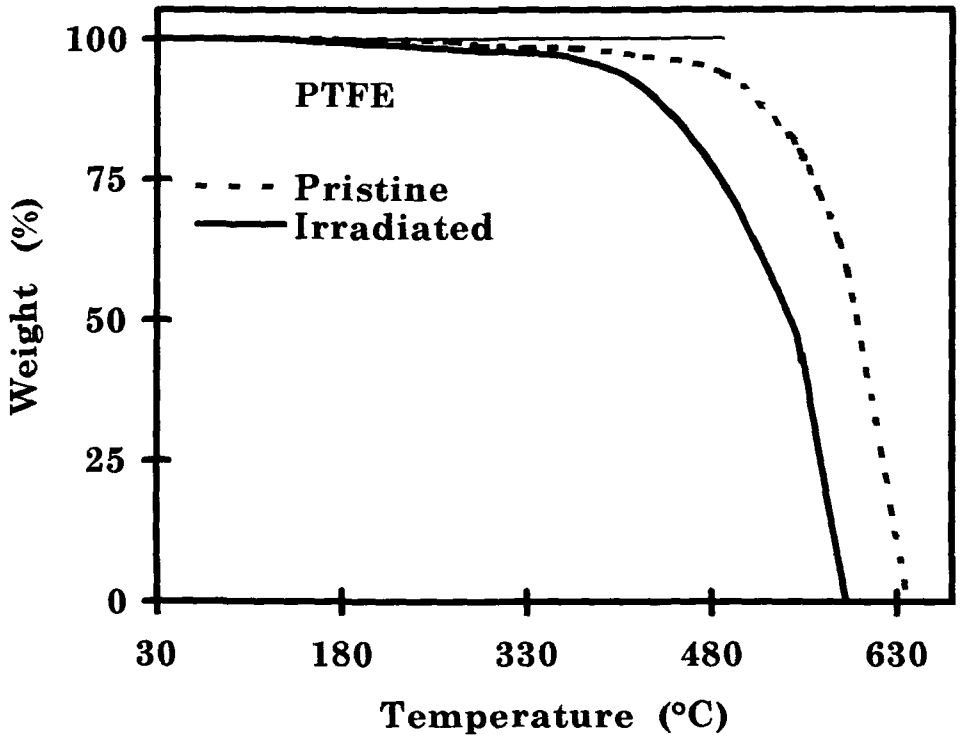

Fig.4.7.6. TGA thermograms of the pristine and the proton irradiated PTFE (80 kGy).

The stable zone of decomposition was reduced from 264°C in the pristine to 125°C for the PTFE irradiated to 80 kGy of proton. Similarly, the slow decomposition zone (of about 5% weight loss) as well as the fast decomposition zone decreased with increase in proton dose.

Table 4.7.3. Thermal decomposition temperatures at different zones for the pristine and the PTFE samples irradiated to different doses (10, 30, 60, 80 kGy).

Dose (kGy)	Stable zone(°C)	Slow decomposition zone (°C)	Fast decomposition zone (°C)
0	30-264	264-470	470-639
10	30-257	257-442	442-631
30	30-244	244-439	439-625
60	30-157	157-425	425-613
80	30-125	125-418	418-607

(ii) Differential scanning calorimetry

DSC analysis revealed a decrease in melting temperature of PTFE with increase in dose of proton irradiation. The DSC thermograms of the pristine and the proton irradiated PTFE (80 kGy) are shown in Fig.4.7.7.

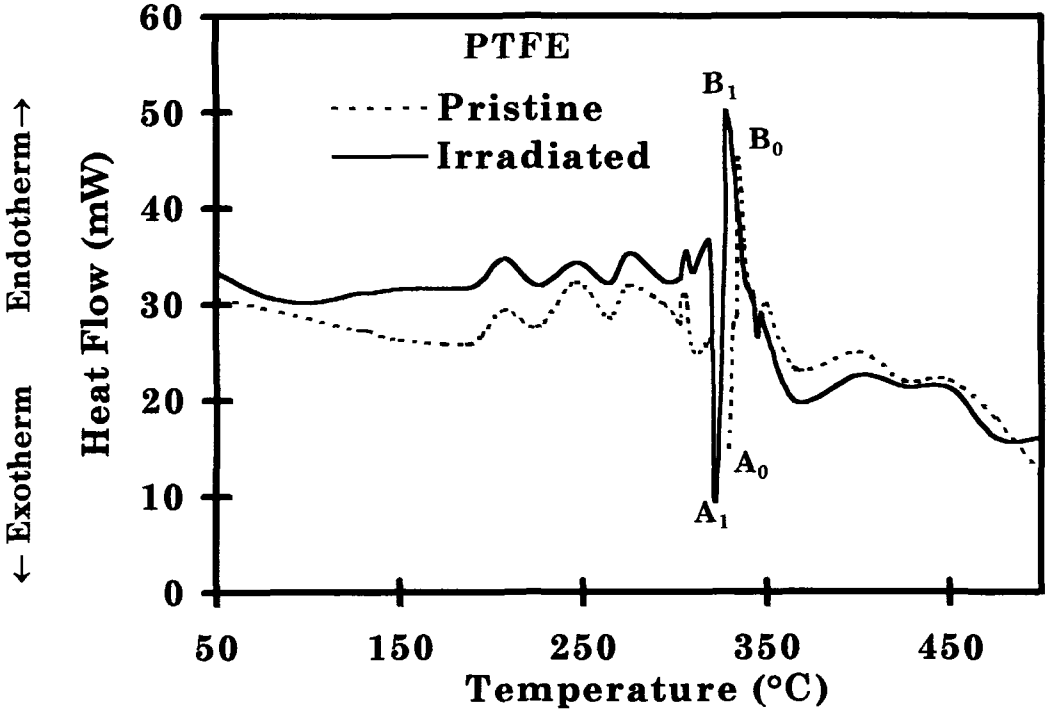

Fig.4.7.7. DSC thermograms of the pristine PTFE and the proton irradiated PTFE (80 kGy).

In the pristine PTFE, endothermic distortions started at around 208°C and continued up to 330°C (A_0), at which a transition from exothermic to endothermic occurred. The melting endotherm was observed at 334°C (B_0). For the irradiated samples, endothermic distortions started at around 205°C and continued up to 327°C (A_1), at which a transition from exothermic to endothermic occurred. The melting temperatures gradually decreased with increase in dose and were found to be 330°C, 328°C, 324°C and 321°C (B_1) for the samples irradiated by 10, 30, 60 and 80 kGy respectively. This finding is in

accordance with the other studies and supports the fact that PTFE underwent chain-scission by proton irradiation.

4.8. POLYALLYLDIGLYCOL CARBONATE (PADC)

The proton irradiated PADC samples of S1, S2, S3 and S4 stacks were characterised by track studies, surface studies, spectroscopic and thermal techniques as described below (section 4.8.1). The fission track development and the effect of fullerene destruction on PADC samples of S5 stack were studied by track technique and are described in section 4.8.2. Effect of proton irradiation through metal foils on heavy-ion track registration property of PADC samples of S6 and S7 stacks is discussed in section 4.8.3.

4.8.1. Analysis of PADC samples of S1, S2, S3 and S4 stacks

(a) Track Studies

The damaged trails in the polymer caused by fission fragments were fixed through suitable chemical treatment, leading to the development of optically visible microscopic tracks. The bulk etch-rate (V_G) was calculated by track diameter method using the equations as described in chapter 3. There were no well-defined tracks for the highly energetic proton ions on their passage through the target

material, which could be developed and fixed through chemical etching. However, pre-proton irradiated PADC was effective in registering the tracks of other heavy ions. Further the higher the dose of proton irradiation, the greater is the energy deposition in the material and hence the fission tracks in PADC were etched at a faster rate. Fig.4.8.1 shows the increase in fission fragment track diameters with etching time in the pristine and the irradiated PADC samples.

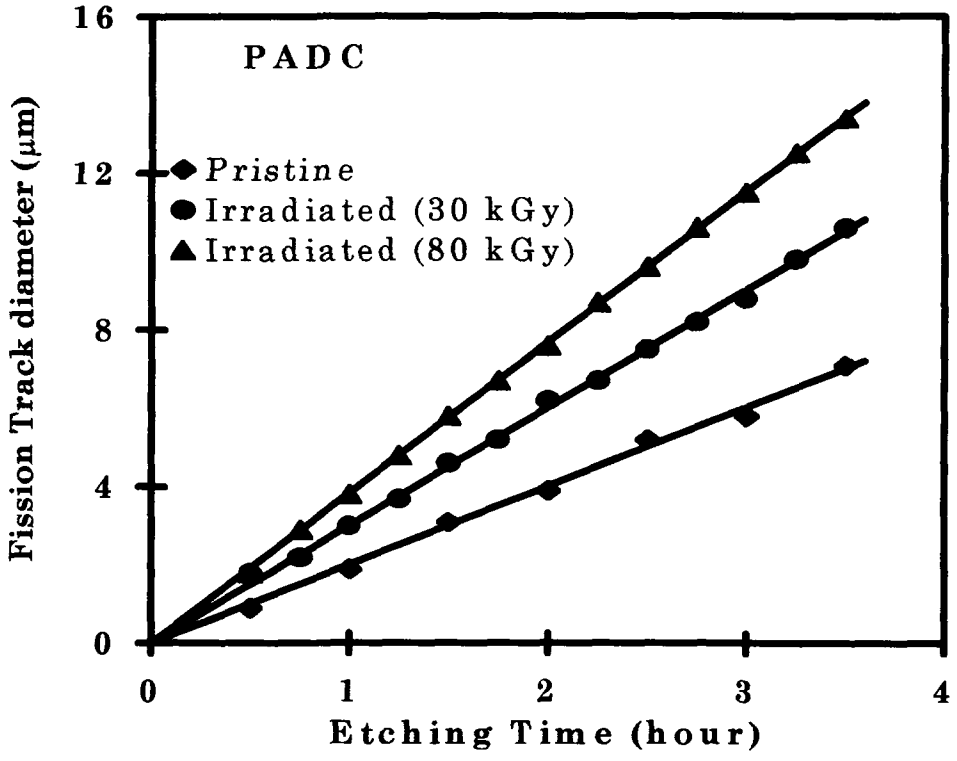

Fig.4.8.1. Plot of fission track diameters versus etching time for the pristine and the PADC samples irradiated by 30kGy and 80kGy of 62 MeV proton.

The V_G was found to be 1.0 μm/h for the pristine PADC which increased to 1.3, 1.5, 1.7 and 1.9 μm/h for the PADC samples irradiated at 10kGy, 30kGy, 60kGy and 80kGy of 62 MeV proton respectively. The proton irradiation has made the polymer very sensitive to bulk etching response.

(b) Surface Studies

Atomic force microscopy (AFM) was done in ambient atmosphere to obtain the surface image of the pristine and the proton irradiated PADC (80kGy). Fig.4.8.2 represents the AFM micrographs of the samples. The surface roughness (R_q), averaged over 20 different fields was found to be 5 ± 0.4 nm for the pristine and 4.4 ± 0.4 nm for the irradiated sample. This reduction of surface roughness by about 12% indicates that the surface becomes smooth after irradiation. This might be due to the production of defects and chemical modification in the bulk and material ejection at the surface as it expected when the insulators are irradiated to energetic ions [62]. Thus, if the energetic ions hit the target material in a regularly distributed manner all over its surface, then the smoothness of the surface would increase at the nanoscopic level.

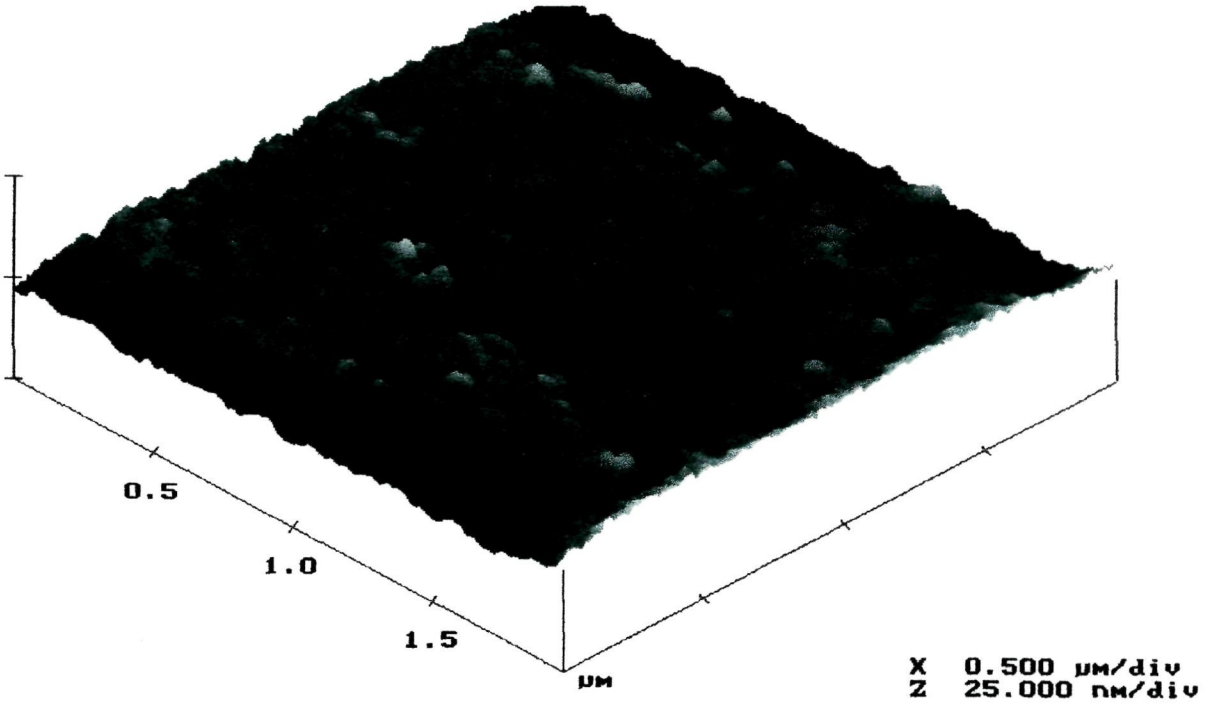

Fig.4.8.2 (i). AFM image of the pristine PADC.

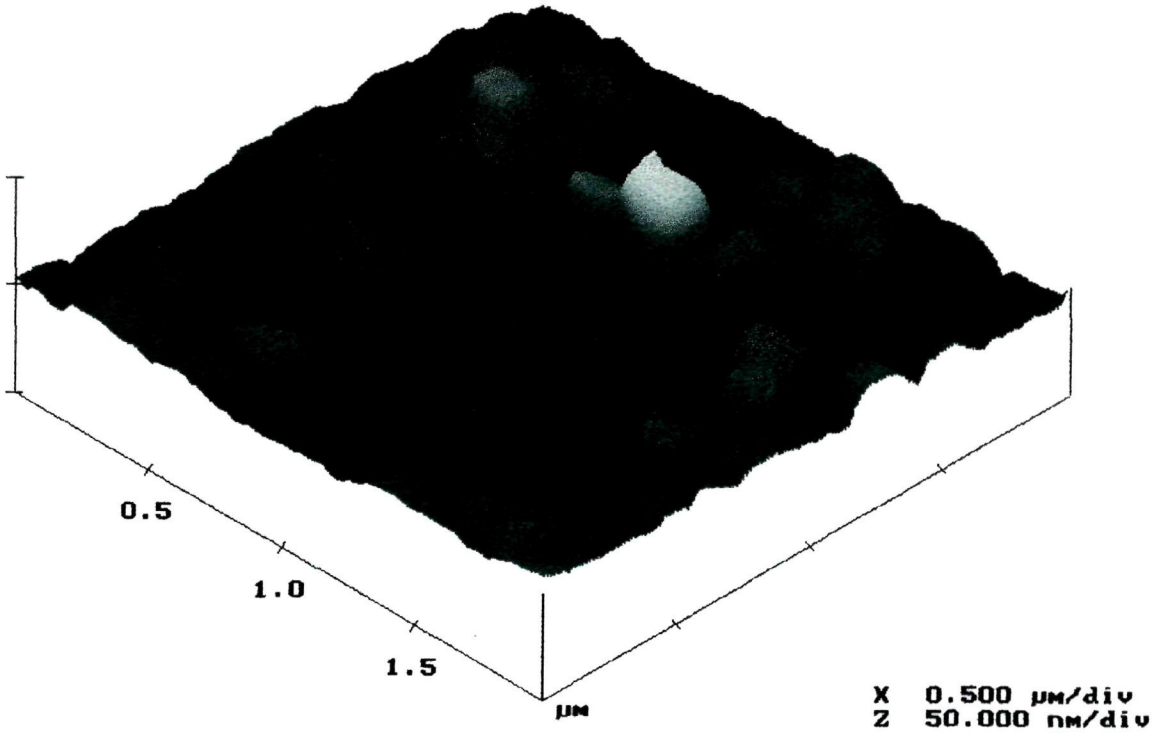

Fig.4.8.2 (ii). AFM image of the irradiated PADC (80 kGy).

(c) Spectral Analysis

The pristine as well as the irradiated PADC samples were characterised by three spectroscopic techniques, viz. (i) UV-Visible (ii) Fourier Transform Infra-red and (iii) Electron spin resonance to check the alternation in band gap, structural changes and free radical formation respectively due to proton irradiation at various doses.

(i) UV-Visible Spectroscopy

The absorption edges in the UV-Vis spectra of the pristine and proton irradiated PADC samples do not suffer any considerable shift, thereby maintaining the constancy of the band-gap (E_g). Using the equations 2.11 and 2.12 as described earlier in chapter 2, the wavelength-gaps (λ_g) and the energy band-gaps (E_g) are derived for the pristine and the proton irradiated PADC samples at four different doses. The E_g was found to be 3.5 ± 0.1 eV for the pristine PADC, which remained unchanged even for the PADC sample irradiated at the highest dose (80 kGy) of 62 MeV proton.

(ii) Fourier Transform Infrared Spectroscopy

FT-IR spectra of the pristine and proton irradiated PADC samples at different doses were recorded as shown in Fig.4.8.3. It can be seen from the spectra that there is a considerable change in the

positions of the absorption bands. Most of the peaks vanished completely after irradiation.

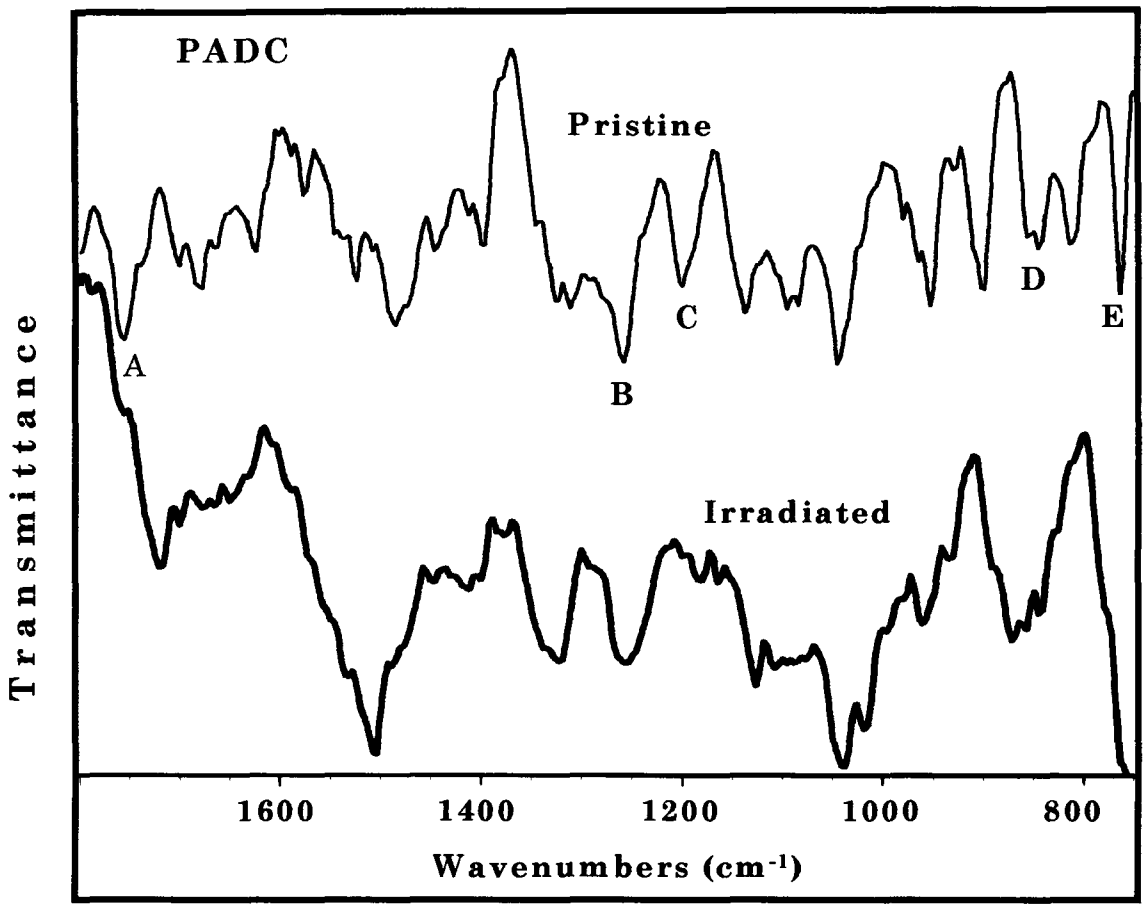

Fig.4.8.3. FT-IR spectra of the pristine PADC and proton irradiated PADC (80kGy) in the range of 1800-750 cm^{-1}.

The absorption bands, as obtained from the spectrum of pristine PADC, are identified as: (A) 1751 cm^{-1} (νC=O), (B) 1276 cm^{-1} (νC-O), (C) 1193 cm^{-1} (νC-O-C, νC-C), (D) 875 cm^{-1} (rC-H) and (E) 784 cm^{-1} (γC-H, νC-C) [59]. These are either shifted with reduced transmittance or vanished completely in case of the irradiated PADC samples denoting that degradation is the main effect induced by proton irradiation.

(iii) Electron Spin Resonance Spectroscopy

ESR spectral analysis showed the absence of any free radical in the irradiated PADC. This was probably due to the fact that the irradiated samples were kept at room temperature for a few months during which the free radicals formed might have been annihilated. So from this study, no conclusion could be ascertained regarding the free radical formation.

(d) Thermal Studies

The thermal responses of the PADC samples were verified by two thermal techniques. viz. (i) Thermogravimetric analysis and (ii) Differential scanning calorimetry.

(i) Thermogravimetric analysis

The thermograms shown in Fig.4.8.4 represent the mode of decomposition of the pristine and the irradiated PADC samples. The results derived from the thermograms are given in Table 4.8.1. In all the cases (pristine and irradiated), a stable zone (no weight loss), slow decomposition zone, fast decomposition zone and residual decomposition zone were observed. The stable zone of the pristine PADC was found to be up to 118°C, which reduced as a function of increased proton doses and reached a value of 90°C for the PADC irradiated to the highest dose (80 kGy).

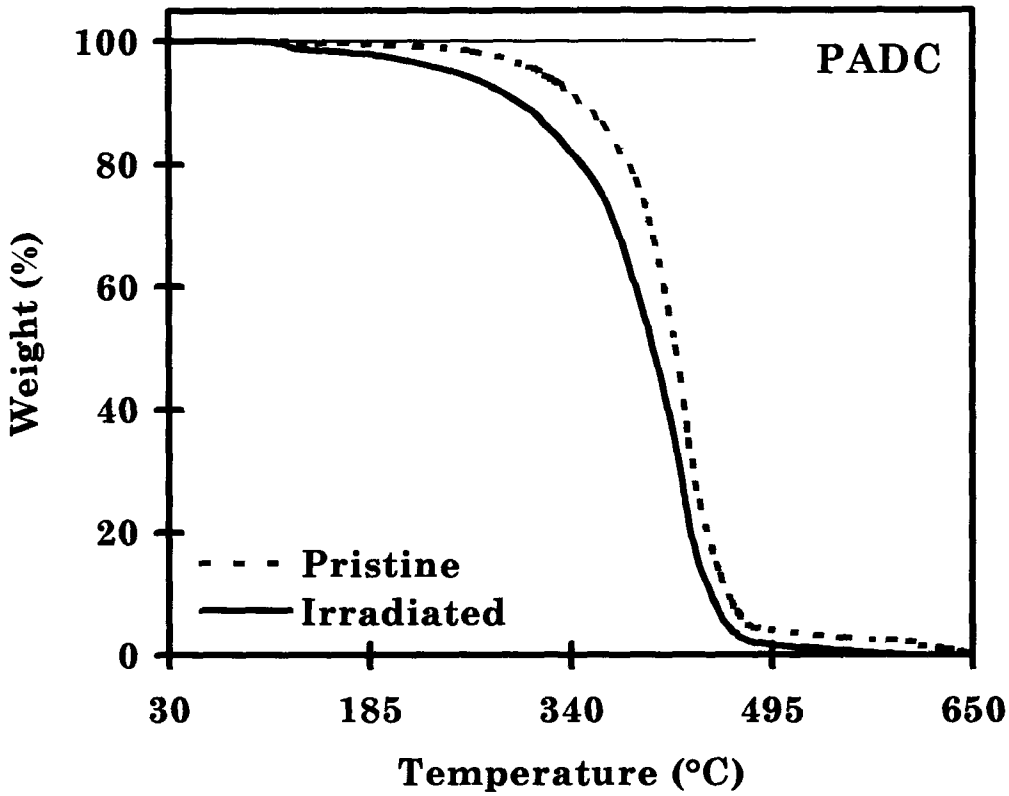

Fig.4.8.4. TGA thermograms of the pristine and the proton irradiated PADC (80 kGy).

A similar kind of trend was observed for all the other zones too. The end point of the fast decomposition zone reduced slowly from 481°C for the pristine PADC to 468°C for the irradiated PADC at highest dose (80 kGy). The remaining 3-7% of total weight that was left behind, decomposed in the residual zone. The whole mechanism was terminated at 650°C for the pristine and at about 600°C for the irradiated PADC samples. The proton irradiation favoured the segmental vibration of the polymeric molecules at an early temperature than that for the pristine suggesting that the polymer

has undergone degradation due to proton bombardment. This effect was also found to be directly related to the dose of irradiation, i.e., the more the dose the less was the tolerance of the polymer to heat.

Table 4.8.1. Thermal decomposition temperatures at different zones for the pristine and the PADC samples irradiated to different doses (10, 30, 60, 80 kGy).

Dose (kGy)	Stable zone (°C)	Slow decomposition zone (°C)	Fast decomposition zone (°C)	Residual decomposition zone (°C)
0	30-118	118-332	332-481	481-650
10	30-110	110-328	328-470	470-610
30	30-90	90-320	320-470	470-600
60	30-90	90-320	320-468	468-600
80	30-90	90-308	308-468	465-600

(ii) Differential Scanning Calorimetry

Fig.4.8.5 shows the DSC thermograms of the pristine and the proton irradiated PADC samples at different doses. One small exotherm at 315°C and a broad exotherm at 407°C were observed in all the cases (Pristine and all irradiated PADC samples). The heat capacities involved in the exothermic process at 407°C are 5.4 $kJ.g^{-1}$ for the pristine and 3.8, 3.8, 3.6 and 3.2 $kJ.g^{-1}$ for the PADC samples

irradiated to the doses of 10, 30, 60 and 80 kGy respectively. The thermograms were recorded with an error of ± 2°C. There was no endotherm within the measured temperature range.

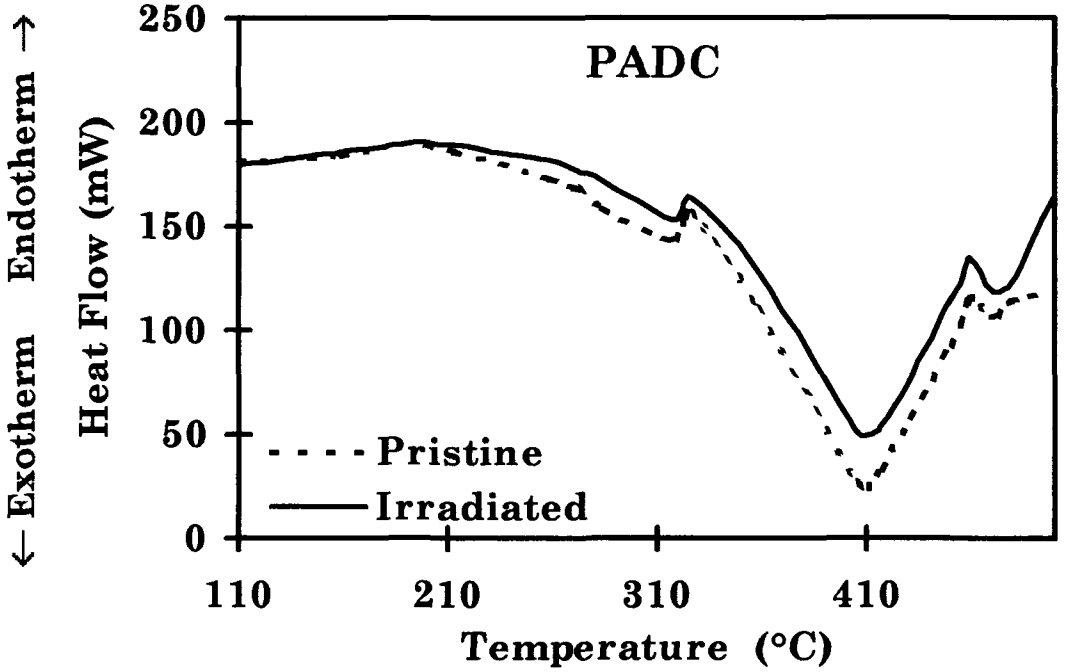

Fig.4.8.5. DSC thermograms of the pristine PADC and the proton irradiated PADC (80 kGy).

4.8.2. Analysis of PADC samples of Fullerene embedded stack (S5)

Out of four PADC samples used in the stack S5, the first three were used (as in the blow up diagram shown in Fig.4.8.6.) for analysis. The etching characteristic of fission tracks on normal and fullerene

(C_{60}) embedded PADC surfaces was evaluated both by optical and electron microscopy. The track diameters on different PADC surfaces as a function of etching time are listed in Table 4.8.2.

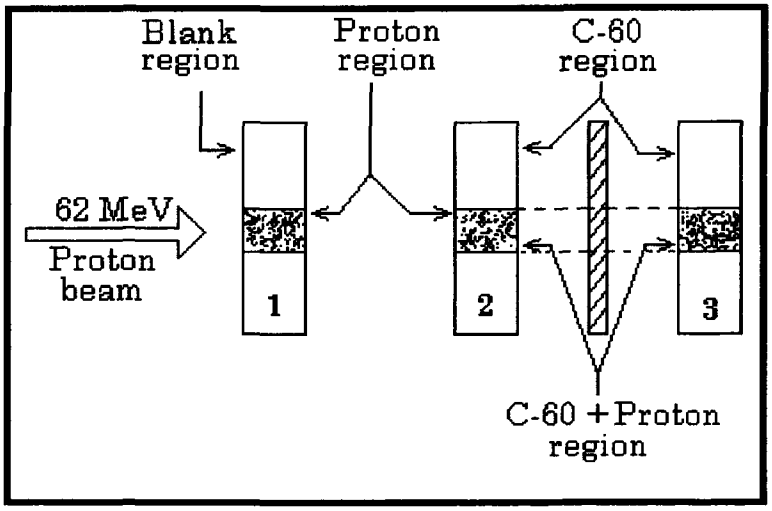

Fig.4.8.6. Blow up diagram of the first three PADC samples of fullerene embedded stack (S5).

Table 4.8.2. Values of fission fragment track diameters in different regions viz. Proton+C_{60}, C_{60}, Proton and blank region in PADC sample of S5 stack, as a function of etching time.

Etching time (hour)	**Diameter of fission tracks (μm) in different regions**			
	(Proton+C_{60})	**C_{60}**	**Proton**	**Blank (Pristine)**
1	1.8	1.8	1.8	1.8
2	5.3	3.6	4.3	3.6
3	7.8	3.9	6.0	3.9
4	11.0	7.8	8.2	7.8
5	15.3	10.7	12.1	10.7

The bulk etch-rates were found to be 1.5 μm/h for proton + C_{60} region, 1.3 μm/h for only proton irradiated region and 1.0 μm/h for the blank region (pristine). Scanning electron micrographs of different regions of the PADC sample etched for 120 minutes are shown in Fig.4.8.7.

The SEM photographs (Fig.4.8.7) show the fission fragment tracks in the pristine PADC (blank region), proton irradiated PADC (Proton irradiated region) and proton irradiated fullerene embedded PADC (Proton + C_{60} region). The increase in track diameters in the (Proton + C_{60}) region may be due to additional material damage caused by the energy released in the destruction of C_{60} molecules by proton irradiation [66]. More open structures and etch craters were observed in this region as evident from the SEM photographs.

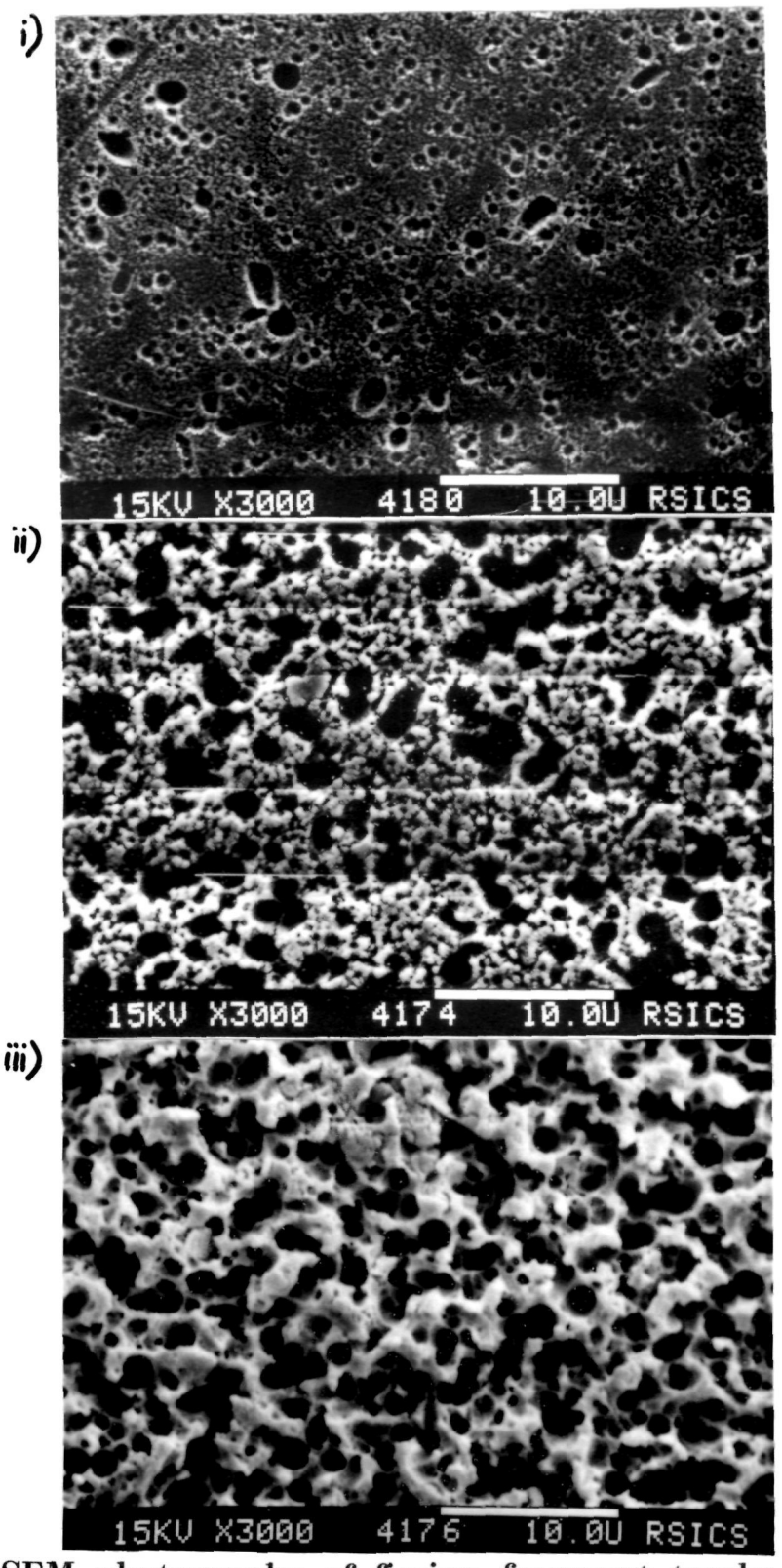

Fig.4.8.7. SEM photographs of fission fragment tracks in PADC samples of stack S5 i) Pristine PADC (blank region) etched for 120 minutes, ii) Proton irradiated region etched for 120 minutes, iii) (Proton + C_{60}) region etched for 120 minutes.

4.8.3. Analysis of PADC samples of Metal foil embedded stacks (S6 and S7)

The second PADC sample (PADC 2) of each stack (as shown in Fig.3.3) were analysed by track studies. The diameters of ^{28}Si ion tracks were found to increase slowly with etching time. It reached to a value of 6.6 μm in the pre-proton irradiated PADC surface adjacent to gold foil of stack S6, 6.1 μm on the surface in contact with aluminum foil of stack S7 and 4.8 μm on the pristine PADC after 3 hours of chemical etching.

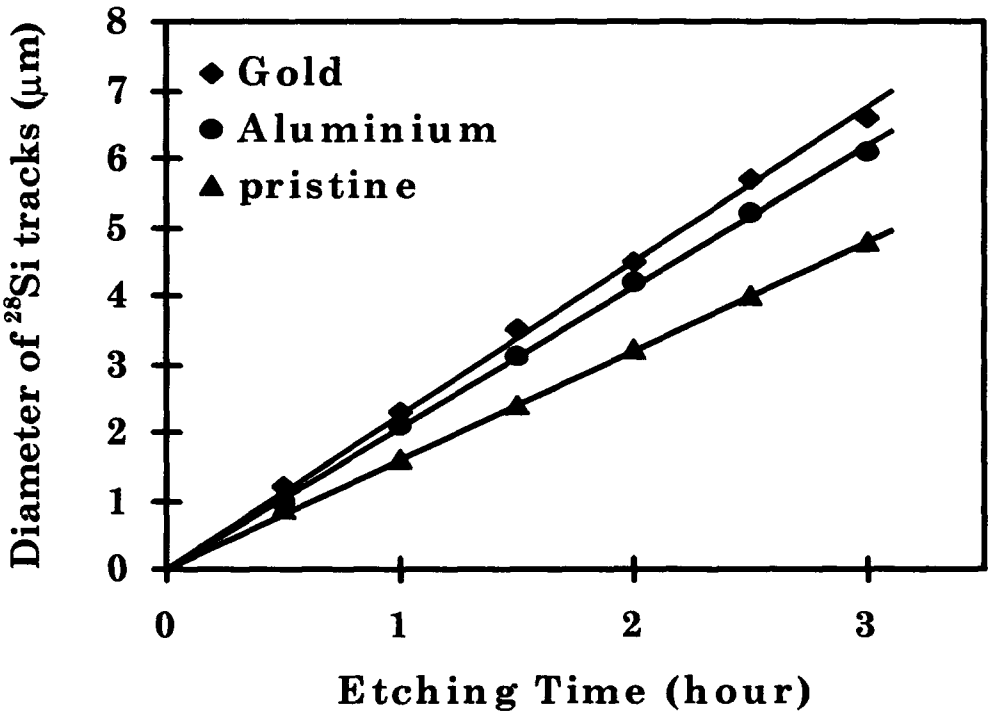

Fig.4.8.8. Etching time versus ^{28}Si track diameters for PADC samples of S6 stack adjacent to gold foil and that of S7 stack adjacent to aluminium foil, along with the pristine.

From the slope of the curves plotted between the track diameters versus etching times (Fig.4.8.8), the bulk etch-rates (V_G) were derived as given in Table 4.8.3. Similarly, the track lengths of ^{28}Si were also found to increase faster for the pre-proton irradiated PADC as compared to the pristine sample. Even the maximum etchable true track lengths of ^{28}Si ions in PADC were longer for the proton irradiated samples as compared to pristine one. The silicon track lengths were found to be maximum for the PADC adjacent to the gold foil, followed by that adjacent to the aluminium foil. The track lengths were plotted against the etching time as shown in Fig.4.8.9.

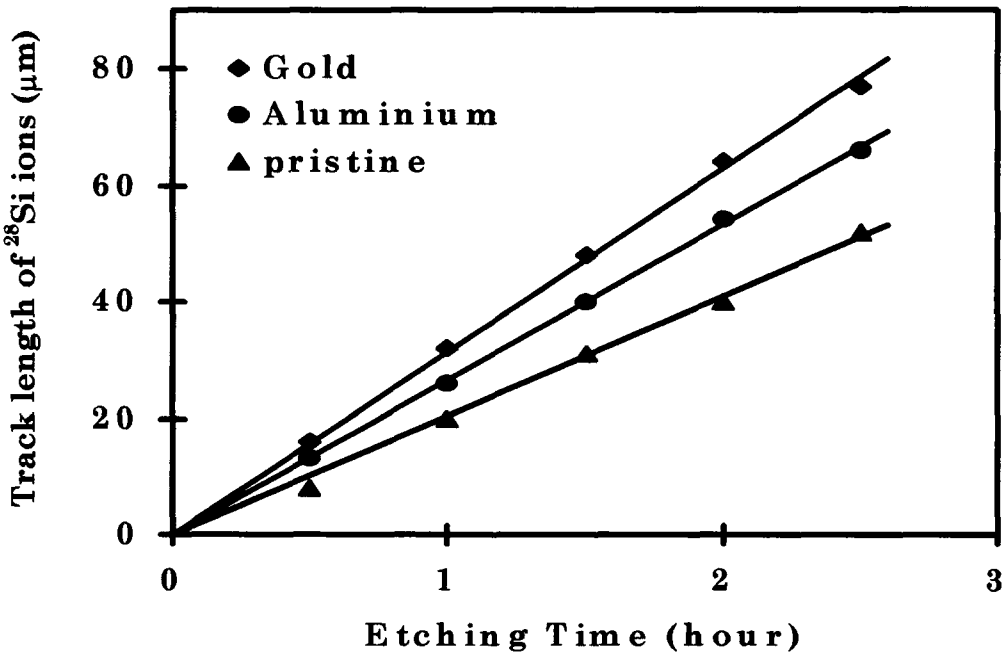

Fig.4.8.9. Etching time versus ^{28}Si track lengths for PADC samples of S6 stack adjacent to gold foil and that of S7 stack adjacent to aluminium foil, along with the pristine.

The corresponding track etch-rates (V_T) were calculated from the slope of the graphs for the different PADC samples and are given in Table 4.8.3. The V_T was found to be maximum for the PADC adjacent to the gold foil. The track lengths and track diameters were measured with a maximum probable error of ± 1.12μm. The errors associated with etch-rate measurements lies between 0.3 to 0.6μm/h. The etching response of a track detector is defined as the ratio of the track etch-rate to the bulk etch-rate (V_T/V_G). The greater its value the better is the track registration sensitivity of the detector.

Table 4.8.3. The bulk etch-rate (V_G), the track etch-rate (V_T) and the etching response (V_T/V_G) of pristine PADC and PADC adjacent to Al and Au foils.

Sample	V_G (μm/h)	V_T (μm/h)	(V_T/ V_G)
PADC (Pristine)	0.8	20.4	25.5
PADC (Al foil)	1.0	26.6	26.6
PADC (Au foil)	1.1	31.5	28.6

In this case, the etching response was found to be increased for the pre-proton irradiated PADC samples, but it has been further found that the sensitivity of the PADC adjacent to the gold foil was more than that adjacent to the aluminium foil. So, there is certainly

an additional effect of these metal foils towards the enhancement of the track registration sensitivity, which can be attributed to some secondary ionisations taking place due to proton irradiation.

62 MeV proton beam incident on the metal target results in the emission of secondary particles like fission fragments, spallation products, etc., having a wide energy range, some of them approaching the energy of the incident proton beam. The emitted secondary particles move preferably in the forward direction and cause additional ionisation in the adjacent polymer. The emission of these secondary particles depends on the charge of the target foil, so the effect of secondary ionisation was more prominent in the PADC adjacent to the gold foil. The SEM photographs of the ^{28}Si tracks in the pristine and the proton irradiated PADC samples of S6 and S7 stacks are shown in Fig.4.8.10. It reveals that the extent of damage in the PADC sample adjacent to the gold foil was more than the other PADC samples.

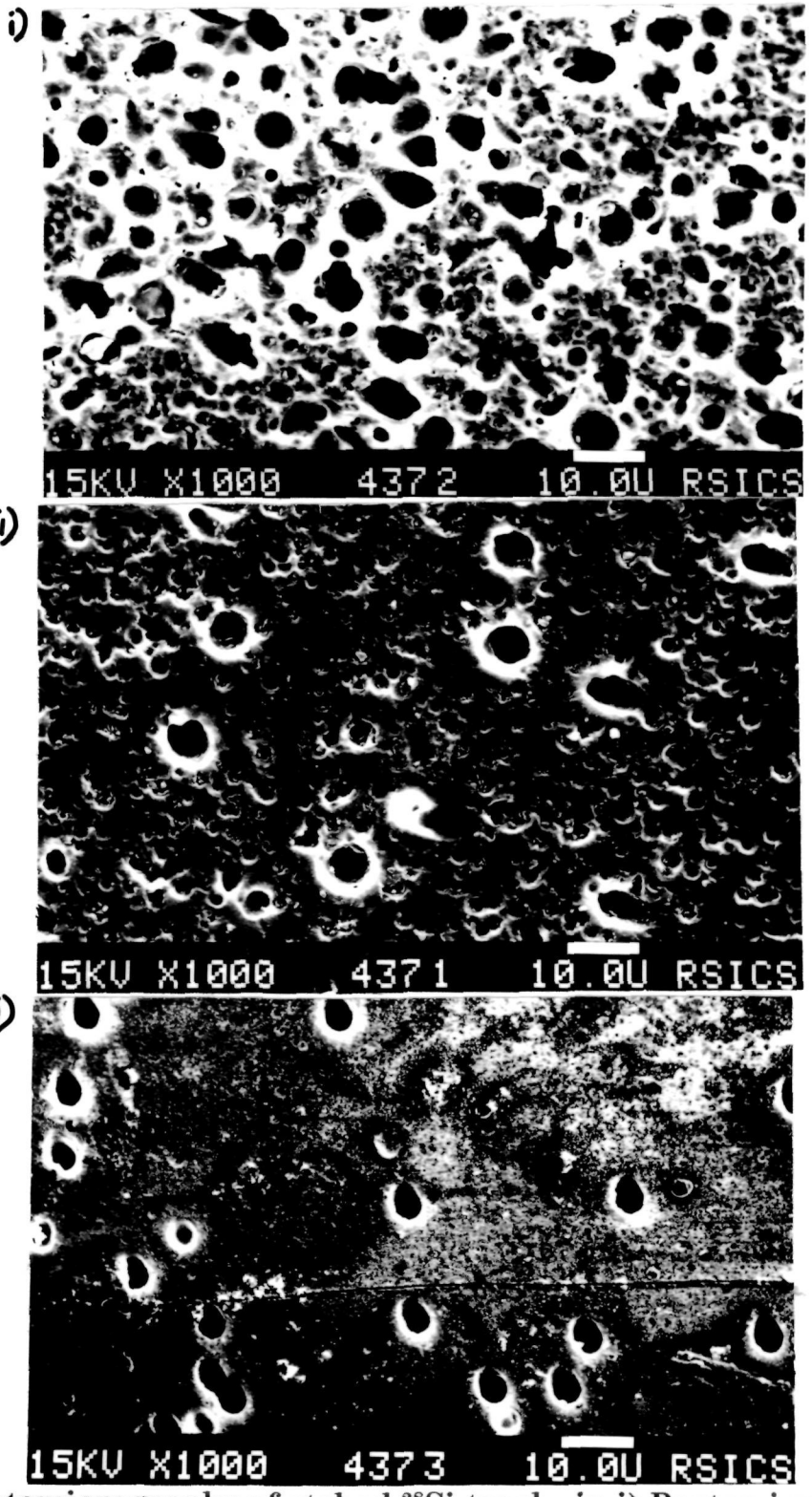

Fig.4.8.10. Photomicrographs of etched ^{28}Si tracks in i) Proton irradiated PADC of stack S6 adjacent to gold foil, ii) Proton irradiated PADC of stack S7 adjacent to aluminium foil, iii) Pristine PADC.

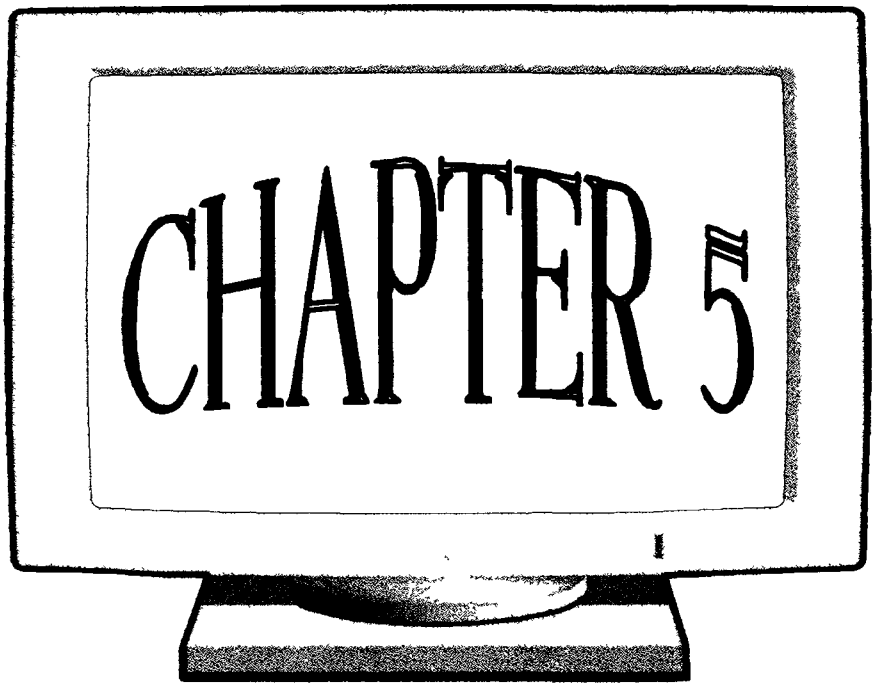
CHAPTER 5

CHAPTER 5

CONCLUSION AND FUTURE PERSPECTIVES

5.1. CONCLUSION

In an attempt to investigate the impact of the proton irradiation on eight different types of polymers, the present work revealed several physico-chemical modifications induced in the polymers due to the proton irradiation. The major findings of the present work are presented below.

5.1.1. Makrofol-N (MFN)

From the track studies it was evident that the bulk etch-rate of MFN increased by about 15-25% for two lower doses (10, 30 kGy) and about 50-75% for two higher doses (60, 80 kGy) than that of the pristine. The activation energy for etching was also found to be decreasing with increase in proton dose, signifying the degradation of the polymer by proton irradiation. There was no considerable change in the optical absorption spectra of MFN by proton irradiation. Only slight decrease in band-gap was observed even at the highest dose. The transmittance (FT-IR) spectra showed that even at the highest dose of proton irradiation new bands were not formed, rather the

transmittance (%) of most of the bands decreased denoting a degradation of the polymer by proton irradiation. Free radical formation was not observed. Thermal stability in the MFN irradiated to the highest dose decreased by about 24%. Exotherms appeared for the proton irradiated MFN (80 kGy), which was absent in the pristine one. There was a decrease (23%) in melting temperature for the sample irradiated to 60 kGy and 80 kGy. These results imply that, degradation is the dominant phenomenon in the polymer due to proton irradiation.

5.1.2. Triafol-TN (TTN)

In spite of slight increase in bulk etch-rate of the proton irradiated TTN, the activation energy for etching remained almost constant. The optical absorption properties were modified for the TTN irradiated to the highest dose (80 kGy), where the optical band-gap was reduced by 8%. No significant change in the vibrational frequencies was observed, which implied that chain-separation was not affected by much by proton irradiation. No free radical formation was observed. Stable zone appeared for the samples irradiated to higher two doses (60, 80 kGy) due to decolourisation of the blue dye by proton irradiation, i.e., the thermal stability of the polymer increased

by proton irradiation at the higher doses (60, 80 kGy). Exothermal temperatures reduced slightly with increase in dose up to 60 kGy, but the peak vanished for the highest dose. Melting temperatures were found at around 315°C for the pristine and the proton irradiated samples.

5.1.3. Polyethylene terephthalate (PET)

The bulk etch-rate of proton irradiated PET was found to be increasing thereby decreasing the activation energy of etching with the increase in dose. The bulk etch-rate increased by about 50-60% for the PET irradiated to the highest dose. It can therefore be inferred that proton irradiation made the polymer easily etchable, implying a degradation of the polymer. Proton irradiation (80 kGy) also increased the surface roughness of the polymer slightly. The XRD spectra showed an increase in the intensity of the main peak with a shift in its position which can be attributed to the differences in density of the pristine and irradiated zones arising out of the restoration of the crystal structure due to the increasing strain on the irradiated PET. Emergence of new peaks has been noticed which might be due to the newly formed fine polymer crystallites in the amorphous zone of irradiated PET. It can be concluded that there was an increase in

crystallinity of PET by proton irradiation. However, the optical band gap did not suffer any change and also there was no sign of free radical formation. The transmittance spectra however showed the change in most of the characteristic peak positions denoting the deformation of the polymeric structure. It also revealed the simultaneous effect of recrystallisation and amorphisation due to proton irradiation. Thermogravimetric analysis showed the disappearance of the stable zone after proton irradiation, permitting the polymer to undergo a slow decomposition as soon as the heat was applied. The decomposition behaviour of the polymer was found to be dose dependent, i.e., the more the dose of the proton beam, the less the thermal stability. This denoted a degradation of the polymer under proton beam irradiation, thus, enabling it to decompose earlier than the pristine. Differential scanning calorimetry indicated a change in melting (endotherms) nature of the proton irradiated PET. Here, we found continuous endothermal distortions spreading over a temperature zone instead of a sharp endothermal peak as in case of the pristine polymer.

5.1.4. Triafol-BN (TBN)

Track studies revealed that the activation energy for bulk-etching was not modified under different doses of proton irradiation, even though the etch-rates were increasing (about 50% at the highest dose). There was an increase in E_g by about 33% for the irradiated polymers, denoting an enhanced insulating nature of TBN due to proton irradiation. This property was independent of the four doses used. No significant change in the vibrational frequencies was observed except the one for stretching vibration of the main-chain. The transmittance (%) of most of the peaks was found to be reduced. This suggested the chain-scissioning leading to degradation in the irradiated TBN samples. Free radical signals were not observed. The stable zone appeared for the irradiated polymers. But, fast decomposition zone reduced. The melting temperature for the pristine TBN was found to be 334°C, which reduced to about 321°C for the irradiated samples denoting bond cleavage in the molecule, which corroborated the results of Thermogravimetric analysis and spectral studies.

5.1.5. Polypropylene (PP)

The proton irradiation on this polymer considerably reduced its surface roughness (by about 31%) in the nanoscopic level. X-ray diffraction study indicated an increase in crystallinity of the polymer due to proton irradiation (80 kGy). A slight shift of the absorption edge in the optical absorption spectra of the PP irradiated at 80 kGy of proton indicated a decrease in optical band-gap from 5.2 to 4.9 eV. The isotactic nature of the polymer was not disturbed even at the highest dose of proton irradiation. An increase in absorbance at all the wave numbers demonstrated the change in the crystallinity matrix and corroborating the results obtained from XRD analysis. Free radicals could not be traced from the ESR spectral analysis. The increase in thermal stability of the polymer was found to be roughly linear with increase in proton dose, which could be attributed to the cross-linking effect caused by proton irradiation enhancing the crystallinity of the material. This dose dependent modification of the thermal property endorsed the findings of the FT-IR and XRD studies. The temperature of crystallisation of PP reduced from 203°C (pristine) to 175°C (irradiated), whereas the melting temperature increased from 212°C (pristine) to 232°C (irradiated).

5.1.6. Polyimide (PI)

The proton irradiation made the polymer easily etchable but the response of bulk material to etching rate at different temperatures remained invariant. The surface roughness of the polymer reduced considerably (about 52%) by proton irradiation. Optical band-gap remained constant (2.2 eV) even after irradiation at the highest dose. No free radicals were detected for the irradiated polymer. Increase in absorbance of the bands corresponding to the phenyl groups further indicated some degradation of the polymer due to proton irradiation. The characteristic absorbance bands corresponding to alkyne groups were not observed for the irradiated samples. Proton irradiation enhanced the thermal resistivity of PI, which was again found to be dose dependent i.e. it increased with increase in dose. The temperature for crystallisation of the polymer increased from 298°C (pristine) to 316°C (irradiated), whereas the melting temperature increased slightly from 316°C (pristine) to 324° (irradiated).

5.1.7. Polytetrafluoro ethylene (PTFE)

The surface roughness of PTFE in the nanoscopic level decreased by about 53% due to proton irradiation (80 kGy). The decrease in intensity and shifting of the main peak in the XRD spectra

denoted some destruction of the orderliness of the original crystal structure due to proton bombardment. A shift in absorption edge from UV to visible region was noticed in the UV-Vis spectra of the irradiated polymer leading to a reduction in optical band-gap by about 27% for the polymer irradiated by 80 kGy of 62 MeV protons. ESR spectral analysis showed the formation of the free radical in PTFE by proton irradiation only at the highest dose (80 kGy). This free radical thus formed could be responsible for decreasing the optical band-gap. FT-IR study revealed that the C-F stretching vibration was affected due to irradiation (80 kGy). Since the C-F coupling is less covalent than C-C coupling due to more electronegativity of fluorine, the C-C bond is relatively less probable towards cleavage by irradiation. Thermogravimetric analysis revealed a decrease in the thermal stability by proton irradiation, which can be attributed to the loss of crystallinity as obtained from the structural analysis. There was no sharp exothermic peak indicating the temperature of crystallisation, rather a numerous thermic distortions were observed that spread over a range from 205°C to 325°C, however, the melting temperature was found to decrease gradually from 334°C (pristine) to 311°C (irradiated) with increase in dose. This result is in accordance with the other

studies and supports the fact that PTFE underwent chain-scission by proton irradiation.

5.1.8. Polyallyldiglycol carbonate (PADC)

The proton irradiation modified the track registration property of PADC. The bulk etch-rate of PADC irradiated to 80 kGy of 62 MeV protons was found to be 90% higher than that of the pristine.

The pre-proton irradiated PADC was found to be more sensitive to register the tracks of other heavy ions. Further, the proton irradiation made the polymer easily etchable. The maximum etchable track diameters of the fission fragments as well as the track lengths and diameters of the ^{28}Si ions in pre-proton irradiated PADC samples were found to increase considerably than in the pristine PADC, which was again found to be an increasing function of dose.

Secondly, it was found that the extra energy released by fullerene destruction due to proton irradiation had an additional impact on the adjacent PADC. The track diameters as well as the bulk etch-rate were more for the (Proton + C_{60}) region, which might be due to additional material damage. More open structures and etch craters were observed in this region.

Thirdly, it was found that proton irradiation through metal foils

resulted in the emission of some secondary particles which increased the etch-rate values of PADC. Moreover, this increase in etch-rate values of PADC was found to be a direct function of the atomic number (Z) of the metal foil. i.e., the bulk etch-rate was more for the PADC adjacent to the gold foil than that for the one adjacent to aluminium foil.

The proton irradiation reduced the surface roughness of PADC by about 12% at nanoscopic levels due to the probable occurrence of a splash phenomenon which can be expected from swelling in atomic scale of the nearby surface around the impinging ions or it might be due to the production of defects and chemical modification in the bulk and material ejection at the surface as it expected when the insulators are irradiated to energetic ions. However, the proton irradiation could not induce any considerable modification in the optical absorption properties of PADC. So, the optical band-gap (3.5 eV) was found to be unaltered after proton irradiation. The free radical formation was also not observed. The transmittance spectra revealed that the position of the transmission lines was considerably changed and most of the transmittance peaks vanished completely after proton irradiation denoting that degradation is the main effect induced by proton

irradiation. The thermogravimetric analysis of the irradiated samples showed a considerable decrease in thermal stability of the polymer by proton irradiation. The irradiation favoured the segmental vibration of the polymeric molecules at a lower temperature than that for the pristine. This supported the fact that the polymer had undergone degradation due to proton bombardment. This effect was also found to be directly related to the dose of irradiation, i.e., the more the dose the less was the tolerance of the polymer to heat. This is in accordance with the results of FT-IR. The DSC thermograms revealed a decrease in heat capacities involved in the exothermic process, which can be explained through the amorphisation of the polymer due to proton irradiation.

From the above results following general conclusion can be drawn:

- The proton irradiation has improved the track registration sensitivity in PADC, PET, MFN, TBN and PI.
- Thermal resistance of some polymers like PI, TBN, TTN and PP is improved by proton irradiation.
- The thermal stability of these polymers has been found to be dose dependent.

- The optical absorption properties of some of the irradiated polymers viz. PP, TTN and PTFE are found to be modified and the optical band-gap is reduced at the highest dose, whereas the optical band-gap of TBN is increased by about 33%.
- The crystallinity of the polymers like PET and PP is improved by proton bombardment, but for PTFE it is found to be diminished.
- The surface roughness of PADC, PI, PP, PTF is reduced except PET, where the roughness is increased slightly after proton irradiation.
- Formation of relatively stable free radical has been detected in PTFE after irradiation with a proton dose of 80 kGy.

5.2. FUTURE PERSPECTIVES

The induced modifications in physico-chemical properties of the polymers by proton irradiation will further enhance their applicability. Some of the feasible applications and the possible extension of the present work are discussed below.

5.2.1. Application of the Modified Polymers

The present investigation and the resultant conclusions drawn above show modified properties of the polymers, which could further enhance their technical importance. Keeping these results in view and

observing the recent trends of international standards in this field, it can be said that this area of research has a wide scope for further exploration, some of which are interpreted below:

- The proton irradiation on fullerene led to its destruction with the emission of a huge amount of energy. This can be utilised for some useful purpose like improvement in the detection and etching sensitivity of polymers (viz. PADC) for detection of energetic lighter particles.
- Thin metal targets of different atomic numbers can be used to induce the additional effects on track registration sensitivity of the polymers.
- The track registration sensitivity of the polymers plays an important role in manufacturing the single or multiple pore micro/nano-filters, which find immense applications in many fields. Improvement in track registration sensitivity of PADC, PET, MFN, TBN and PI by proton irradiation provides an important database for fabrication of designer micro-filters for specific applications.
- PADC also finds its application in detection of alpha particles emitted from the radioactive sources. It has been extensively used in the simultaneous measurement of Radon, Thoron and their

progeny in indoor atmosphere. The improvement in detection efficiency of PADC by proton irradiation will be certainly helpful in its application pertaining to its use as an environmental dosimeter.

- The thermal stability of PI extends its application to surface coatings of supersonic aircrafts, insulation coatings in various electrical appliances and backings in nuclear physics experiment. The present experiment reveals a possibility of further enhancing the thermal stability by proton irradiation. This finding will surely be very useful for its future application relating to space science.
- The decrease in optical band-gap and formation of stable free radicals in PTFE by proton irradiation will find its usefulness in micro-electronic devices.
- PP being one of the lightest polymers is being used extensively in many area of scientific and commercial interest. So, the improved properties like smoothness, thermal resistivity, optical conductivity, etc. by proton irradiation will enhance its usefulness.

5.2.2. Extension of the present work

The present investigations have opened up a wide scope of further detailed research in the field of radiation induced modification of various polymers.

- Most of the characteristic modifications in the properties of the polymers used in the present work occur at the highest dose of the 62 MeV proton. There is a scope to further investigate the modifications induced in the polymers irradiated at higher doses, i.e., more than 80 kGy of 62 MeV protons.
- A systematic ESR study of the irradiated polymers should be carried out either on line or at low temperature immediately after irradiation so that the free radicals formed can be detected before they are annihilated.
- The decrease in the optical band-gap might be due to formation of carbon clusters which can be proved and the cluster size can be measured by SAXS (Small Angle X-ray Scattering) or Neutron scattering experiments on the irradiated polymers.
- The increased throughput of track-irradiated membranes suggests their application as gas selective membranes. Due to their compactness, latent tracks can provide the potential to develop micro-sized chromatographic separators.
- Ion lithography can be done by galvanic deposition, chemical vapour deposition or ion sputter techniques in order to induce the desired modification in polymers. It's a new way to create hard and

conductive polymers. Ion implantation is mainly used for controlled doping of semi-conductors.

- Etched tracks can be utilised for generating ray-optical scattering devices with exactly pre-determined properties.
- For etch cones with diameters and at distances small in comparision with the wavelength of applied radiation, coherent scattering (wave optics) becomes dominant. At sufficient areal density of the ion tracks and sufficient depth of the etched track cones, a drastic reduction of reflected intensity is observed. So the etched tracks can be helpful in developing anti-reflection surfaces.
- Some additional characterisation techniques like thermoluminesence, annealing, hardness measurements, etc. may be prescribed for the irradiated polymers for a better understanding of the mechanisms responsible for the radiation induced modifications.
- The impact of heavy ion irradiation on the same polymers, as used in the present work, can be studied in order to have a comparative study on the effect of low and high LET radiations on polymers.

REFERENCES

[1] Spohr R. Ion tracks and Microtechnology - Principles and applications. Vieweg Bertelsmann Publishing Group International. (1990), 1-13.

[2] Gowariker V. R., Viswanathan N. V. and Sreedhar Jayadev. Polymer Science. New Age International (P) Limited Publishers. 9th Edition. (1996), 1-12.

[3] Rodriguez F. Principles of Polymer Systems. Tata Mcgraw Hill Publishing Company Ltd. (1974), 26-49.

[4] Venkatesan T. High energy ion beam modification of polymer films. Nucl. Instr. and Meth. B7/8 (1985), 461-467.

[5] Vacik J., Cervena J., Hnatowicz V., Fink D., Apel P. Yu. and Strauss P. Ion transmission - New technique for analysing ion tracks in polymers. Nucl. Instr. Meth. B146 (1998), 475-479.

[6] Apel P. Yu. Conductometric studies of multiply charged ion track structure in various polymers. Nucl. Tracks. Radiat. Meas. 19 (1991), 29-34.

[7] Nikezic D. and Kostic D. Simulation of the track growth and determining the track parameters. Radiat. Meas. 28 (1997), 185-190.

[8] Puglisi O., Liccialdello A., Calcagno L. and Foti G. Molecular weight distribution and solubility changes in ion bombarded polystyrene. Nucl. Instr and Meth. B19/20 (1987), 865-871.

[9] Lovinger A. J., Forrest S. R., Kaplon M. L., Schmidt P. H. and Venkatasen T. Structural and morphological investigation of the development of electrical conductivity in ion-irradiated thin films of an organic material. J. Appl. Phys. 55 (1984), 476-482.

[10] Marletta G. Chemical reactions and physical property modifications induced by keV ion beams in polymers. Nucl. Instr. and Meth. B46 (1990), 295-305.

[11] Davenas J., Xu X. L., Boiteaux G. and Sage D. Relation between structure and electron properties of ion irradiated polymers. Nucl. Instr. and Meth. B39 (1989), 754-763.

[12] Fink D., Müller M., Chadderton L. T., Cannington P. H., Elliman R. G. and Mc Donald D. C. Optically absorbing layers on ion beam modified polymers: A study of their evolution and properties. Nucl Instr. and Meth. B32 (1988), 125-130.

[13] Elman B. S., Thakur M. K., Sandman D. J. and Newkirk M. A. Ion implantation studies of polydiacetylene crystals. J. Appl. Phys. 57 (1985), 4996-4999.

[14] Marletta G., Pignataro S. and Oliveri C. Reflection electron energy loss (REELS) of conductive polymers obtained by keV/bombardment. Nucl. Instr. Meth. B39 (1989), 773-777.

[15] Forrest S. R., Kaplon M. L., Schmidt P. H. Venkatesan T. and Lovinger A. Large conductivity changes in ion-beam-irradiated organic thin films. J. Appl. Phys. Letters. 41 (1982), 706-710.

[16] Macchi F., Daudin B., Hillairet J., Lauzier J., N'Goma J.B., Cavaille J.Y. and Legrand J. F. Micromechanical properties of electron irradiated PVDF-TrFE copolymers. Nucl. Instr. and Meth. B46 (1990), 334-337.

[17] Lee E. H., Lewis M. B., Blau P. J. and Mansur L. K. Improved surface properties of polymer materials by multiple ion treatment. J. Mater. Res. 6 (1991), 610-628.

[18] Biersack J. P. and Kallweit R. Ion beam induced changes of the refractive index of PMMA. Nucl. Instr. and Meth. B46 (1990), 309-312.

[19] Darraud-Taupiac C., Bennamane B., Decossas J. L. and Vareille J. C. CR-39 (poly(diethylene glycol bis(allyl carbonate)) under γ-rays & proton beams. Nucl.Instr. and Meth.B131, (1997), 198-204.

[20] Le Möel A., Duraud J. P., Lecomte C., Valin M. T., Henriot M., Le Gressus C., Darnez C., Balanzat E. and Demanet C. M. Modifications induced in Polyvinylidene Fluoride by energetic ions. Nucl. Instr. and Meth. B32 (1988), 115-119.

[21] Komaki Y., Ishikawa N. and Sakurai T. Effects of gamma rays on etching of heavy ion tracks in Polyimide. Radiat. Meas. 24 (1995), 193-196.

[22] Dwivedi K. K., Ghosh S., Fink D., Mishra R., Tripathy S. P., Kulshreshtha A. and Khathing D. T. Modification of Track Registration Response of PADC detector by energetic protons. Radiat. Meas. 31 (1999),127-132.

[23] Mishra R., Tripathy S. P., Kulshrestha A., Srivastava A., Ghosh S., Dwivedi K. K., Khathing D. T., Muller M. and Fink D. Impact of Electron Irradiation on particle track etching response in Polyallyldiglycol carbonate (PADC). Pramana 54(2000), 777-784.

[24] Zhai P. J., Xing Y. X., Zhang Y., Feng S. L., Kang Y. X., Tang X. W., Wang Y. G., Zhao W. J., Yan S. Observation and study of latent tracks on the surface of HOPG induced by H^+ ions. Radiat. Meas. 28 (1997), 97-100.

[25] Durrani S. A., Khan H. A., Malik S. R., Aframian A., Fremlin J. H. and Tarney J. Charged particle tracks on Apollo 16 lunar glasses and analogous materials. In Proc. Fourth Lunar Sci. Conf., Geochim. Cosmochim. Acta, Suppl. 4. Pergamon, New York. (1973), 2291-2305.

[26] Al-Jarallah M. I., Abu-Jarad F., Hallak A. B, Coban A. and Islam M. Investigation of proton response of CR-39. Nucl. Tracks Radiat. Meas. 22 (1993), 191-194.

[27] Afarideh H., Hatami P. and Hosseini A. A. Low energy protons and deutrons track registration in CN-85 SSNT detector. Nucl. Tracks Radiat. Meas. 19 (1991), 9-10.

[28] Ogura K., Benton E. V., Frank A. and Atallah T. Proton response of CR-39. Nucl. Tracks Radiat. Meas. 12 (1986), 527-530.

[29] Ogura K., Hattori T., Hirata M., Asano M., Yoshida M., Tamada M., Omichi H., Nagooka N., Kubota H. and Katakai R.

Development of copolymer of CR-39 with high sensitivity to low LET particles. Radiat. Meas. 25 (1995), 159-162.

[30] Ogura K., Hattori T., Asano M., Yoshida M., Omichi H., Nagooka N., Kubota H., Katakai R. and Hasegawa H. Proton response of high sensitivity CR-39 copolymer. Radiat.Meas.28 (1997),197-200.

[31] Pinheiro Filho J. D., De Almeida E. S., Bilbao E. Z., Santos R. C., Da Silva A. X., Sciani V. and Rela P. Thermal annealing of proton tracks with energies of 4 to 6 MeV in CR-39 polymer detectors. Radiat. Meas. 23 (1994), 743-748.

[32] Mircea I. Chipara. ESR investigations on ion irradiated polymers. Nucl. Instr. Meth. B131 (1997), 85-90.

[33] Edmonds E. A. and Durrani S. A. Relationship between thermo-luminescence, radiation induced spin resonance and track etchability of Lexan polycarbonate. Nucl. Tracks. 3 (1979), 3-11.

[34] Akber R. A., Nadeem K., Majid C. A., Hussain A., Zaman N., Chaudhary M. A. and Khan H. A. Studies of structural changes produced by high doses of gamma rays in some plastic track detectors. Nucl. Instr. Meth. B173 (1980), 217-221.

[35] Sinha D., Sarker G. K., Ghosh S., Kulshreshtha A., Dwivedi K. K. and Fink D. Gamma ray photon induced modifications in Triafol-TN and Triafol BN polymeric track detectors. Radiat. Meas. 29 (1998), 599-504.

[36] Nouh S. A. Effect of UV radiation on the optical properties of cellulose triacetate. Radiat. Meas. 27 (1997), 499-503.

[37] Steckenreiter T., Balanzat E., Fuess H. and Trautmann C. Chemical modifications of PET induced by SHI. Nucl. Instr. Meth. B131 (1997), 413-417.

[38] Eßer M. and Fuhrmann J. Polymer chain orientation in latent ion tracks Nucl. Instr. Meth. B151 (1999), 118-122.

[39] Steckenreiter T., Balanzat E., Fuess H. and Trautmann C. Pyrolytic Effects induced by energetic ions in Polymers. Nucl. Instr. and Meth. B151 (1999), 161-168.

[40] Apel P. Yu, Didyk A. Yu., Kravets L. I., Kuznetsov V. I. and Fursov B. I. Registration temperature effect in Polypropylene detectors. Nucl. Tracks Radiat. Meas. 22 (1993), 93-96.

[41] Apel P. Yu, Kuznetsov V. I., Luppov V. G., Levkovich A. V., Altynov V. A. and Orelovich O. L. Effects of atomic hydrogen on polymeric track detectors. Nucl. Tracks Radiat. Meas. 22 (1993), 97-100.

[42] Davenas J., Boiteux G. and Jardin C. Electronic and mass transport in ion beam nano structured polymers: Role of the irradiation energy. Nucl. Instr. and Meth. B131 (1997), 91-96.

[43] Xu X. L., Yuehui Yu., Zixin L., Lizhi C., Fang F., Zuyao Z., Shichang Z., Gendi D. and Guanqun X. Shrinkage of Polyimide films under ion beam irradiation. Nucl. Instr. and Meth. B59/60(1991),1267-1270.

[44] Marletta G. and Iacona F. Chemical and Physical property modifications induced by ion irradiation in Polymers. Materials

and Processes for surface & interface Engineering. Kluwer Academic Publishers (1995), 600-605.

[45] Yoshida K. and Iwaki M. Structure and Morphology of ion-implanted Polyimide films. Nucl. Instr. and Meth. B19/20 (1987), 878-881.

[46] Betz N., Petersohn E. and Le Möel A. Swift heavy ion effects in fluoro polymers: radicals and crosslinking. Nucl. Instr. and Meth. B116 (1996), 207-211.

[47] Schierholz K., Lappan U., Lunkwitz K. Electron beam irradiation of polytetrafluoroethylene in air: investigations on thermal behavior. Nucl. Instr. and Meth. B151 (1999), 232-237.

[48] Frank A. L. and Benton E. V. Dielectric plastics as high exposure gamma ray detectors. Radiat. Eff. 2 (1970), 269-272.

[49] Zamani M., Sampsonidis D., Charalambous S. Dose rate effects on CR-39 SSNT detector. Nucl. Tracks 12 (1986), 125-128.

[50] Portwood T. and Henshaw D. L. The effect of gamma dose on alpha response of CR-39. Nucl. Tracks 12 (1986), 105-108.

[51] Sharma S. L., Pal T., Rao V. V. and Enge W. Effect of gamma irradiation on bulk etch rate of CR-39. Nucl. Tracks Radiat. Meas. B18 (1991), 385-389.

[52] Sinha D., Ghosh S., Srivastava A., Dedgaonkar V. G., Dwivedi K. K. Effect of gamma rays on PADC detectors. Radiat. Meas. 28 (1997), 145-148.

[53] Abu-Jarad F., Hala A. M., Farhat M., Islam M. Effect of high gamma dose on the CR-39 properties. Radiat. Meas. 28 (1997), 111-116.

[54] Sinha D., Dwivedi K. K. Modifications of radiation detection response of PADC track detectors by photons. Radiation Physics and Chemistry 53 (1998), 99-105.

[55] Oda K., Yoshida K., Yamauchi T., Honda Y., Ikeda T. and Tagawa S. Effects of low LET radiations on CR-39 track detector. Radiation Measurements 28 (1-6) (1997), 85-88.

[56] Dwivedi K. K. and Mukherji S. Heavy ion track lengths in Solid dielectric track detectors. Nucl. Instrum. Methods B161 (1979), 317-326.

[57] Saxena A. and Dwivedi K. K. Chemical etching characteristics of glass detectors. Nucl.Tracks and Radiat. Meas.12 (1986), 161-164.

[58] Fink D., Chung W. H., Klett R., Schmoldt A., Cardoso J., Montiel R., Vazquez M. H., Wang L., Hosoi F., Omichi H. and Goppelt-Langer P. Carbonaceous Clusters in irradiated polymers as revealed by UV-Vis spectrometry. Radiat. Eff. and Def. in Solids. 133 (1995), 193-208.

[59] Gagnadre C., Decossas J. L. and Vareille J. C. IR spectroscopic studies of polycarbonate irradiated by H^+ and Li^+ ions. Nucl. Instr. and Meth. B73 (1993), 48-52.

[60] Alpert N. L., Keiser W. E. and Szymanski H. A. IR- Theory and Practice of Infrared Spectroscopy. A Plenum/Rosetta edition,

Published by Plenum Publishing Corporation, New York. (1970), 184-300.

[61] Fink D., Hosoi F., Omichi H., Sasuga T. and Amaral L. IR transmission of ion iradiated polymers. Radiat. Eff. and Def. in Solids. 132 (1994), 313-328.

[62] Papaléo R. M., Farenzena L. S., De Araújo M. A. and Livi R. P. Surface tracks in polymers induced by MeV heavy ion impacts. Nucl. Instr. and Meth. B151 (1999), 135-139.

[63] Nouh S. A., Wahab L. A. and Eissa H. M.. The effect of UV radiation on the thermal degradation of Cellulose triacetate.Radiat. Meas.30 (1999), 753-757.

[64] Caro J. C., Lappan U. and Lunkwitz K. Sulphonation of fluoro polymers induced by electron beam irradiation. Nucl. Instr. and Meth. B151 (1999), 181-185.

[65] Spinks J. W. T. and Woods R. J. An Introduction to Radiation Chemistry. Wiley Interscience Publication. 3rd Edition. (1990), 452-471.

[66] Fink D., Chung W. H., Dwivedi K. K., Ghosh S., Klett R., Stritzker B., Richter A. and Chadderton L. T. Effects of Fullerene destruction. Radiat. Eff. And Def. in Solids.143 (1998), 311-332.

RESUME

Name : **Shyama Prasanna Tripathy.**

Date of birth : **30th November, 1972.**

Educational qualifications:

Exam. Passed	Board/ University	Year	Result	% of marks
H.S.C.	B.S.E.Orissa.	1988	1st Div	75
+2 Science.	C.H.S.E.Orissa.	1990	1st Div	71.5
+3 Science.	Utkal University	1993	1st Div.	74.5(Hons.)
(Physics)			(Distinc.)	65.1(Aggt.)
M.Sc.(Physics)	Utkal University.	1995	1st Div.	78.1(Rank 3)
P.G.D.C.A.	Utkal University.	1996	1st Div.	60.5
M.Phil. (Physics)	Utkal University	1997	PASS.	***
Ph.D.(Physics)	N.E.H.University.	1997	Continuing	***

Computer proficiency: MS-DOS, Windows 9x, UNIX, FORTRAN, BASIC, PASCAL, MS-Word, Excel, HPG, Web designing.

CONFERENCE / WORKSHOP:

(I) ATTENDED:

[1] School on accelerator based technology. April 14-24, 1998, Nuclear Science Centre, New Delhi.

[2] National Workshop on Radon/Helium Precursors for Earthquake Studies. October 12-17, 1998, G. N. D. University, Amritsar.

[3] School on Swift Heavy Ions in Materials: Basic phenomena and Applications. October 24, 1998, Nuclear Science Centre, New Delhi.

[4] Awareness programme on Applications of radioisotopes and radiation technology, November 26-27, 1999, R. S. I. C., Shillong.

[5] National Workshop on recent trends in Electron Microscopy. April 26-27, 2000, R. S. I. C., Shillong.

(II) PARTICIPATED:

[1] Eleventh National Symposium on "Solid State Nuclear Track Detectors". October 12-14, 1998, G. N. D. University, Amritsar.

[2] International Conference on "Swift Heavy Ions in Materials Engineering and Characterisation (SHIMEC-98)", October 20-22, 1998, Nuclear Science Centre, New Delhi.

[3] Nuclear and Radiochemistry Symposium (NUCAR'99), Bhabha Atomic Research Center, Mumbai. Paper awarded.

Scholarship/ Fellowship awarded:

[1] Merit Scholarship. : 1985-1988.
[2] National Scholarship. : 1989-1993.
[3] Jindal Scholarship. : 1993-1995.
[4] State Loan Scholarship. : 1995-96.
[5] Junior Research Fellowship (NSC-UGC): July'97 - Nov'99.
[6] Senior Research Fellowship (DAE) : Dec'99-March'2000.
[7] Senior Research Fellowship (CSIR) : April'2000-Mar'2003.

List of Publications:

[1] **Ranges and Energy Loss Measurement of 1.0-4.7 MeV/u ^{28}Si ions in Makrofol-G using PADC as detector .**
R. Mishra, **S. P. Tripathy**, A. Kulshreshtha, A. Srivastava, K. K. Dwivedi and D. K. Avasthi. *Radiation Effects and Defects in Solids. vol.147 (1999) 273-281.*

[2] **Modifications in Track Registration Response of PADC detector by energetic protons.**
K. K. Dwivedi, S. Ghosh, D. Fink, R. Mishra, **S. P. Tripathy**, A. Kulshreshtha and D. T. Khathing. *Radiation Measurements. vol.31 (1999) 127-132.*

[3] **Assessment of Indoor Radon Level in Shillong.**
M. Sen, R. Mishra, **S. P. Tripathy**, D. Sinha, A. Kulshreshtha, K. K. Dwivedi, P. Deka and B. Bhattacharjee. *J. As. Sc. Soc. 39(3) (1998) 106.*

[4] **Concentration of Radon and Thoron in some dwellings of North Eastern India.**
R. Mishra, **S. P. Tripathy**, L. Pachuau, C. Laldawngliana, R. Lalramengzami, S. Ghosh, K. K. Dwivedi, D. T. Khathing, T. V. Ramachandran. *Indoor+ Built Environment. vol.8 (1999) 322-326.*

[5] **Optical and Electrical properties of some electron and proton irradiated polymers.**
R. Mishra, **S. P. Tripathy**, D.Sinha, D. T. Khathing, K. K. Dwivedi, S. Ghosh, M. Muller, D. Fink and W. H. Chung. Presented in NUCAR'99, BARC(**Awarded**). *Nuclear Instrumentation and Methods in Physics Res. B, 168 (2000) 59-64.*

[6] **Optical Absorption and Track studies of Gamma- irradiated ZnP glass.**
A. Kulshreshtha, D. Sinha, R. Mishra, **S. P. Tripathy**, K. K. Dwivedi, S. Ghosh and D. Fink. Presented in the 19th International Conference on Nuclear Tracks in Solids, Besancon, France. *Radiation Measurements. vol.32(3) (2000) 169-172.*

[7] **Impact of Electron Irradiation on particle track etching response in Polyallyldiglycol carbonate (PADC).**
R. Mishra, **S. P. Tripathy**, A. Kulshrestha, A. Srivastava, S. Ghosh, K. K. Dwivedi, D. T. Khathing, M. Muller and D. Fink. *Pramana, vol.54(5) (2000)* 777-784.

[8] **Effect of high gamma doses on etch rate values of different types of PADC detectors.**
D. Sinha, R. Mishra, **S. P. Tripathy**, K. K. Dwivedi. *Radiation Measurements, 000 (2000) 000.*

[9] **Simultaneous Determination of Radon, Thoron and their progeny in dwellings.**
K. K. Dwivedi, R. Mishra, **S. P. Tripathy**, A. Kulshreshtha, D. Sinha, A. Srivastava, P. Deka, B. Bhattacharjee, T. V. Ramachandran and K. S. V. Nambi. *Radiation Measurements, 000 (2000) 000.*

[10]**Electron Induced Modification in Poly(ethylene terephthalate).**
R. Mishra, **S. P. Tripathy**, K. K. Dwivedi, D. T. Khathing, S. Ghosh, M. Muller and D. Fink. *Radiation Effects and Defects in Solids. 000 (2000) 000.*

[11] **Effect of proton irradiation through metal foils on PADC.**
S. P. Tripathy, R. Mishra, A. Kulshreshtha, K. K. Dwivedi, D. T. Khathing, A. Srivastava, S. Ghosh and D.Fink. Presented in SHIMEC'98, NSC, Delhi. *Radiation Measurement, 000 (2000) 000.*

[12] **Electron irradiation on polyallyldiglycol carbonate.**
R. Mishra, **S. P. Tripathy**, A. Kulshreshtha, D. T. Khating, K. K. Dwivedi, S. Ghosh and D. Fink. Presented in the International conference SHIMEC '98, NSC, Delhi. *Radiation Effects and Defects in Solids. 000 (2000) 000.*

[13] **Gamma-photon induced modification of Polyvinylchloride (PVC) film.**
D. Sinha, **S.P.Tripathy**, R.Mishra, K.K.Dwivedi. *Radiation Effects and Defects in Solids, 000 (2000) 000.*

[14] **Optical absorption studies in heavy ion irradiated polymers.**
S. P. Tripathy, R. Mishra, A. Kulshreshtha, D. T. Khathing, K. K. Dwivedi, A. Srivastava, S. Ghosh and D.Fink. Presented in 11th National Symposium on SSNTDS, 1998, GNDU, Amritsar. *Radiation Effects and Defects in Solids, 000 (2000) 000.*

[15] **Electron Induced Modification in Polypropylene.**
R. Mishra, **S. P. Tripathy**, K. K. Dwivedi, D. T. Khathing, S. Ghosh, M. Muller and D. Fink. *Radiation Measurements, 000 (2000) 000.*

[16] **Modifications in etching characteristics and surface topography of some electron irradiated polymers.**
R. Mishra, **S. P. Tripathy**, K. K. Dwivedi, D. T. Khathing, S. Ghosh and D. Fink. Presented in International conf. on Nucl. Tracks, 2000, Slovenia. *Radiation Measurements, 000 (2000) 000.*

[17] **Modificatins induced by proton irradiation in Polyallyl diglycol carbonate.**
S. P. Tripathy, R. Mishra, K. K. Dwivedi, D. T. Khathing, S. Ghosh and D. Fink. Presented in International conf. on Nucl. Tracks, 2000, Slovenia. *Radiation Measurements, 000 (2000) 000.*

[18] **Range and Energy loss rate of 118 MeV ^{28}Si in some Polymers using PADC as Detector.**
D. T. Khathing, **S. P. Tripathy**, R. Mishra, B. K. Verma and K. K. Dwivedi. Presented in International conf. on Nucl. Tracks, 2000, Slovenia. *Radiation Measurements, 000 (2000) 000.*

[19] **Proton Induced Modification in Polyethylene Terephthalate (PET).**
K. K. Dwivedi, **S. P. Tripathy**, R. Mishra, D. T. Khathing, S. Ghosh and D.Fink. Presented in International con. on Nucl. Tracks, 2000, Slovenia. *Radiation Measurements, 000 (2000) 000.*

[20] **Optical and electrical properties of gamma irradiated PADC detector.**
D. Sinha, T. Phukan, **S. P. Tripathy**, R. Mishra and K. K. Dwivedi. Presented in International conf. on Nucl. Tracks, 2000, Slovenia. *Radiation Measurements, 000 (2000) 000.*

[21] **Range of ^{28}Si ions in Makrofol.**
S. P. Tripathy, R. Mishra, S. Shyam, A. K. Mawar, K. K. Dwivedi, D. T. Khathing and A. Srivastava. Presented in 11th National

Symposium on SSNTDS, 1998, GNDU, Amritsar. *Radiation Measurements, 000 (2000) 000.*

[22] **Effect of Electron irradiation on Polytetrafluoro ethylene.**
R. Mishra, **S. P. Tripathy**, K. K. Dwivedi, D. T. Khathing, S. Ghosh, M. Muller and D. Fink. *Nuclear Instrumentation and Methods in Physics B. 000 (2000) 000.*

[23] **Spectroscopic and Thermal Studies of Electron irradiated Polyimide.**
R. Mishra, **S. P. Tripathy**, D. T. Khathing, K. K. Dwivedi, S. Ghosh, M. Muller and D. Fink. *Radiation Physics and Chemistry, 000 (2000) 000.*

[24] **Modification in some properties of Polypropylene (PP) by 62 MeV Protons.**
S. P. Tripathy, R. Mishra, K. K. Dwivedi, D. T. Khathing, S. Ghosh and D. Fink. *Nuclear Instrumentation and Methods in Physics Res. B.*

[25] **Modification induced in Polytetrafluoro ethylene (PTFE) by 62 MeV Protons.**
S. P. Tripathy, R. Mishra, K. K. Dwivedi, D. T. Khathing, S. Ghosh and D. Fink. *Radiation Physics and Chemistry.*

[26] **On the Isothermal and Isochronal Annealing of ZnP glass track detector.**
S. P. Tripathy, R. Mishra, K. K. Dwivedi and D. T. Khathing. *Journal of Phys: D, Applied Physics.*